Development of an Engine Testing Facility for Spark Ignition Engine Fuels

by
Wilhelm Jordaan Kenny

Thesis presented in fulfilment of the requirements for the degree of Master of Science in the Faculty of Engineering at Stellenbosch University

Supervisor: Mr Richard Walter Haines

March 2013

Declaration

By submitting this thesis electronically, I declare that the entirety of the work contained therein is my own, original work, that I am the sole author thereof (save to the extent explicitly otherwise stated), that reproduction and publication thereof by Stellenbosch University will not infringe any third party rights and that I have not previously in its entirety or in part submitted it for obtaining any qualification.

Date: March 2013

Abstract

This thesis comprises of the development of a facility were spark ignition engine fuels can be tested. Development of the facility included the installation of a standard spark ignition engine, an engine dynamometer, control and monitoring equipment, control and monitoring software, and an in-cylinder pressure measurement setup.

The system was tested using petrol as well as a petrol-ethanol blend. The results indicated good accuracy and repeatability of the system. Analysis of the performance and combustion of the petrol-ethanol blend showed no significant difference in comparison to the petrol fuel. The petrol-ethanol blend showed a slight increase in oxygen content and fuel consumption as well as an increase in CO_2 emissions and a decrease in CO emissions.

During the project, a comparison was also made between the performance of fibre optic transducers and a piezoelectric transducer. It was found that the fibre optic transducers performed similarly to the piezoelectric transducer during low engine load conditions. At high load conditions however, the fibre optic transducers were not able to produce the same accuracy as the piezoelectric transducer.

Opsomming

Hierdie tesis bestaan uit die ontwikkeling van 'n fasiliteit waar brandstowwe vir 'n vonkontsteking binnebrandenjin getoets kan word. Ontwikkeling van die fasiliteit sluit in die installering van 'n standaard vonkontsteking binnebrandenjin, 'n enjin rem, beheer en monitering toerusting, beheer en monitering sagteware, en 'n in-silinder drukmeting opstelling.

Die fasiliteit is getoets met suiwer petrol sowel as 'n petrol-etanol mengsel. Die resultate het hoë vlakke van akkuraatheid en herhaalbaarheid getoon. Ontleding van die werksverrigting en verbranding van die petrol-etanol mengsel het geen beduidende verskil getoon in vergelyking met die suiwer petrol brandstof nie. Die petrol-etanol mengsel het 'n effense toename in suurstofinhoud, brandstofverbruik, sowel as CO_2 vrylating en 'n afname in CO vrylating getoon.

Tydens die projek is 'n vergelyking getref tussen die akkuraatheid van optiese vesel drukmeters en 'n piësoëlektriese drukmeter. Daar is bevind dat die akkuraatheid van die optiese vesel drukmeters soortgelyk is aan die piësoëlektriese drukmeter gedurende lae enjin lastoestande. By hoë las omstandighede was die optiese vesel drukmeters egter nie in staat om dieselfde akkuraatheid as die piësoëlektriese drukmeter te handhaaf nie.

This report is dedicated to God and to my family,

Yolande Kenny

Wilhelm Kenny

Andrew Kenny

L'lani Kenny

Thank you for all your support, love and patience during my studies.

Acknowledgements

The author wishes to thank the following persons:

- Mr RW Haines for his continuous support and motivation during the project.
- The staff at the Mechanical and Mechatronic Engineering workshop for their advice and high quality workmanship.
- Mr E Grobbelaar for his assistance during the project.

Table of Contents

List of Figures

Page

List of Tables

Page

Nomenclature

ABDC	After bottom dead centre
AC	Alternating current
ATDC	After top dead centre
AVSR	Anti-valve seat recession
BBDC	Before bottom dead centre
BDC	Bottom dead centre
BMEP	Break mean effective pressure
BSFC	Break specific fuel consumption
BTDC	Before top dead centre
CI	Compression ignition
CLD	Chemiluminescence detector
CV	Constant velocity
DAQ	Data acquisition
DC	Direct current
DISI	Direct injection spark ignition
ECU	Electronic control unit
EGR	Exhaust gas recirculation
ETBE	Ethyl tertiary-butyl ether
FID	Flame ionization detector
FFV	Fuel flexible vehicle
FMEP	Friction mean effective pressure
FVI	Flexible volatility index
HC	Hydrocarbon
IC	Internal combustion
IMEP	Indicated mean effective pressure
IVC	Inlet valve closing
MAP	Manifold absolute pressure
MMT	Methylcyclopentadienyl manganese tricarbonyl
MON	Motor octane number
MTBE	Methyl tertiary-butyl ether
PCV	Positive crankcase ventilation
PFI	Port fuel injection
PLC	Programmable logic controller

PMEP	Pumping mean effective pressure
PRT	Platinum resistance thermometer
RON	Research octane number
SCADA	Supervisory control and data acquisition
SI	Spark ignition
TAME	Tertiary amyl methyl ether
TDC	Top dead centre
TEL	Tetraethyl lead
TML	Tetramethyl lead
TWC	Three way catalytic converter
ULP	Unleaded petrol
VR	Variable reluctance
WWFC	Worldwide Fuel Charter

1. Introduction

In today's modern society the automobile is one of the main contributors to CO_2 emissions due to the fossil fuels it uses. This has led to the widespread interest in biofuels for use in spark ignition (SI) as well as compression ignition (CI) engines. Carbon in the plant matter used for producing biofuels originates from the CO_2 absorbed from the atmosphere. Burning of biofuels therefore forms a closed loop carbon cycle. In contrast, fossil fuels, when burnt, release carbon into the atmosphere which has been trapped under the ground for millions of years (Milnes et al., 2010).

However, for these biofuels to be considered as viable options for internal combustion (IC) engines they have to be tested in laboratories as well as in vehicles. Laboratory testing of biofuels, in CI engines, at Stellenbosch University has been possible since 2008 due to previous projects. A need was therefore identified to also develop a SI engine testing facility at the University to enhance fuel testing capabilities. For the project, a SI engine, which is capable of running on petrol as well as petrol-biofuel blends, was sponsored. This engine had to be coupled to a dynamometer and all the relevant sensing and control equipment installed.

In-cylinder pressure is extremely useful for analysing the combustion process in IC engines. Combustion duration and the thermodynamic effects of different engine conditions and fuels can be studied when in-cylinder pressure data is available. Due to this, an in-cylinder pressure measurement setup also had to be developed for the test facility.

The pressure transducers that are mostly used for in-cylinder pressure measurement are based on the piezoelectric effect. These transducers are however costly. For this reason, fibre optic transducers has recently been developed which are far more cost effective than their piezoelectric counterparts. However, the performance of fibre optic transducers in comparison to piezoelectric transducers has not been widely published. The project therefore also aimed to study the performance of fibre optic transducers during different engine operating conditions.

The objectives that were therefore identified for the project are as follows:

1. Develop a repeatable and accurate SI engine and dynamometer setup for fuel testing,
2. Develop a highly accurate and repeatable in-cylinder pressure measurement setup for combustion analysis,
3. Compare the performance of piezoelectric in-cylinder pressure transducers to fibre optic transducers, and
4. Test the completed setup for sensitivity to fuel changes.

2. Literature Review

In order to gain a good understanding of engine testing facilities, a literature review was undertaken. Of the literature that was studied, the most important aspects are summarized in this chapter. The literature review includes requirements for engine testing, workings of modern SI engines, properties of petrol and bioethanol as well as the requirements for in-cylinder pressure measurement.

2.1 Engine Testing

In this section the requirements of an engine and dynamometer test setup is discussed. These include the parameters to be measured and controlled, installation of the engine and dynamometer and the operating principle of certain engine dynamometers.

2.1.1 Overview

The development of an engine testing facility requires a wide range of engineering skills which include design, procurement, installation, fault finding and software programming. These skills however need to be integrated during the development and completion of the facility to ensure that the specifications set at the beginning of the project are satisfied. (Plint & Martyr, 1995)

An engine testing facility generally consists of the test cell infrastructure, a ladder frame test bed, a test engine, a dynamometer, sensors and actuators, control equipment as well as control software. Before the equipment is installed in the test cell, certain criteria have to be met to ensure user friendly and safe operation of the setup. Typical criteria to consider are overall floor size, engine layout (orientation), noise isolation, safety barriers during engine operation (doors, windows, walls, roof), lighting, location of the control room and fire extinguishing system. Furthermore, criteria also have to be met to ensure sufficient ventilation and water flow into and out of the test cell as well as electricity supply and exhaust extraction. (Plint & Martyr, 1995)

Although all of the above mentioned aspects have to be taken into account during the development of an engine testing facility, the most important aspect to consider is safety. Plint and Martyr (1995) recommends that hard wired emergency stops be installed in the control room as well as the test cell itself. Furthermore it is recommended that computerized alarm systems are installed which can shut down the engine in case of a high or low parameter reading. These readings include temperatures, pressures, speed, load and fire suppression systems.

2.1.2 Measured parameters

Typical parameters that have to be measured in an engine testing facility include torque, speed, air and fuel flow, temperature and pressure. Note, all parameters with the prefix *brake* refers to measurements made at the engine flywheel i.e. the net output of the engine. Standard SI units were used in the project.

a) Engine torque and speed

Engine torque is measured using a load cell which is installed on the dynamometer at a distance *R* from the centre of the dynamometer, as shown in Figure 1. More information on engine dynamometers will be given in section 2.1.6.

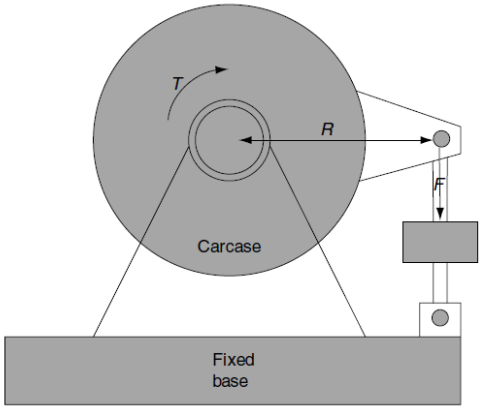

Figure 1: Dynamometer and load cell setup (Plint & Martyr, 1995)

Engine rotational speed, which is required for calculations and control purposes, is measured using a speed sensor attached to the rear of the dynamometer. The speed sensor mostly used is a variable reluctance (VR) speed sensor (also referred to as a passive magnetic speed sensor). It consists of a permanent magnet, pole piece and a coil as can be seen in Figure 2.

A toothed wheel rotates, in close proximity, past the tip of the sensor. The approach and passing of one of the teeth, changes the strength of the magnetic field. This in turn induces an AC voltage in the coil. The amplitude and frequency of the induced voltage is proportional to the speed of the toothed wheel and therefore the speed of the engine. (Honeywell sensing and control, 2012) (Presto, [S.a.])

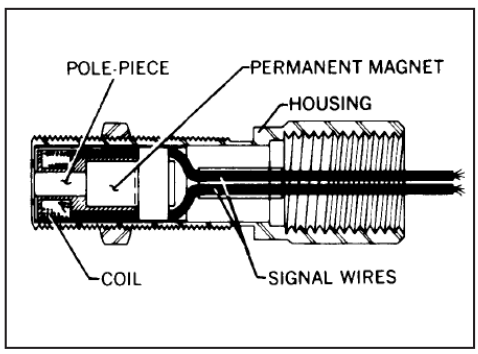

Figure 2: Speed sensor internal configuration (Presto, [S.a.])

b) Fuel and air flow

Measurement of fuel flow is a very important parameter for comparative fuel testing. It is used to determine the brake specific fuel consumption (BSFC), the thermal efficiency of the engine as well as to calculate the heat release rate of the fuel (see section 2.5.3). BSFC is a measure often used to compare different fuels seeing as it takes into account engine torque, speed and fuel consumption. The formula for BSFC is as follows:

$$BSFC = \frac{\dot{m}_f}{P_b} = \frac{1}{\eta_T Q_{hv}} \quad (1)$$

where P_b is the brake power developed by the engine, $\dot{m}_f$ is the fuel mass flow rate, η_T is the thermal efficiency of the engine, and Q_{hv} is the mass based energy content of the fuel (Ferguson & Kirkpatrick, 2001). An accurate measurement of fuel flow rate is therefore essential for accurate determination of BSFC.

Fuel flow is measured either cumulatively or instantaneously. With cumulative fuel flow meters, fuel is supplied to the engine from a measuring vessel. Fuel flow is then calculated (either on a volumetric or gravimetric basis) by measuring the time required for a certain volume or mass of fuel to be drained from the vessel (Lilly, 1984). Instantaneous flow meters (e.g. Coriolis effect flow meter) measures the flow rate in real time. The advantage this has over cumulative flow meters is that it can be used for transient testing (Ferguson & Kirkpatrick, 2001).

Seeing as IC engines use air as the working fluid, the inlet air flow rate is a commonly measured parameter. Equipment used to measure air flow include an orifice plate, venturi meters, viscous flow meters, turbine meters and hot wire or film anemometer devices. With viscous air flow meters, an element consisting of a large number of small passages (pipes) is used. These pipes produce a pressure drop across them proportional to the flow through them (Ferguson & Kirkpatrick, 2001).

c) Temperature and pressure

Temperature and pressure are two parameters which are very important for monitoring purposes. Sensors that can be used to measure temperature include thermocouples, platinum resistance thermometers (PRT) and thermistors, out of which thermocouples are mostly used for engine testing. Where high accuracy temperature measurement is required, PRTs are used. Thermistors can be installed in space limited positions due to their small size and simplicity. (Lilly, 1984)

Pressure measurement can be achieved by using either mechanical or electronic methods. The selected method depends on the application of the measured pressure value.

Electronic pressure measurement is usually done using a pressure transducer whereas with mechanical measurement, manometers and barometers are mostly used. (Figliola & Beasley, 2006)

2.1.3 Engine installation considerations

IC engines are a significant source of vibration. These vibrations are absorbed in a vehicle by rubber engine mountings designed for that specific engine. It is therefore recommended that these specific mountings are used for mounting the engine onto a test bed. Depending on the size of the engine, the vibrations it produces can induce vibration to the test cell structure. It is therefore common practice to mount the test bed onto a seismic block carried on flexible mountings, or to mount the test bed on isolation feet which reduces the vibration transmission to the floor. (Plint & Martyr, 1995)

Apart from the engine mountings it is also recommended to install the exhaust system from a vehicle in which the engine is used (Plint & Martyr, 1995). If the exhaust system has to be modified, the back pressure in the exhaust system may change which will affect the volumetric efficiency and therefore power output of the engine. These changes therefore have to be taken into account when modifications to the exhaust system are made.

2.1.4 Engine speed and load control

Test sequences using an engine coupled to a dynamometer consist of sets of predetermined torque and speed points. These points can be achieved by adjusting the dynamometer torque setting and the engine throttle position via a throttle actuator.

Two modes of dynamometer operation can be used with proper control systems, namely torque and speed. With torque mode, the dynamometer will maintain a fixed load on the engine for any throttle setting. If the engine throttle setting is therefore increased or decreased, the engine speed will also increase or decrease. In speed mode, the dynamometer maintains a constant speed setting for any throttle setting. A change in throttle setting would therefore cause a change in the applied torque. For partial load testing speed mode is preferred. (Plint & Martyr, 1995)

Engine testing can either be done on a steady-state or transient basis. With steady-state testing the performance of the engine during constant load and speed points can be analysed. This is representative of the conditions experienced by an engine in a vehicle when driving at a constant velocity (freeway driving). With transient testing, changes in engine load and speed conditions (e.g. acceleration, gear shifts and deceleration) can be simulated. For transient testing, dynamometers capable of absorbing and producing power are required. Furthermore, fast response (less than 50 ms) is required from the hardware after a change is applied by the control system. (Plint & Martyr, 1995)

2.1.5 Dynamometer installation considerations

In a testing facility the engine and dynamometer are generally coupled using a single drive shaft contained in a shaft guard. In a vehicle, the engine is coupled to the wheels through a gearbox, differential and side shafts, all of which have inherent damping and lower inertia than certain types of dynamometers. Typical inertia values for the wheels of passenger vehicles are in the region of 1,38 $kg \cdot m^2$ (Ubysz, 2010) while certain dynamometers (AC and DC dynamometers in particular) can have inertias in the region of 1,76 $kg \cdot m^2$ (Horiba, 2013).

Coupling a dynamometer to the engine using a single drive shaft therefore requires an analysis of the inertia, damping and stiffness requirements before specifying the drive shaft components. The stiffness of the assembled shaft must be such that its natural frequencies lie outside the range of speeds the test engine will be run. The use of the engine's clutch should also be considered seeing as it aids in vibration damping and serves as a torque limiter. (Plint & Martyr, 1995)

2.1.6 Dynamometer operating principal

A dynamometer (also called a brake) consists of two main components namely the rotor and the stator (which is the absorbing element). The stator is mounted on trunnion bearings coaxial with the machine shaft which allows the stator to rotate due to the braking torque developed. This torque is then restrained and measured using a load cell as shown Figure 1. Dynamometer types that are mostly used for engine testing are hydraulic (water brake) or electrical motor based (Ferguson & Kirkpatrick, 2001).

With hydraulic dynamometers an engine braking torque is developed by transfer of momentum from the rotating rotor to the stator (casing) using water. The braking torque developed can be varied by adjusting the amount of water in the casing. The motion between the rotor and the casing causes turbulent shear stresses in the water and therefore heat. This serves the purpose of absorbing the engine power and cooling the dynamometer. (Ferguson & Kirkpatrick, 2001)

Electrical motor based dynamometers transform the absorbed engine power into electrical energy. The electrical energy developed is then dissipated in the form of electricity or heat. The heat is dissipated using either a cooling medium or a forced air stream. Electrical dynamometers available include direct current (DC), alternating current (AC) and eddy current dynamometers. DC and AC dynamometers are capable of absorbing and producing power and can therefore be used for transient testing (Plint & Martyr, 1995). These dynamometers convert engine shaft power into electricity which can be supplied to the electricity grid which reduces operational costs. For this project, an eddy-current dynamometer was used of which a sectional view of a similar model is given in Figure 3.

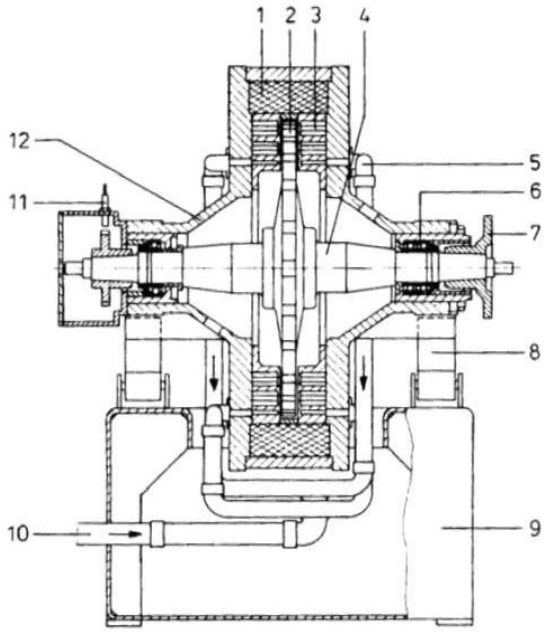

Figure 3: Schenck eddy current dynamometer cross section (Schenck Pegasus GmbH, 1997)

Descriptions for the numbers are as follows:

1. Excitation coil
2. Rotor
3. Cooling chamber (loss plate)
4. Rotor shaft
5. Water outlet
6. Rotor bearing
7. Coupling flange
8. Pendulum supports
9. Frame
10. Water inlet
11. Speed sensor
12. Casing

The toothed rotor is made from high-permeable steel and it rotates between the steel loss plates. Braking of a prime mover is achieved by using the principle of electromagnetic induction. The coil in the dynamometer generates a magnetic field parallel to the axis of the machine. Rotation of the rotor in this magnetic field generates eddy currents at the inner surfaces of the loss plates. These eddy currents then generate an additional magnetic field and it is the interaction between the two magnetic fields which causes the braking torque (Schenck Pegasus GmbH, 1997). The torque can be varied by changing the supply current to the coils.

The braking torque developed, and therefore power absorbed, causes an increase in temperature of the loss plates. These plates are cooled by circulating water

through passages located within them. Additional cooling is achieved by air flow in the gaps between the rotor and the loss plates.

2.2 Spark Ignition Engines

The first four stroke SI engine was built by Nicolaus Otto in 1876. Thereafter, Karl Benz and Gottlieb Daimler developed a light, high speed engine from which most modern SI engines descended. In this section, the workings of modern SI engines as well as their combustion characteristics will be discussed.

2.2.1 Overview

In this section, certain parts of a SI engine that were applicable to the project will be discussed. For basic engine operating principals, the reader is referred to *Internal Combustion Engine Fundamentals* by JB Heywood or to *Internal Combustion Engine Handbook* by R Basshuysen and F Schäfer.

a) Air-fuel mixture formation

For the majority of SI engines the fuel is mixed with ambient air outside the combustion chamber. In more sophisticated engines, mixing takes place in the cylinder during the compression stroke. Older engines used carburettors to inject the fuel while modern engines use electronic fuel injection where fuel is injected using an injector. With port fuel injection (PFI) SI engines this injector is located in the manifold while with direct injection SI engines (DISI) the injector is located in the combustion chamber. PFI results in a homogenous mixture of fuel and air being supplied to the combustion chamber whereas DISI results in either homogenous or stratified mixtures, depending on the moment of injection (Van Basshuysen & Schäfer, 2004).

Before ignition of the mixture can occur, the fuel droplets have to vaporise. Vaporisation (and mixing) takes place during the intake and compression stroke where the latter is responsible for the largest part of the evaporation. The fuel can only burn completely when the relative air-fuel ratio (called lambda) of the mixture is greater than or equal to 1 (Van Basshuysen & Schäfer, 2004). Lambda is the ratio of the actual air-fuel ratio of the mixture entering the engine to the stoichiometric required ratio. It is used as an indication of the amount of oxygen present in the mixture. The lambda values for stoichiometric, lean and rich air-fuel mixtures are 1, greater than 1 and less than 1 respectively.

DISI was developed due to a demand for less CO_2 emissions and therefore reduced specific fuel consumption. As the name implies, fuel is injected directly into the combustion chamber either early during the intake stroke or late during the compression stroke. The latter, known as stratified DISI, is used mostly during part load whereas the former, known as homogeneous DISI, is mostly used during full load. Stratified operation results in an excess air factor greater than 1 (lean-burn phase), while stoichiometric homogeneous injection results in an excess air

factor equal to 1. Although stratified operation creates an overall lean mixture, the local air-fuel ratio at the spark plug should be close to the stoichiometric ratio to ensure reliable ignition. This is achieved by concentrating the injected fuel around the spark plug using either jet directed, wall-directed or air-directed processes which depends on the intake system, piston crown and combustion chamber design. (Van Basshuysen & Schäfer, 2004)

b) Electronic control unit and sensors

For the project, the engine utilizes a PFI system. Figure 4 shows the sensors as well as the electronic control unit (ECU) that can be found on a modern PFI engine. The ECU uses the readings from the various sensors to control the air-fuel ratio as well as the ignition timing.

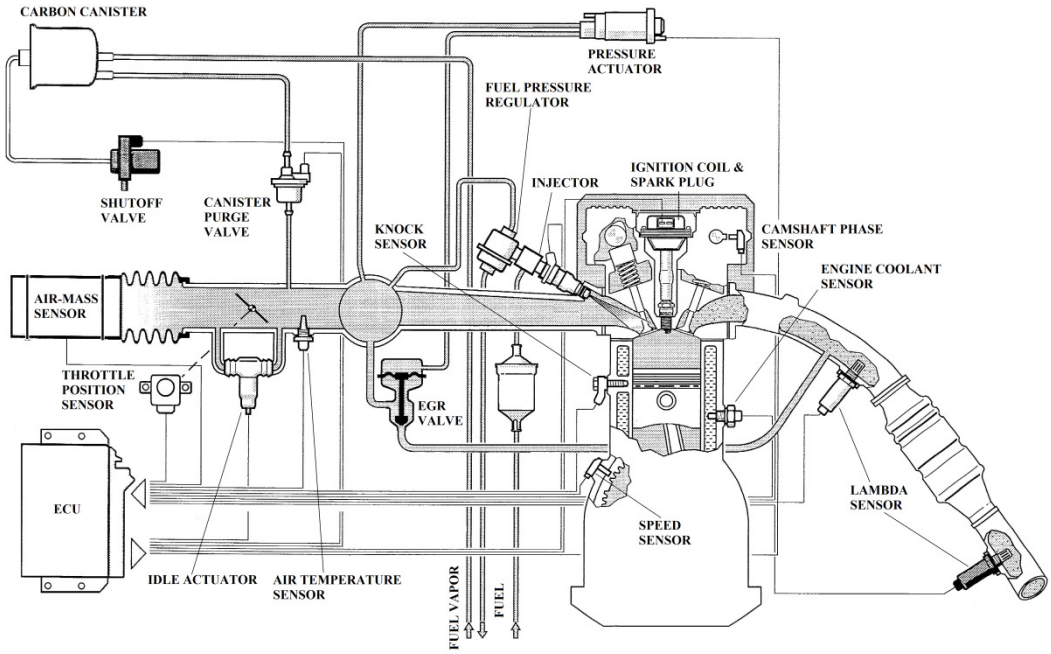

Figure 4: PFI engine management system (Bosch, 1995)

Engine load is monitored using either an intake air mass sensor or a manifold absolute pressure (MAP) sensor, coupled to an intake air temperature sensor. These sensors are located in the air intake system of the engine. (Bosch, 1995)

During engine starting and warm-up, a rich mixture has to be supplied to the cylinders to enable sufficient fuel vaporisation. The ECU uses the coolant temperature sensor to determine engine starting and warm-up conditions. It also uses this sensor to determine when the engine is overheating. Extra fuel also has to be supplied to each cylinder during acceleration which is detected by monitoring the rate of change of the throttle blade angle. For this purpose, the ECU uses a throttle position sensor which consists of a potentiometer connected to the throttle shaft (Ferguson & Kirkpatrick, 2001).

The throttle position sensor and valve is located in the throttle body (shown in Figure 5) which is bolted to the inlet of the intake manifold.

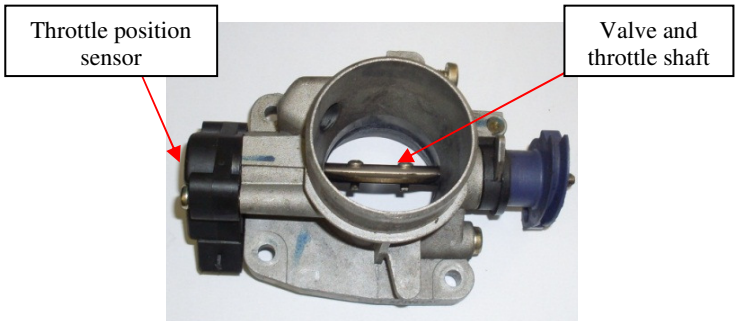

Figure 5: Throttle body

A lambda sensor enables the ECU to determine the amount of oxygen in the exhaust and therefore whether the engine is running rich, lean or stoichiometric. Two types of lambda sensors are available namely binary and linear, both of which consist of a zirconium dioxide (ZrO_2) electrolyte. This electrolyte is coated on its interior and exterior surfaces with porous platinum which creates the electrodes of the sensor. One of the electrodes is exposed to the exhaust gases while the other is exposed to ambient air. A voltage, dependant on the oxygen ion flow rate, is then produced across the electrolyte which is fed back to the ECU. (Ferguson & Kirkpatrick, 2001)

For exact control of the moment of ignition as well start of injection, the ECU has to be able to identify the angular position of the crankshaft as well as the camshaft with reference to top dead centre (TDC). For this purpose, engines are fitted with a crankshaft and camshaft position sensor. The crankshaft position sensor provides information on the position of the pistons while the camshaft position sensor provides information on the current cycle of one of the cylinders. The crankshaft sensor is also used to measure engine speed. (Bosch, 1995)

The ignition timing for optimum engine efficiency and for unwanted combustion (knock) is very close together and engines are therefore fitted with knock sensors. When knocking occurs, the engine generates characteristic vibration patterns which can be measured and fed back to the ECU by the sensor (Bosch, 1995).

The ECU has two control modes namely open and closed loop control. Closed loop control is used when the engine is running at steady-state conditions and in this mode the ECU receives input from the lambda sensor in the exhaust. Under transient conditions however, the lambda sensor response is too slow and therefore the ECU uses open loop control. In this mode the ECU adjusts the fuelling according to a data table known as the ECU *map* which is stored in its memory.

The *map* consists of a number of engine load and rpm combinations and the corresponding fuelling and timing requirements which is compiled by the engine manufacturer. (Chevron, 2009)

2.2.2 Combustion in spark ignition engines

The combustion process in a SI engine is initiated by a spark produced at the electrodes of the spark plug. The spark is triggered by the ECU and causes an exothermic chemical reaction in close proximity to its electrodes. This reaction then expands through the combustion chamber by means of a self-sustaining flame front. In order for the spark to develop between the spark plug electrodes, a high-voltage (in the region of 25 kV) is supplied by the ignition coil. The ignition coil and spark plug combination is referred to as the ignition system. (Van Basshuysen & Schäfer, 2004)

The mixture that is present in the vicinity of the spark plug must have an air-fuel ratio between 0.8 and 1.2 to ensure reliable combustion. Furthermore, the mixture must be heated by the spark to a temperature in the range of 3000 to 6000 K. (Van Basshuysen & Schäfer, 2004)

Propagation of the flame front can be best explained using Figure 6. The figure shows curves for in-cylinder pressure and mass fraction of fuel burnt which is the ratio of mass fuel burnt to mass fuel injected. After the flame development period, which is the time elapsed from spark discharge to a mass fraction fuel burnt of 10 %, the bulk of the fuel is burnt during the rapid-burning period (section between 10 and 90 % mass fraction burnt). The slope of mass fraction burnt curve is known as the burn rate of the fuel which can be used as an analysis tool of the combustion process. For different fuels and engine load and speed points, the burn rate will vary. (Heywood, 1988)

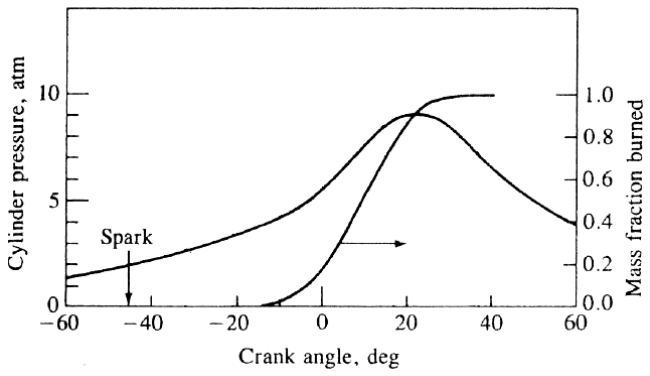

Figure 6: Cylinder pressure and mass fraction burnt curves (Heywood, 1988)

With SI engines, fluctuations in the in-cylinder pressure readings during constant load and speed, is a typical phenomenon. It is caused by cycle-to-cycle variations in the mixture motion at the time of spark as well as variations in the mixture composition (Heywood, 1988).

In Figure 7, a typical in-cylinder pressure versus crank angle curve for different cycles of a PFI engine is shown, in which the fluctuations in pressure can clearly be seen.

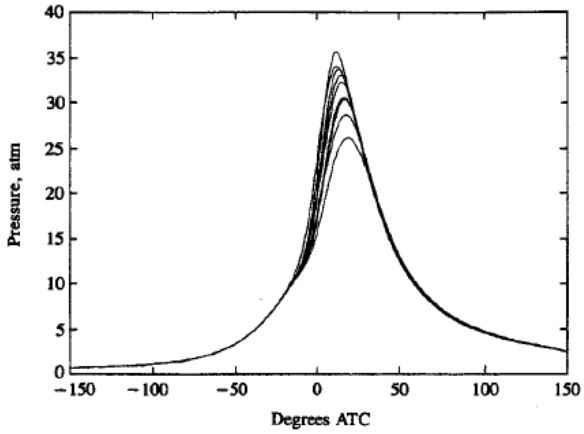

Figure 7: Combustion pressure fluctuations (Heywood, 1988)

Normal combustion in a SI engine results in a smooth pressure rise as can be seen in Figure 7. When engine knock occurs, sharp fluctuations in the cylinder pressure are present, as shown in Figure 8, and the following engine characteristics can be perceived: (Chevron, 2009)

- "Pinging" noise
- Loss of power
- Overheating of engine parts
- Engine damage

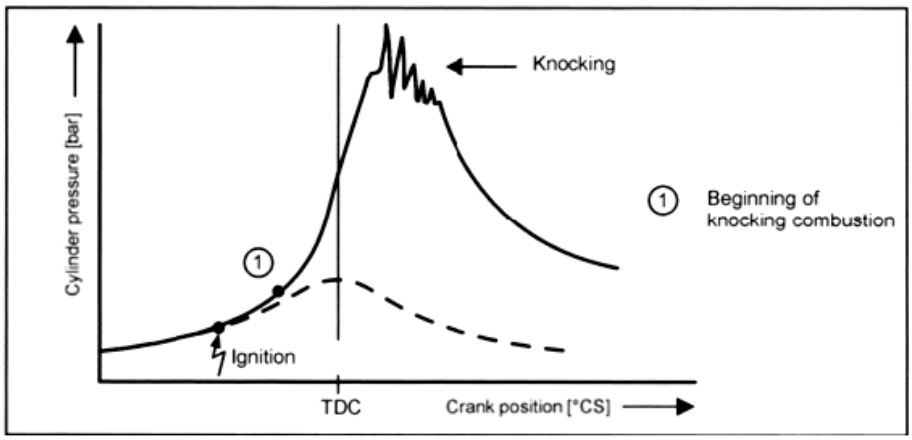

Figure 8: Knock pressure curve (Van Basshuysen & Schäfer, 2004)

To counter knock, the engine's ECU will retard the ignition timing or enrich the air-fuel mixture until normal combustion has been restored (Ferguson & Kirkpatrick, 2001) (The fuel expert, 2010). The cause of engine knock is given in section 2.3.1.

2.2.3 Emissions from spark ignition engines

The main components of an SI engine's exhaust gases are carbon dioxide (CO_2), carbon monoxide (CO), unburnt and partially burnt hydrocarbons (HC) as well as nitrogen oxides (NO_x). Nitrogen oxide emissions include NO, NO_2, N_2O, N_2O_3, N_2O_3, N_2O_4 and N_2O_5 of which NO and NO_2 form the largest part. Formation of NO is influenced by temperature, oxygen concentration, dwell time and pressure, with maximum formation occurring at temperatures between 2200 K and 2400 K. DISI engines produce less NO_x than PFI engines due to lower average combustion temperatures. (Van Basshuysen & Schäfer, 2004)

CO_2 is produced due to complete combustion of the HCs in the fuel and the concentration produced depends on fuel consumption and composition. CO is produced due to incomplete combustion and it depends on the air-fuel ratio and therefore the amount of oxygen present in the mixture (Van Basshuysen & Schäfer, 2004). During normal combustion, a small percentage of fuel is not burnt which causes HC emissions. Reasons for incomplete combustion include trapped fuel in the crevices and oil layers, carbon deposits, liquid fuel (and not fuel vapour) present in the mixture as well as exhaust valve leakage. (Ferguson & Kirkpatrick, 2001)

CO_2 and CO can be measured using a non-dispersive infrared analyser (NDIR) which is based on the infrared absorption spectrum of gases. The other two pollutants, HC and NO_x, can be measured using a flame ionization detector (FID) and a chemiluminescence detector (CLD) respectively. The FID burns the HC present in the exhaust gas sample with a hydrogen-air flame. This process produces electrons and positive ions which are proportional to the number of carbon atoms present in the sample. During measurements using a CLD, photons are emitted due to a chemical reaction between the exhaust sample and ozone (O_3). The amount of photons emitted is proportional to the amount of measured pollutant present in the sample. (Ferguson & Kirkpatrick, 2001)

SI engine exhaust gas emission can be reduced using positive crankcase ventilation (PCV), exhaust gas recirculation (EGR) or a three way catalytic converter (TWC). With PCV, the gases that leaks by the piston rings (called blow by) are vented back into the intake air system which reduces HC emissions. EGR reroutes exhaust gas into the intake air system which reduces NO_x emissions (Chevron, 2009). Three way catalytic converters are however able to reduce HC, CO and NO_x emissions and are therefore favoured for reduction of emissions (Bosch, 1995). For SI engines operating at the stoichiometric point (lambda equal to 1) TWC's are needed to meet current emissions legislation limits (Van Basshuysen & Schäfer, 2004).

2.3 Spark Ignition Engine Fuels: Petrol

Petrol has been produced from crude oil since 1859. However, usage of it as a SI engine fuel only gained interest with the invention of the automobile in 1892. The early SI engines that were produced could run on any liquid that was highly flammable. However, it was the increased demand for better engines that resulted in petrol becoming the fuel of interest. This has also been the cause for the interdependence of fuel and engine development (Chevron, 2009). Engines are designed considering the available fuels and the fuels are produced considering the requirements of the engine in which it will be used.

2.3.1 Petrol production and properties

Petrol production starts off with fractional distillation of crude oil. Distillation separates the different HCs in the crude oil into naphtha (or straight-run petrol), kerosene, diesel and atmospheric bottoms. The products from distillation are then either used directly or processed further. Further processing that is commonly done is cracking, reforming and alkylation.

Cracking is the process of breaking hydrocarbons with higher boiling points into hydrocarbons with lower boiling points. Reforming converts hydrocarbons of one class into another (e.g. paraffins into aromatics) while alkylation is used to combine gaseous hydrocarbons to form liquid hydrocarbons. (Chevron, 2009)

For crude oil derived fuels there are currently numerous standards which must be met. These standards ensure that the fuel properties are compatible with the current vehicle fleet as well emissions requirements (SAPIA, 2008). The properties include octane number, volatility, residue and existent gum, copper strip corrosion, sulphur content, total aromatics, oxygenates, oxidation stability induction period and density.

a) Octane number

The octane number of a fuel is an indication of the fuels resistance to auto-ignition. Three types of auto-ignition are found in SI engines namely knock, pre-ignition and post-ignition. These phenomena can cause severe engine damage due to the uncontrolled combustion taking place.

Knock occurs when the unburnt mixture ahead of the flame front is compressed to a high enough pressure, and therefore temperature, that it automatically ignites. Knocking is an uncontrolled process and can occur during high load conditions (e.g. hard acceleration and hill climbing). Pre- and post-ignition is typically initiated by a hot spot in the combustion chamber. Pre-ignition occurs before spark delivery whereas post-ignition occurs after spark delivery. (Chevron, 2009)

The octane number of a fuel is determined by comparing the antiknock quality of a fuel sample to that of blends of iso-octane and n-heptane. Iso-octane has an octane number of 100 while n-heptane has an octane number of 0 (SAPIA, 2008).

An octane number of 95 therefore indicates that the fuel under consideration has the same anti-knock quality as a mixture of 95 % iso-octane and 5 % n-heptane.

Two laboratory test methods exist for measuring octane number. The one test gives the research octane number (RON) while the other gives the motor octane number (MON). The former is representative of a fuel's anti-knock quality at low speed, mild-knocking conditions whereas the latter is more representative of higher speed, higher temperature knocking conditions. To determine these two values a single cylinder, variable-compression, knock-test engine is used. The engine is operated under various conditions (speed, spark advance and mixture temperature) and compression ratios to determine at which setting a knock of standardized intensity is produced. The engine is then run under the same conditions with blends of iso-octane and n-heptane until the same knock characteristic is achieved. The sensitivity of a fuel can be determined by subtracting MON from RON. Sensitivity indicates the effect of changes in operating conditions on a fuel's performance. (Chevron, 2009)

The octane number of a fuel is of great significance for SI engines. Each engine has a fixed compression ratio, which is the ratio of maximum to minimum cylinder volume. This has a major effect on the pressures that will be reached in the cylinder and therefore the chance of knock occurring (SAPIA, 2008). The compression ratio of an engine therefore has to be finalised according to the octane number of available fuels.

b) Volatility

Volatility is the tendency of a fuel to vaporise. This is very important in IC engines because it is the vapour above the atomized liquid fuel and not the liquid itself that burns. Therefore, if the fuel is not volatile enough (or too volatile) at a specific time, satisfactory combustion will not take place.

The volatility of a fuel must be such that it enables easy cold starting but, does not cause vapour lock when the engine is hot. Furthermore, a fuel that is too volatile, will cause excessive evaporation from the fuel tank which causes unwanted environmental emissions and poses health threats. (SAPIA, 2008)

There are a number of aspects that define a fuel's volatility namely: (SAPIA, 2008)

- Distillation profile,
- Vapour pressure,
- Flexible volatility index (FVI), and
- Drivability index.

The distillation profile of petrol is a set of volumes, evaporated at specific temperatures which include 70 °C, 100 °C, 150 °C and 180 °C. In Figure 9 a

typical distillation profile of petrol is shown. T50 and T90 denote the temperatures at which 50 % and 90 % by volume have evaporated.

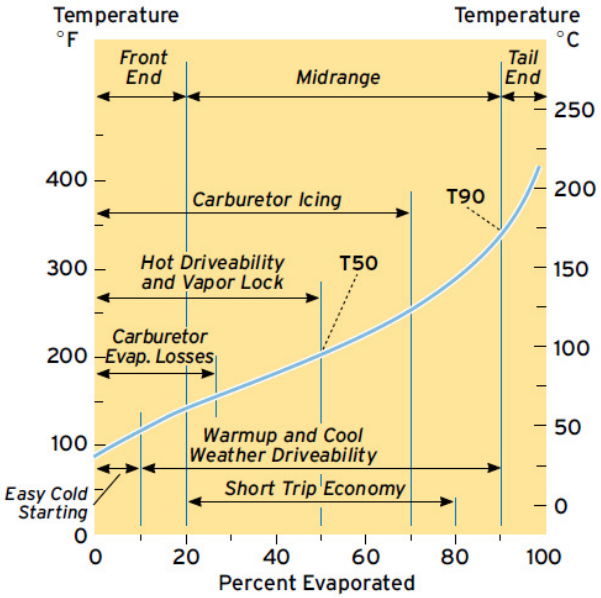

Figure 9: Petrol distillation profile (Chevron, 2009)

Vapour pressure relates to the lighter components in the fuel. It is extremely important as it affects cold-start and warm-up driveability. Higher vapour pressures result in better cold-start performance whereas low vapour pressures aid in preventing vapour lock from occurring (Chevron, 2009). Measurement of the vapour pressure is however very complicated and therefore a simplified parameter is used which is referenced to a standard temperature of 37,8 °C. This parameter is called the Reid vapour pressure (SAPIA, 2008).

The FVI is an indicator of the tendency of a fuel to cause vapour lock (hot running performance). A low FVI value is typical of fuels with high resistance to vapour lock. In contrast to the FVI the driveability index is a measure of a fuel's performance during cold start and warm-up.

Volatility is also affected by ambient conditions and therefore fuel specifications regarding volatility must not only take engine design into account, but also the conditions in which it will operate.

c) Total aromatics

Aromatics are HCs with a molecular structure based on benzene rings which occur naturally in crude oil. Other common aromatics found in petrol are toluene and xylene. The name *aromatic* comes from the early days of the discovery of these compounds when they were grouped due to their fragrant odours.

Increased levels of aromatics in petrol will increase the octane rating of the fuel due to high octane rating of aromatics (SAPIA, 2008). However, aromatic emissions are toxic. Benzene specifically is carcinogenic and can also damage certain elastomers used in seals and gaskets.

2.3.2 Petrol additives

In order to change the characteristics of petrol, additives are used. These additives include octane enhancing additives, oxidation inhibitors, corrosion inhibitors, oxygenates, metal deactivators (captures metal ions which can cause oxidation), demulsifiers (separates petrol and water), deposit control additives, dyes (used to distinguish between different fuels) and anti-valve seat recession (AVSR) additives (Chevron, 2009). In this section, the most significant additives will be discussed.

a) Octane enhancers

Currently there exist many substances that can be used as octane enhancers. These include lead products, manganese compounds and oxygenates. The lead products that are typically used are tetraethyl lead (TEL) and tetramethyl lead (TML) (Chevron, 2009). Lead however reduces the efficiency of catalytic converters and has negative effects on human health (SAPIA, 2008) and has therefore been phased out worldwide.

The manganese compound that can be used as an octane enhancer is methylcyclopentadienyl manganese tricarbonyl (MMT). MMT however has been found to cause neurological damage in humans for moderate or high levels of exposure. MMT also causes damage to catalytic converters and spark plugs. Due to these negative effects, MMT is being phased out as an octane enhancer. (Sierra Research, 2008)

b) Oxygenates

Oxygenates are added to petrol mainly to reduce CO and HC emissions. Added advantages of oxygenates are an increase in octane rating and reduced particulate matter emissions. The reason for the reduced emission is the increased oxygen content given by oxygenates which decreases the chance of incomplete combustion occurring. (SAPIA, 2008)

There are two main groups of oxygenates namely alcohols and ethers. The alcohols include ethanol, methanol, isopropyl alcohol and tertiary-butyl alcohol. Of these, ethanol will be discussed in more detail as it was the only alcohol tested in the project. The ethers include methyl tertiary-butyl ether (MTBE), ethyl tertiary-butyl ether (ETBE) and tertiary amyl methyl ether (TAME). Out of these oxygenates, ethanol and MTBE are used most frequently. Ethanol is however preferred due to concerns over health effects and water contamination when using MTBE. (California Environmental Protection Agency, 1998)

Oxygenates can however cause driveability issues, depending on the engine management system, due to over-leaning. Petrol-oxygenate blends can also increase the vapour pressure of the fuel which results in an increase in evaporative emissions. This effect is most significant with methanol which can cause a 35 % increase in vapour pressure even at low concentrations. (SAPIA, 2008)

c) Deposit control additives

Deposits can form on any surface that comes into contact with the fuel. This includes the fuel system, combustion chamber, valves, cylinders, etc. Deposits can cause decreased engine performance, increased exhaust emissions, increased fuel consumption and deposit interference between the piston and the cylinder (Additive Technical Committee, [S.a.]). In Figure 10 the deposit formation on the cylinder head as well as on top of the piston of a *BMW* engine is shown.

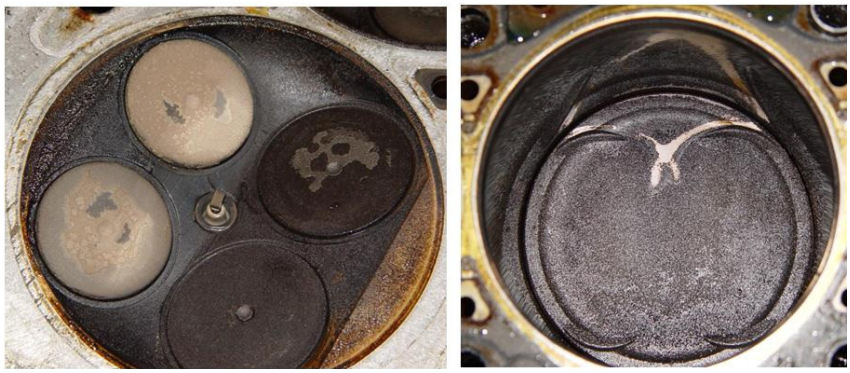

Figure 10: Engine combustion chamber deposits (M5 Board, [S.a.])

The additives that are currently available for deposit control are able to clean, and keep clean, the areas where deposits are commonly found. Chemical compounds that are used for controlling deposit formation include amides, amines, amine carboxylates, polyether amines and polyolefin amines. These compounds are used with carrier fluids which include polyalphaolefins, polyethers, mineral oils and esters. (Additive Technical Committee, [S.a.])

d) AVSR additives

Due to the high speed and continuous movement of valves in an engine cylinder head, recession of the valve seats as well as valve wear can occur. In older vehicles, additives are needed to prevent this from happening. In modern vehicles, this is less prone to happen due to the use of more suitable valve and seat materials. The additives that can be used are MMT, phosphorus, potassium or sodium based. Phosphorus can however degrade the performance of catalytic converters. (NICNAS, 2004)

2.4 Spark Ignition Engine Fuels: Bioethanol

Ethanol is a very popular biofuel and is produced either synthetically or through fermentation (bioethanol). Synthetic ethanol is produced from crude oil whereas bioethanol is produced from biodegradable feedstock. Synthetic ethanol is however mainly used for industrial purposes (Tamers, [S.a.]).

2.4.1 Bioethanol production

Two types of sources are normally used to produce bioethanol namely first and second generation. First generation sources include starch based crops (e.g. wheat and corn) or sugar cane while second generation sources include lignocellulosic material (woody biomass or waste residues from forestry). The various feedstocks used for bioethanol production are shown in Figure 11.

The materials used are firstly broken down into sugars where after alcohol (ethanol) is produced through fermentation. The processes used with the different feedstocks are very similar except that hydrolysis is not used with sugar cane. Furthermore, the lignocellulosic material requires a more complicated hydrolysis process than starch feedstocks. (EUBIA, [S.a.])

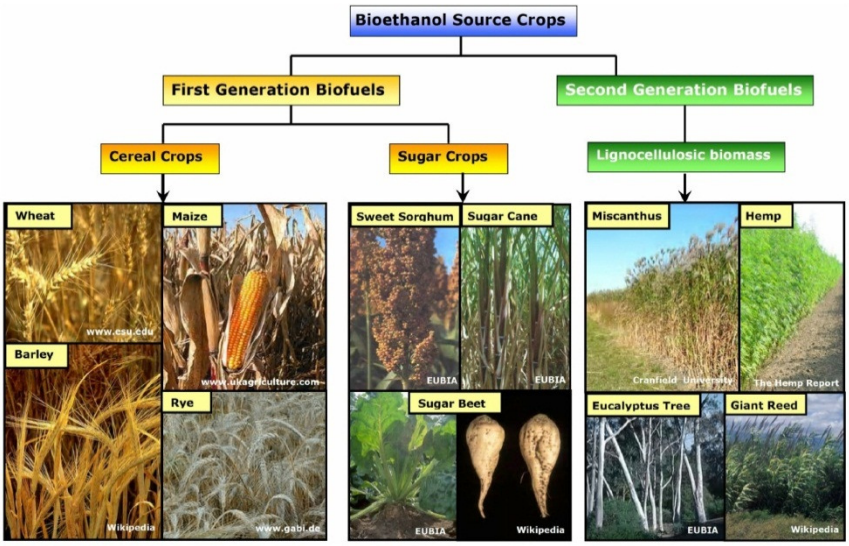

Figure 11: Bioethanol feedstocks (EUBIA, [S.a.])

2.4.2 Bioethanol properties

Bioethanol can be used without mixing with petrol. However, a mixture of 100 % bioethanol and 0 % petrol (known as E100) cannot be used in standard vehicles. This is due to the corrosive nature of ethanol. In order to use petrol-ethanol blends with high ethanol content, changes to certain engine components have to be made. These include certain plastic, rubber and metal components which can be damaged by ethanol. Vehicles that can run on low or high content ethanol blends are called fuel flexible vehicles or FFVs (Milnes et al., 2010).

The following list contains certain properties of ethanol: (SAPIA, 2008)

- High octane rating.
- Increases fuel volatility when added to petrol.
- 34,7 % more oxygen content by weight than petrol.
- Ethanol burns with limited visibility (fire hazard).
- Ethanol is infinitely soluble in water (causes corrosion problems).
- Ethanol is highly intoxicating when consumed.

The Worldwide Fuel Charter (WWFC) has set out specific guidelines for the properties of ethanol. These properties are however specifically for anhydrous ethanol for use in up to E10 blends. The properties specified are purity, water content, density, electrical conductivity, phosphorus content, sulphur content, heavy metal content, non-volatile material content (can cause deposits), pH value (as close to neutral as possible), and appearance (must be clear and bright) (Koc et al., 2009). Heavy metals, phosphorus and sulphur content are regulated due to poisoning of catalytic converters (WWFC, 2009).

The purity of ethanol is affected by the amount of saturated alcohols (C3-C5), methanol and water present in the sample. For petrol-ethanol blends of up to 10 % ethanol, a minimum of 99,5 % is specified for the purity of ethanol. Density is another measure of the purity of ethanol. The density of a sample of ethanol should be very close to that of pure ethanol. (WWFC, 2009)

2.4.3 Effects of bioethanol on emissions and engine performance

Ethanol reduces the emissions of CO and HCs while CO_2 emissions increase when it is mixed with petrol. The reduced CO and HC emissions are a result of the increased oxygen available for combustion (Koc et al., 2009). However, combustion of ethanol produces toxic acetaldehyde and the eye irritant peroxyacetyl. The scale of these emissions can however be controlled through emissions control technologies (SAPIA, 2008).

The advantage on a carburettor engine's performance, when adding ethanol to petrol, is increased brake torque and power as well better thermal and volumetric efficiency (Al-Hasan, 2003). The increased brake torque and power is again due to the improved combustion while the improved volumetric efficiency is due to higher latent heat of vaporisation. Furthermore, when blended with petrol, ethanol increases the octane rating of the fuel which allows the use of higher compression ratios (Topgül et al., 2006). However, due to ethanol having a lower calorific value the fuel consumption increases when ethanol is used in SI engines (Al-Hasan, 2003).

Due to the increase in oxygen content when ethanol is blended with petrol the stoichiometric air-fuel ratio changes. For E10 the stoichiometric ratio changes from 14,7:1 to 14,1:1 (Ricardo Inc., 2010). Modern engine control systems using closed loop control are able to change the air-fuel ratio and are therefore able to

adjust to the addition of ethanol. With carburetted engines the air-fuel ratio is fixed and the addition of ethanol can damage these engines due to overheating (Australian Historical Motoring Federation, 2010).

2.5 In-cylinder Pressure Measurement

In-cylinder pressure measurement is done on a crankshaft angle (also referred to as crank angle) basis (AVL, 2002). The advantage that crank angle based measurement has, is that the different phases of the engine cycle can be studied in detail (Heywood, 1988). Others pressures that are commonly measured on a crank angle basis include intake and exhaust system pressure (AVL, 2002). In-cylinder pressure is a very important parameter in engine testing as it can be used to calculate important combustion related parameters in conjunction with cylinder volume.

2.5.1 Pressure measurement

In order to measure the in-cylinder pressure during the different engine cycles, a pressure transducer is used. These transducers are installed either directly into the cylinder head or through modification of the spark plug (in SI engines) or glow plug (in CI engines). Technologies that are used for these transducers are piezoelectric crystals and fibre optics.

a) Piezoelectric transducers

Piezoelectric transducers are the most popular for use in IC engines with *Kistler* and *AVL* being the foremost manufacturers. The construction of a water cooled *AVL* and *Kistler* pressure transducer is shown in Figure 12, with the main difference being the design of the measuring element. With the *AVL* the measuring element produces a charge on the face where the force (caused by deformation of the diaphragm due to the applied pressure) is applied, whereas with the *Kistler*, the charge is produced on the face perpendicular to the force (AVL, 2002). The former is known as the longitudinal effect while the latter is known as the transversal effect. The charge that is developed is converted to a voltage output using a charge amplifier.

The crystal materials used are quartz (SiO_2) and Gallium Orthophosphate ($GaPO_4$). The piezoelectric properties of quartz are highly influenced by temperature, whereas the properties of Gallium Orthophosphate are not. Temperatures in the combustion chamber can, at the measuring positions, reach temperatures in excess of 400 °C and therefore cooling is needed when using a quartz transducer (AVL, 2002). This makes the transducer relatively large and therefore installation into the engine difficult due to space requirements and constraints. $GaPO_4$ does not require cooling due its insensitivity to temperature which in turn allows for a smaller pressure transducer, making it easier to install into an IC engine.

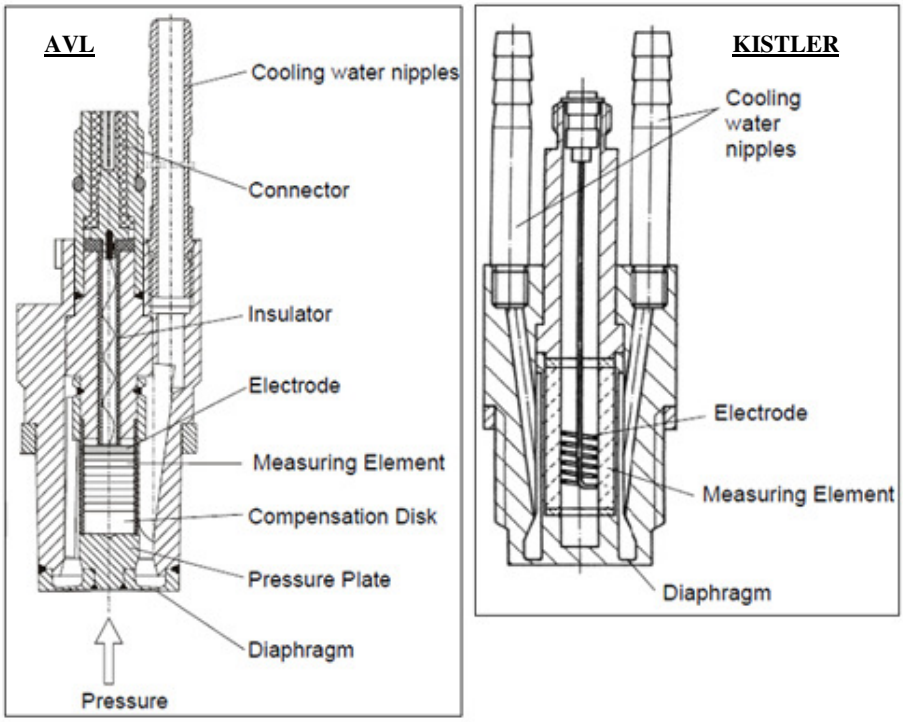

Figure 12: AVL and Kistler transducer cross sections (AVL, 2002)

b) Fibre optic transducers

Due to the high cost involved with piezoelectric pressure transducers, a company called *Optrand Inc.* has developed, specifically for automotive applications, a more cost effective transducer which uses fibre optics. The sensor consists of three main components namely the sensing head with a metal diaphragm, a cable containing two multimode optical fibres and a signal conditioner which contains all the optical and electronic components. In Figure 13, a schematic of the sensor is given. The diaphragm is welded to the metal housing which contains a fibre holding ferrule to which the optical fibres are bonded. (Wlodarczyk et al., [S.a.])

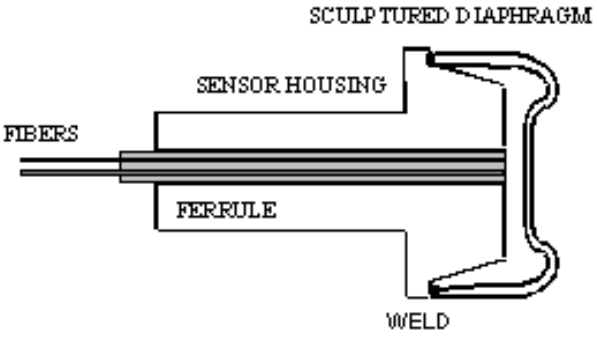

Figure 13: Optrand sensor cross section (Wlodarczyk et al., [S.a.])

Light is supplied through one of the fibres to the sensor head by an LED in the signal conditioner. This light is then reflected off the metal diaphragm (experiencing deflection due to the applied pressure) and then sent back through the other fibre. At the signal conditioner, a photodiode measures the returning light where after the electronics convert the difference in light intensities between the light signals into a voltage. (Wlodarczyk et al., [S.a.])

c) Pressure transducer installation in cylinder head

Installation of the transducer directly into the cylinder head allows the researcher to select the most suitable position in the combustion chamber. However, due to limited space in modern engine cylinder heads, a trade-off has to be made between the most suitable position and the space constraints.

The transducer position in the combustion chamber determines the pressures that will be measured. This is due to the fact that the pressure is not uniform throughout the entire combustion chamber. Installation in the squish gap (gap between the cylinder head roof and the top land of the piston) will cause rapid acceleration and oscillations of the combustion gases (AVL, 2002). This in turn causes substantial differences in pressures measured above the piston bowl and the squish gap.

Installation of the transducer above the piston bowl will cause much higher heat flow loads (heat flux), which results in higher cyclic temperature drift. This is also true when installing the transducer in the vicinity of the exhaust valves (AVL, 2002). If the transducer's thermal sensitivity is high, high cyclic temperature drift will cause large errors in the measured pressure value.

Once the measuring position has been chosen, the design of the installation method has to be executed. One design that can be used is machining a bore through the cylinder head into the combustion chamber.

This bore is then threaded to allow installation of the transducer. This design however requires an installation position which meets the following criteria:

- Sufficient wall thicknesses for machining and tapping the bore
- The bore must not penetrate any oil or water galleries

The other design that can be used is installing a threaded sleeve into the threaded bore in the cylinder head. This sleeve is also threaded internally to allow installation of the transducer. The advantage of this design is it allows for penetration of oil and water galleries and therefore presents more installation options. However, a sealing method is required with the installation of the sleeve to ensure that the oil and water galleries are sealed off from each other and that the water gallery is sealed off from the combustion chamber.

There are various errors that can occur during pressure measuring due to the selected measuring position. The most significant of these errors are due to pipe oscillations, dead volumes, interference to gas flow in the combustion chamber, fuel deposits and temperature differences. Pipe oscillations can occur when the transducer is installed recessed and not flush with the combustion chamber roof. This recess creates an indicating channel which acts as an acoustic resonator. It is therefore recommended to design the installation position such that the measuring face of the pressure transducer is flush with the combustion chamber roof. (AVL, 2002)

d) Pressure transducer installation in spark plug

An alternative to machining the cylinder head of an SI engine is modification of the engine's spark plugs to allow pressure measurement through an indicating channel. The pressure transducer is then installed in this indicating channel. In Figure 14 an example of this is given.

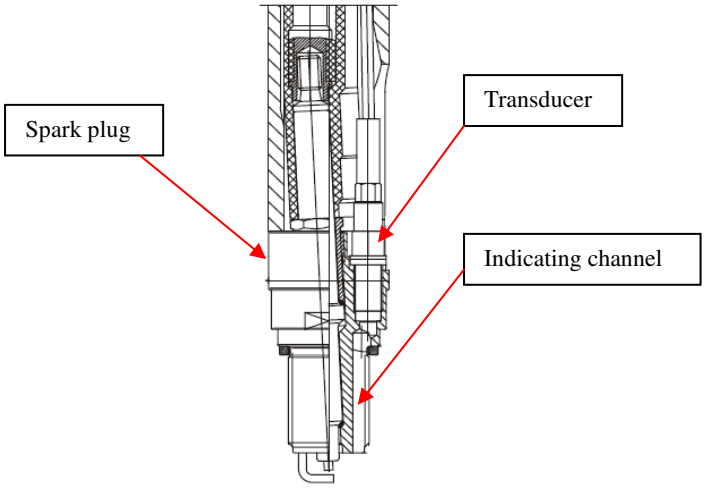

Figure 14: Spark plug installed transducer (AVL, 2002)

2.5.2 Crank angle measurement

Crank angle measurement can be done with a variety of sensors. However, the required accuracy limits the applicable sensors. Sensing technology that are mostly used are optical, magnetic and inductive sensing. Of these three, optical sensing is the most suitable option for engine indicating purposes due to their high accuracy (less than 1 ° accurate) (AVL, 2002).

This type of sensor (see Figure 15) consists of a transparent glass disk inscribed with a pattern of opaque lines, a LED light source, a photo sensor (photodiode array) and signal conditioning circuitry. The photodiode picks up the light from the LED as it passes through the transparent glass disk.

A sinusoidal waveform is then produced by the circuit electronics which is then transformed into a square wave. (Encoder Products Company, [S.a.])

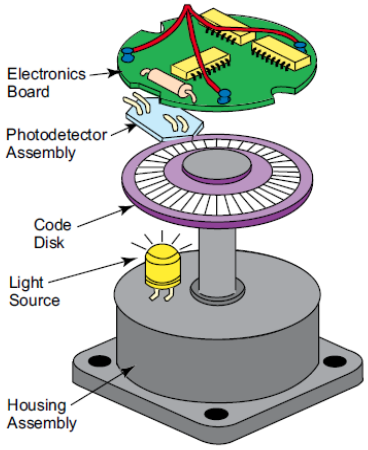

Figure 15: Shaft encoder components (Encoder Products Company, [S.a.])

Angle measurement can either be on an absolute or incremental (relative) basis. The former is a method by which a unique output is given for each shaft position, while the latter outputs only a pulse after each increment in crank angle. The latter is more suited to engine indicating. Incremental encoders either have a single or two channel (quadrature) output (see Figure 16). With a two channel encoder, the output of the two channels (called A and B) are electrically 90 ° out of phase.

The advantage this has over a single channel is that the direction of rotation can be determined by detecting the leading or lagging signal of A and B. Some incremental encoders also have a third channel output called the marker or index (channel Z). This channel outputs a pulse once per revolution, at the same point during each revolution, which can be used as a reference or as a trigger for data acquisition (DAQ). For engine indicating the shaft encoder index is assigned to TDC of the piston used for pressure measurement.

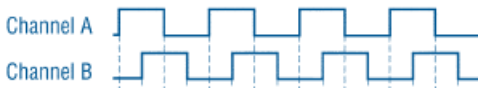

Figure 16: Shaft encoder output channels (Danaher Industrial Controls, 2003)

Mounting of the encoder at the flywheel of the engine can cause measurement errors due to crankshaft torsion and it is therefore recommended that the piston adjacent to the crankshaft pulley is used for pressure measurement. (AVL, 2002).

2.5.3 Parameters calculated from in-cylinder pressure

Parameters that can be calculated from in-cylinder pressure data include indicated mean effective pressure (IMEP), heat release from the fuel and the mass fraction of fuel burnt. The significance and calculation of these parameters will be discussed in this section.

a) IMEP

In-cylinder pressure can be used to determine the indicated (implies a combustion related parameter) work per cycle per cylinder developed by the engine. In four stroke engines the indicated work developed during the compression and expansion stroke is referred to as *gross indicated work* ($W_{i,g}$), whereas the indicated work for the entire cycle is referred to as *net indicated work* ($W_{i,n}$) (Heywood, 1988). The latter is calculated by subtracting the pumping work required during the intake and exhaust strokes from the gross indicated work. The indicated power available per cylinder per cycle can be calculated from the indicated work using the following equation:

$$P_i = \frac{W_i N}{n_r} \tag{2}$$

where N is the rotational speed of the engine and n_r is the number of crankshaft revolutions for each power stroke. For four stroke engines n_r is equal to 2 and for two stroke engines it is equal to 1.

Dividing the indicated work by the swept volume of the cylinders gives the IMEP which is a fundamental parameter for calculating engine mechanical efficiency (Heywood, 1988). IMEP represents the mean positive pressure exerted on the piston during the power stroke. The equation used is as follows:

$$IMEP = \frac{W_i}{V_d} = \frac{\oint p\, dV}{V_d} \tag{3}$$

where W_i is the indicated work, V_d is the displaced volume of the cylinder, V is the crank angle dependant cylinder volume and p is the combustion pressure. The difference between the net and gross IMEP is referred to as the pumping mean effective pressure (PMEP).

Due to frictional losses and accessory work (pumps, fans, alternator, etc.), the engine brake power is less than the indicated power. This is due to friction and is usually expressed as the friction mean effective pressure (FMEP). The FMEP can be calculated by subtracting the break mean effective pressure (BMEP) from the net IMEP. BMEP is a useful parameter for comparing different engines because it takes into account the swept volume and therefore size of the engine (Heywood, 1988).

It is obtained as follows:

$$BMEP = \frac{4\pi T_b}{V_d} \tag{4}$$

where T_b is the torque applied by the dynamometer.

b) Apparent rate of heat release

Two other parameters that can be calculated from in-cylinder pressure data is the apparent rate of heat release and the mass fraction of fuel burnt which are useful tools for comparing the performance of different fuels (Ceviz & Kaymaz, 2005). With these two parameters the length of the combustion process and its thermodynamic effect can be evaluated (Van Basshuysen & Schäfer, 2004).

Heat release is a technique used for determining the amount of fuel energy that is released per degree of crankshaft rotation during an engine cycle. The formula for a simple heat release rate model is developed from the first law of thermodynamics for a control volume representing the engine combustion chamber. This method is known as the zero dimensional approach. With a multidimensional approach the Navier-Stokes equations are taken into account in addition to the first law of thermodynamics (Verhelst & Sheppard, 2009).

The period that is analysed for heat release is from spark delivery to the end of the power stroke (Ceviz & Kaymaz, 2005). The formula for a zero dimensional apparent heat release rate model (ignoring the effects of crevices) is given in equation 5 of which the derivation can be found in appendix B.2. Note that the model is based on a crank angle (θ) and not time basis.

$$\frac{dQ_{ch}}{d\theta} = \frac{V}{\gamma-1}\frac{dp}{d\theta} + \frac{\gamma}{\gamma-1}p\frac{dV}{d\theta} + \frac{dQ_{ht}}{d\theta} \tag{5}$$

where dQ_{ch} is the gross heat release, dQ_{ht} is the heat transfer to the walls, p is the combustion pressure, V is the cylinder volume and γ is the specific heat ratio. If dQ_{ht} is omitted from equation 5, dQ_{ch} represents the net heat release from the fuel. The following equation can be used to calculate dQ_{ht}:

$$\frac{dQ_{ht}}{d\theta} = A\,h_c\,(T - T_w) \tag{6}$$

where A is the instantaneous surface area within the combustion chamber, h_c the in-cylinder heat-transfer coefficient, T the mean gas temperature and T_w the mean wall temperature. The equations for calculating the surface area and cylinder volume can also be found in appendix B.2.

The mean gas temperature can be calculated using the ideal gas equation. Inlet valve closing (IVC) is used as the reference point for the temperature calculations. The equation is as follows:

$$T = \frac{T_{ref}}{p_{ref}\, V_{ref}}\, p\, V \tag{7}$$

There exist many correlations for the heat transfer coefficient of which mostly used is the coefficient proposed by Woschni, Eichelberg, Hohenberg and Annand. The coefficient proposed by Eichelberg was used for the project and it is given by the following equation: (Lounici et al., 2010)

$$h_c = 7.67 \times 10^{-3}\, {V_{mp}}^{0.333} \left(\frac{p}{T}\right)^{0.5} \tag{8}$$

where V_{mp} is the mean piston speed. Eichelberg's coefficient was chosen due to its simplicity of implementation. Furthermore, it has been shown by previous researchers that Eichelberg's coefficient is sufficiently accurate for heat transfer calculations (Lounici et al., 2010).

For calculating the specific heat ratio (γ), numerous models have been developed which are classified either as single or two zone models. With single-zone models the gas in the cylinder is seen as a single homogenous gas whereas with two-zone models a distinction is made between the burnt and unburnt gases (Verhelst & Sheppard, 2009). These two-zone models, although more accurate, are more complicated than single-zone models.

Values for γ can either be assumed to remain constant (in the range of 1,25 and 1,35) or to be dependent on temperature during the heat release period. Chun and Heywood (1987) however recommended that separate models be used for the compression, combustion and expansion cycles. Numerous temperature dependent polynomials have been developed by different researchers. For the project the following polynomial was used: (Ceviz & Kaymaz, 2005)

$$\gamma = 1.338 - 6 \times 10^{-5}\, T + 1 \times 10^{-8}\, T^2 \tag{9}$$

Other models that have been developed include a linear function, and an exponential function. These models however have adjustable parameters that require tuning which is not the case with the model used in this project (Klein, 2007). The model that was chosen has also been shown to give results close to that of more complicated two-zone models (Ceviz & Kaymaz, 2005) (Shehata, 2010).

Typical zero dimensional, single-zone heat release rate curves of a SI engine, using different models for γ, are shown in Figure 17.

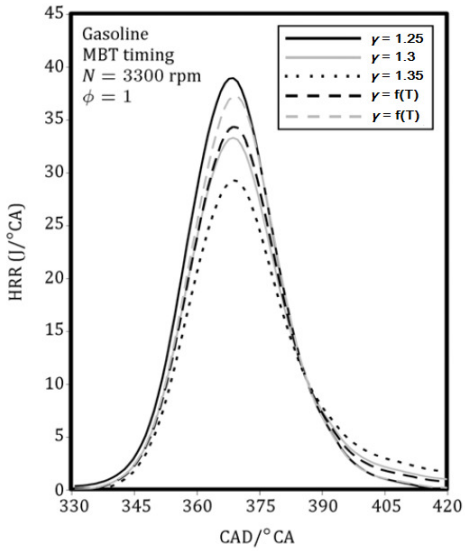

Figure 17: Heat release rate curve (Ebrahimi, 2011)

c) Mass fraction of fuel burnt

The mass fraction of fuel burnt can be calculated theoretically as well as from experimental data. One well known experimental method was developed by Rassweiler and Withrow. With their model, the mass fraction burnt (x_b) is given as follows: (Ceviz & Kaymaz, 2005)

$$x_b = \frac{\sum_{ign}^{i} \Delta p_c^*}{\sum_{ign}^{N} \Delta p_c^*} \tag{10}$$

where Δp_c^* is the corrected pressure rise due to combustion, N refers to the crank angle at end of combustion, ign is the crank angle at ignition and i is increments in crank angle. The corrected pressure can be calculated as described by equation 11 where V_{TDC} refers to the cylinder volume at TDC and n to the polytropic exponent.

$$\Delta p_c^* = [p_i - (V_{i-1} - V_i)^n p_{i-1}](V_{i-1} - V_{TDC}) \tag{11}$$

A theoretical approach that can be used to predict the mass fraction burnt is the Wiebe (or Vibe) function. It is defined as follows: (Chun & Heywood, 1987)

$$x_b = 1 - e^{-a(\frac{\theta-\theta_0}{\Delta\theta})^{m+1}} \tag{12}$$

where θ is the crank angle, $\theta_0$is the angle at the start of combustion, $\Delta\theta$ is the total combustion duration and a and m are adjustable parameters. Values for a and m can be obtained by fitting the Wiebe function to experimental data (Blair, 1999).

2.5.4 Pressure phasing and referencing

The accuracy of parameters calculated from engine pressure depends on many different assumptions and parameters. One parameter that has a significant effect is the alignment between the shaft encoder reference trigger pulse and TDC of the piston used for pressure measurement (Goering, 1998). Lapuerta et al (2000) showed that a 1 ° deviation in the alignment can cause a 75 % error in IMEP calculations.

The most convenient method for adjusting the phasing is by plotting a hot motoring pressure trace against the cylinder volume on a log scale (known as a log P - log V plot). Motoring refers to running the engine without combustion taking place. For correct phasing, the compression and expansion lines will not cross each other, will be straight without any curvature and will have a sharp tip at the TDC point on the log scale plot. Curvature can be due to incorrect pressure referencing, transducer linearity problems and an incorrect clearance volume measurement. Cross over occurs when the captured pressure trace is retarded with regard to TDC (Lancaster et al., 1975).

Referencing (pegging) of the pressure values are required to convert the gauge pressures measured by the transducer to absolute pressures. For this purpose, the measured intake MAP, at IVC, is used to peg the pressure values for both the fibre optic and piezoelectric transducers. A properly phased and referenced hot motoring pressure trace is shown in Figure 18.

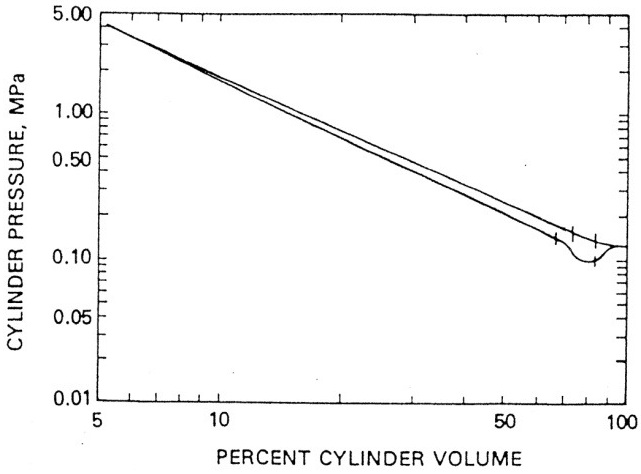

Figure 18: log P - log V plot of properly phased data (Callahan et al., 1985)

3. Test Facility Design and Installation

In this chapter the facility that was developed will be discussed. All of the mechanical, electrical and electronic aspects will be described in detail.

3.1 System Overview

The main components that were used in the project are a SI engine, a *Schenck* W130 eddy current dynamometer, an *AVL* fuel flow meter, an *Allen Bradley* programmable logic controller (PLC) and a *National Instruments* DAQ device. The layout of the system is shown in Figure 19. The 19" cabinet shown in the figure contains all of the controllers that were installed. In Figure 20 photographs of the completed setup are given.

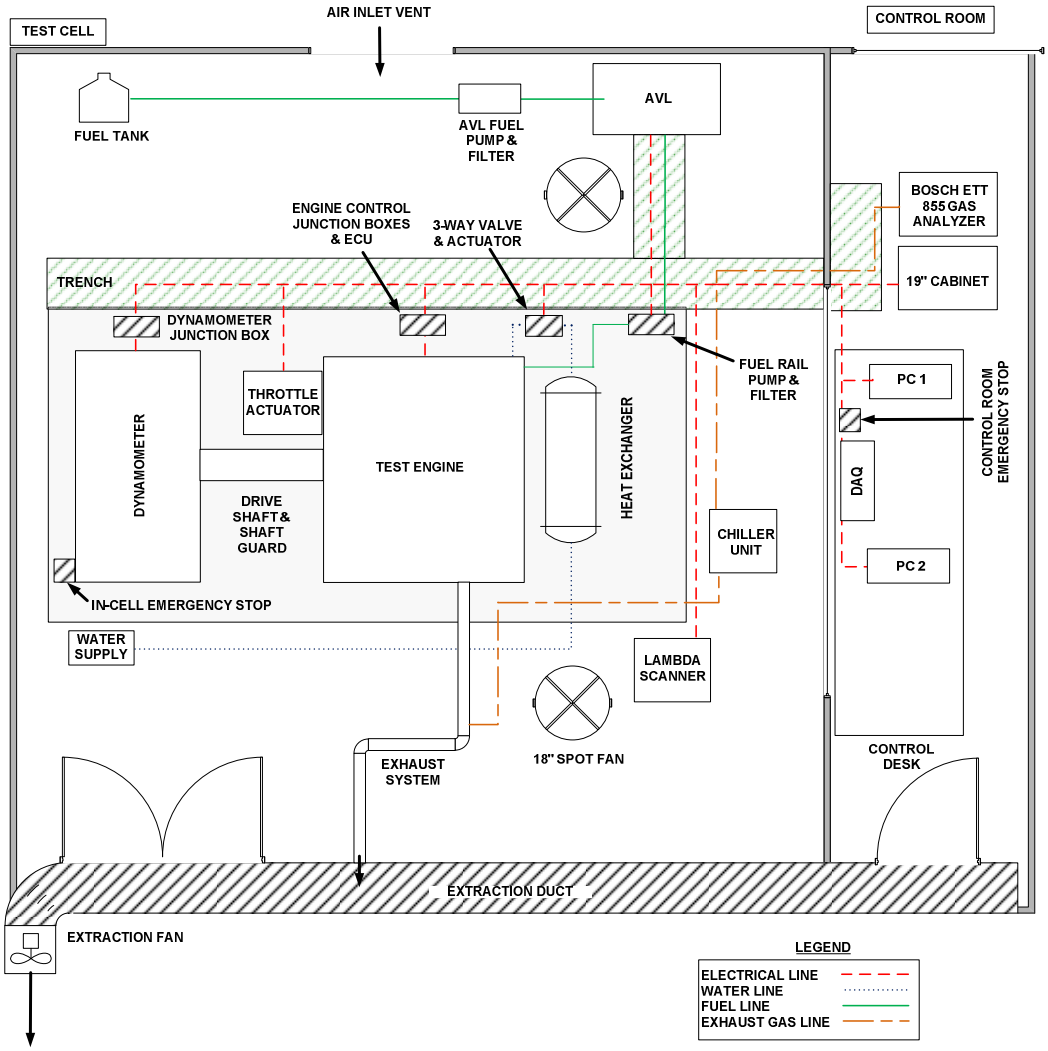

Figure 19: Testing facility layout

Rear right view

Rear left view

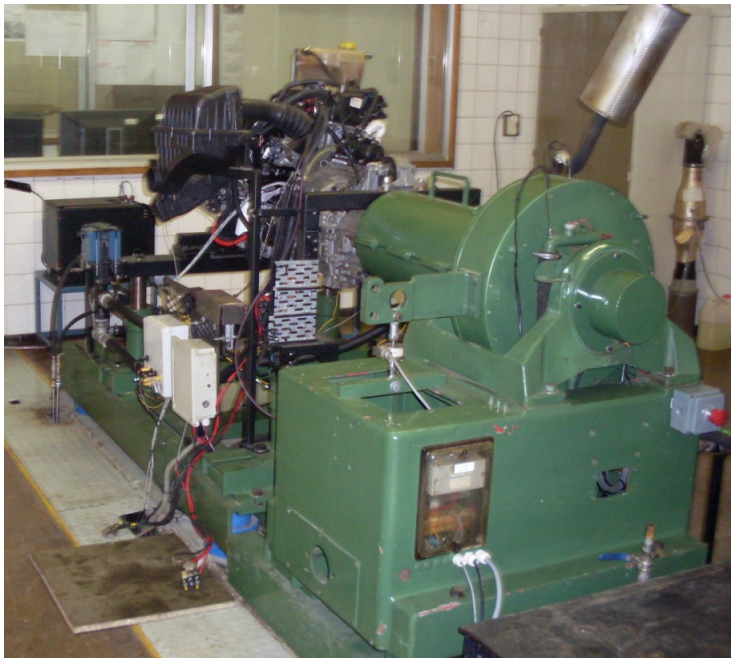

Figure 20: Testing facility photographs

The specific engine that was used for the project is a four cylinder, 1.6 L SI engine with PFI and is suitable for biofuel research due to its proven reliability record and use locally and overseas. The eddy-current dynamometer was chosen due to its mechanical simplicity (allowing easy maintenance), low inertia and stability during steady-state testing.

3.2 Engine and Dynamometer Installation

During the initial stage of the project the engine as well as the dynamometer had to be installed onto a test bed. Drive shaft arrangements were also made to enable coupling of the engine to the dynamometer. The details are discussed in this section.

3.2.1 Test bed

To save costs and design time an existing test bed was used for the project. It consists of two sections; one for the engine and one for the dynamometer, both of which are made up of 10 mm thick steel channels and angle iron. The bed for the engine was mounted on vibration blocks to aid in minimizing vibration transfer to the test cell infrastructure itself and to allow for installation of larger engines in the future.

In order to adjust the height of the engine as well as the alignment between the engine and dynamometer, screw jacks and steel cross members were installed. The bed, screw jacks and cross members are shown in Figure 21. Also shown in the figure are the engine's stands and mountings used for supporting the engine.

The dynamometer was then installed and levelled (using spacers) before the engine was installed. This sequence was used due to the fixed height of the axis of the dynamometer relative to the floor. The engine was then installed and its axis aligned with that of the dynamometer. The engine was also levelled, as per installation requirements, to ensure correct running conditions.

Figure 21: Test bed and engine mounting accessories

3.2.2 Drive shaft and coupling

The engine was coupled to the dynamometer using a custom designed and manufactured drive shaft. A standard drive shaft with two constant velocity (CV) or universal joints could also be used however, this causes more vibration transfer to the dynamometer as well as increased joint wear due to torsional oscillations. For safety purposes a shaft guard was also designed and manufactured using available 16 mm thick pipe. The drive shaft and shaft guard are shown in Figure 22.

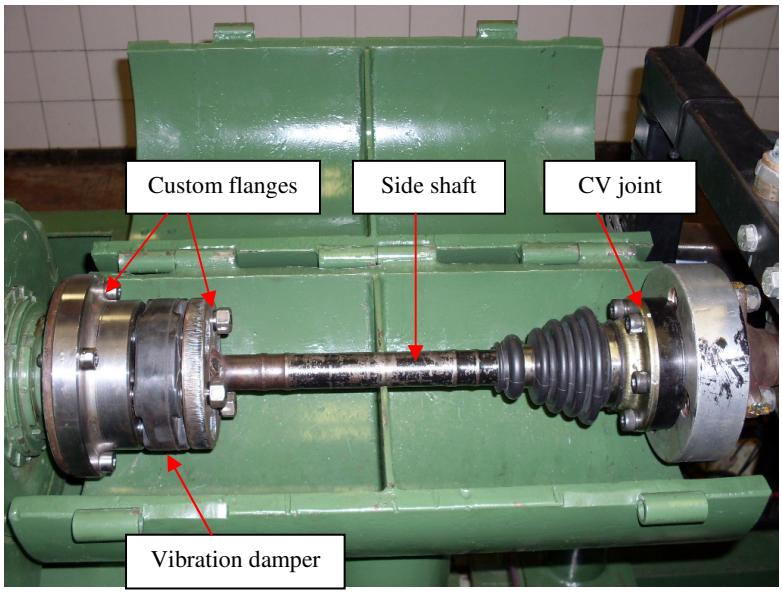

Figure 22: Drive shaft and shaft guard

The shaft that was designed and manufactured consists of a standard *BMW 5 series* side shaft, a standard *BMW 5 series* CV joint, a standard *Mercedes* rubber vibration damper, two custom flanges for connection to the dynamometer, a custom flange for connection to the engine and an *IKO* spherical plain bearing for alignment purposes. Drawings of the drive shaft can be found in appendix A.1.

Due to the unknown properties of the drive shaft components calculations proving their suitability for use on the engine could not be done. The components therefore had to be selected according to the rated specifications of each component.

The suitability of each component was supported as follows:

- The side shaft, CV joint and vibration damper were manufactured for engines with higher maximum torque ratings than the engine used in the project.
- All the fasteners that were used are made from high tensile steel and *Loctite* thread locker was used during assembly.
- The custom flanges were checked for strength and manufactured without sharp corners to minimize stress concentrations.

3.3 Cooling Systems

The facility required development of a cooling system for the engine as well as for the dynamometer. The layout of the cooling system that was developed is shown in Figure 23 while the system wiring can be found in appendix E.

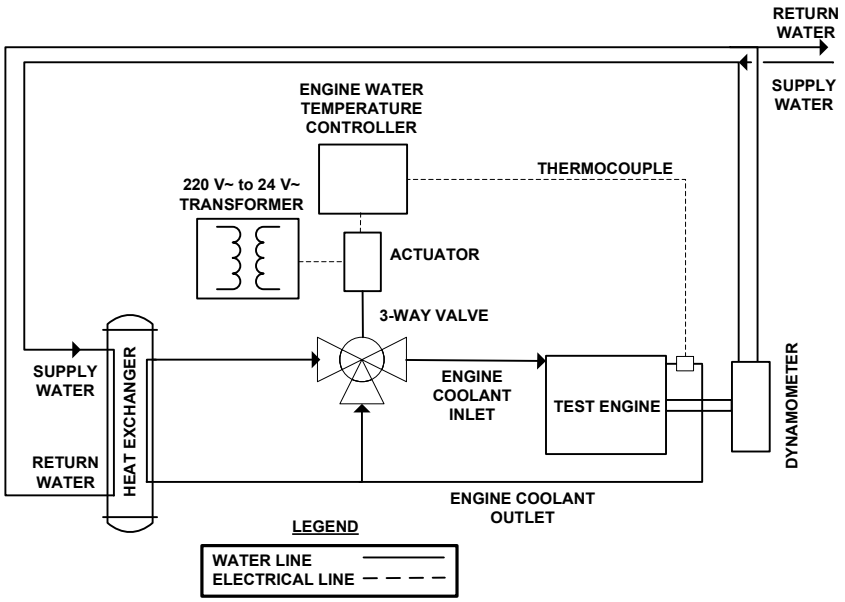

Figure 23: Cooling system layout

In order to keep the engine temperature within design limits, coolant (water mixed with an additive) is pumped through the engine block as well as the cylinder head. In vehicles the heat is then dissipated from the coolant to the atmosphere using a radiator. When using a radiator in a test cell, additional ambient air flow and circulation is required to maintain engine temperature and prevent a substantial increase in the test cell air temperature.

To achieve the additional air flow and circulation, large fans need to be installed in the test cell. Due to the fan size required, installation of a water to water heat exchanger is more beneficial for engine test cells. The capacity of the heat exchanger that was available for the project is however too large for the engine.

Due to this, a three way mixing valve (sized according to typical coolant flow rates in SI engines) was installed to enable control of the engine temperature. This valve is adjusted by an actuator which in turn is controlled using a stand-alone PID controller. The valve and actuator is shown in Figure 24 while the controller is shown in section 3.6.2.

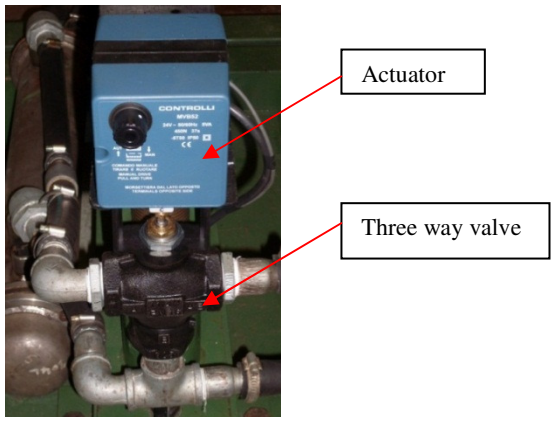

Figure 24: Three way valve and actuator

A choice had to be made between using the engine inlet water temperature as the control parameter or using the outlet water temperature and blocking (jamming) the engine thermostat in fully open mode. The latter was chosen for the project due to the possibility of thermostat failure which could cause overheating of the engine.

To protect the dynamometer, safety switches for temperature and flow rate are located in the outlet water pipes of the dynamometer. These switches were provided with the dynamometer and they form a simple closed loop electronic circuit. When the outlet water exceeds 60 °C or the water flow rate becomes insufficient, the corresponding switch will open and break the circuit. This in turn is monitored by the dynamometer controller which will shut down the engine.

3.4 Fuel System

The engine used for the project utilizes a fuel rail which supplies fuel to the injectors. Injection pressure is kept nearly constant at 270 kPa by a pressure regulator in the return port of the injection rail. To supply fuel to the fuel rail a roller cell pump was used. Fuel enters the low pressure side of the pump and is then pumped by rotating cells. This pump is referred to as the fuel rail pump in this document and it is switched on by a relay which is controlled by the user (see section 3.6.2).

Fuel is fed to the low pressure side of the rail pump from an *AVL* fuel flow meter mounted against the test cell wall. The flow meter (shown in Figure 25) is based on a gravimetric measuring principle. Fuel is supplied to the engine from the measuring vessel and any excess fuel is returned to this vessel.

The vessel is supported frictionless on a blade spring which is connected to a highly sensitive capacitive displacement transducer. This transducer senses any change in fuel mass in the vessel. Fuel flow is then calculated by measuring the change in the fuel mass over a certain measuring time (AVL, 1984). Calibration of the unit is done by running the built-in calibration routine on the controller.

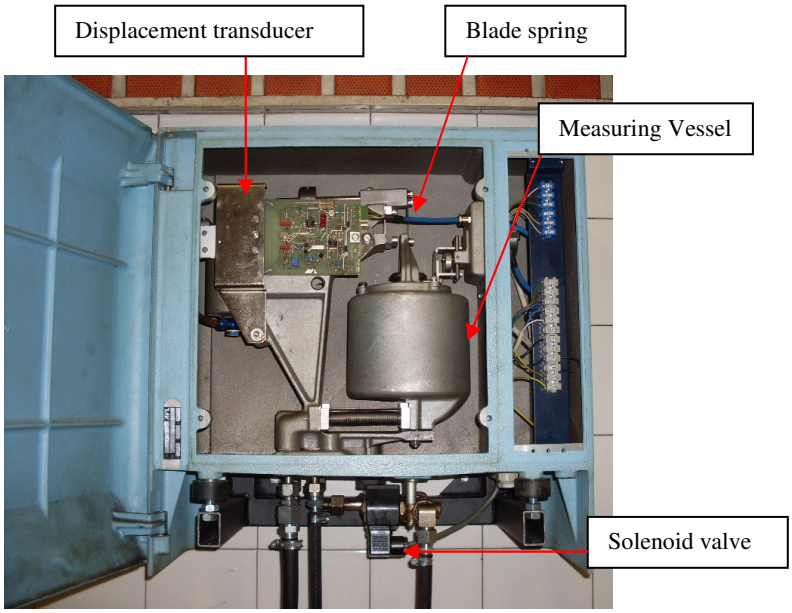

Figure 25: AVL dynamic fuel balance

To fill the measuring vessel, fuel is pumped from a 25 L container using a roller cell pump. To prevent the fuel from flowing out of the vessel once full, a solenoid actuated valve is located in the fuel supply line. The solenoid is energized once the vessel is empty and de-energizes once it is full. The relay which controls the pump was wired to the same terminals as the solenoid valve causing the pump to switch on when the valve is opened and switch off when the valve closes.

In Figure 26 a schematic of the fuel system is given. As can be seen in the figure, an overflow pipe was installed between the fuel flow meter and the fuel container. This was done to prevent fuel spills in the event that the solenoid valve (and therefore the header pump) is not switched off during filling.

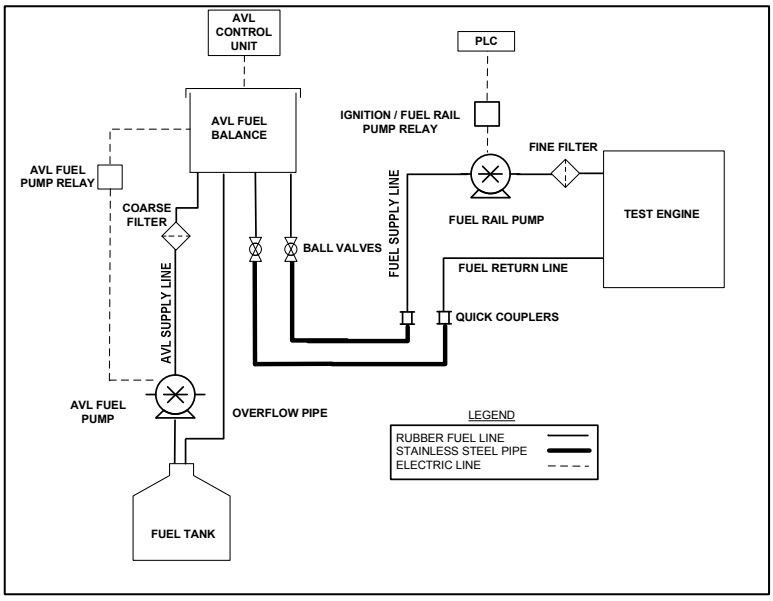

Figure 26: Fuel system layout

3.5 Exhaust Gas Extraction and Cell Ventilation

For the project a standard exhaust system (without a catalytic converter) from a vehicle using the same engine was installed. A photograph of the exhaust is given in Figure 27. This exhaust system was coupled to the existing air extraction system in the test cell using flexible steel tubing.

Figure 27: Engine exhaust system

Due to the minimal airflow across the engine in the test cell, the engine oil can overheat when running at high load conditions. Portable fans were therefore installed to achieve cooling of the oil. One of these fans can be seen in Figure 20.

3.6 System Instrumentation and Control Hardware

In order to monitor and control the engine and dynamometer, a number of electrical and electronic devices were necessary. These include sensors, relays, controllers and actuators which will be discussed in this chapter. The wiring diagrams of all the instrumentation can be found in appendix E.

3.6.1 Sensors and emergency stops

The sensors that were installed in the test cell are thermocouples, pressure transmitters, a relative humidity sensor, a lambda sensor, a load cell and a speed sensor. Thermocouples were installed for measurement of the following temperatures:

- Engine coolant outlet temperature
- Engine coolant inlet temperature
- Engine oil temperature
- Intake air temperature
- Ambient air temperature
- Fuel temperature
- Dynamometer outlet water temperature
- Exhaust gas temperature

Three pressure transmitters were installed for measuring the following:

- Fuel rail pressure
- Oil pressure
- Atmospheric pressure

The relative humidity transmitter was installed to enable calculation of a power correction factor. This factor is needed when the engine is used in atmospheric conditions different from that specified by the manufacturer (Sodré & Soares, 2003). There are numerous different calculation methods for this factor and the one that was used for the project is the SAE J1349. For this factor, the atmospheric pressure, temperature and relative humidity in the test cell is required. This factor can however only be used at full load conditions.

To monitor the mixture air-fuel ratio while the engine is running, a lambda sensor was installed in the first section of the exhaust. This sensor was connected to an *ETAS* model LA4_E lambda scanner which has an analogue output of 0-10 V. The sensor and scanner can be seen in Figure 28.

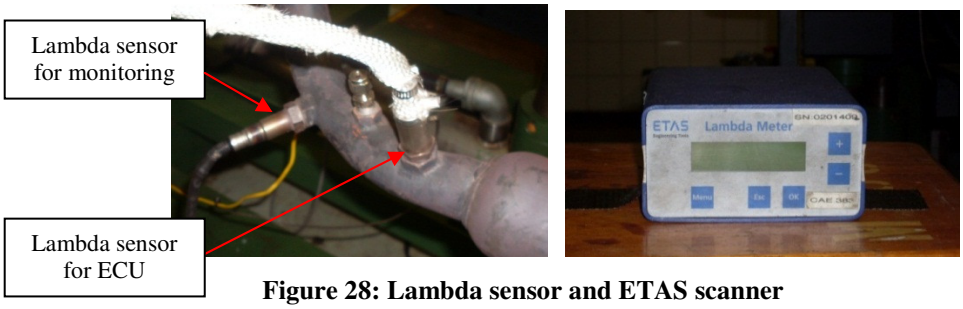

Figure 28: Lambda sensor and ETAS scanner

The installation of emergency stops was a fundamental safety concern in the project. Two of these were installed; one in the test cell itself and the other in the control room (see Figure 29). These emergency stops, wired in series, both have normally closed contacts which were hardwired to shut down the engine when depressed.

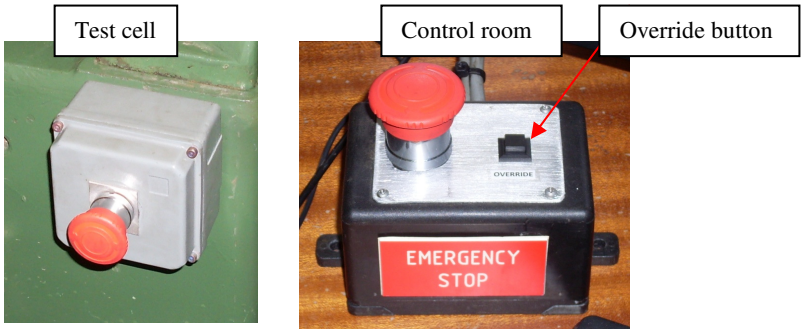

Figure 29: Emergency stops

3.6.2 Controllers and actuators

The controllers that were used for the project were all installed in a 19" cabinet in the control room. This cabinet and all the installed controllers are shown in Figure 30.

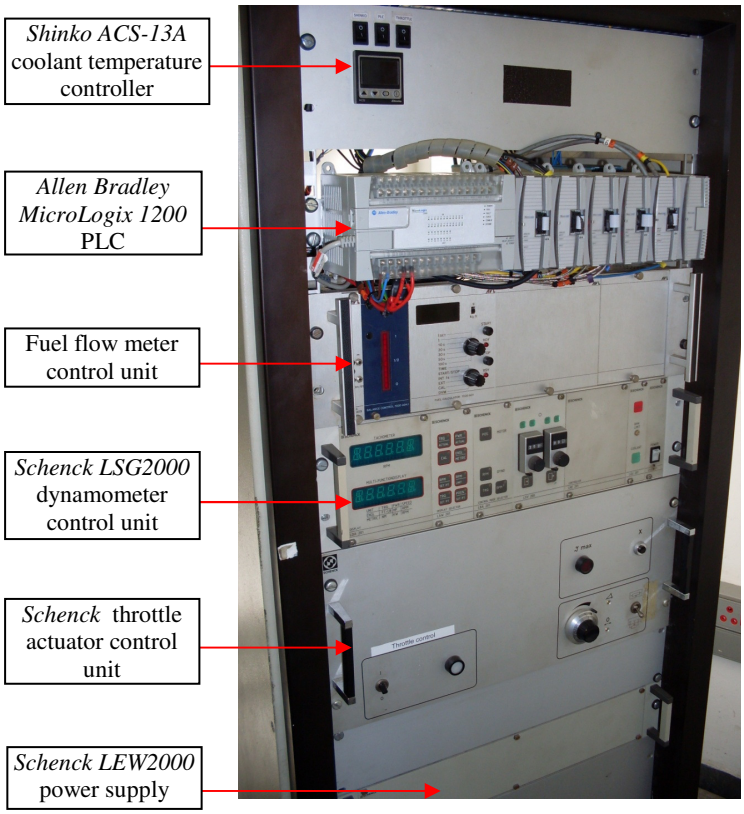

Figure 30: 19" cabinet

a) Dynamometer and throttle

The dynamometer coil is supplied with a DC current from the *Schenck LEW 2000* power supply. The amount of current that is supplied is controlled using the *Schenck LSG 2000* control unit which receives input from the operator. The controller can be used to either control the torque or speed of the dynamometer or the position of the engine throttle. For the project only the speed mode was used for reasons that will be explained in section 3.7.2.

Input to and output from the controller is a 0-10 V signal. The input is received from the PLC which is the hardware that was installed for controlling the engine and dynamometer setup (see section 3.6.2(d)). The response and stability of the *LSG 2000* dynamometer controller was adjusted by tuning the built in PID controller setting while the engine was running.

To enable control of the engine's throttle, a *Schenck* throttle actuator and controller was installed which was connected to the throttle using a steel cable. This actuator is shown in Figure 31. The controller for the actuator also receives a 0-10 V signal, depending on the desired throttle position of the user, from the PLC.

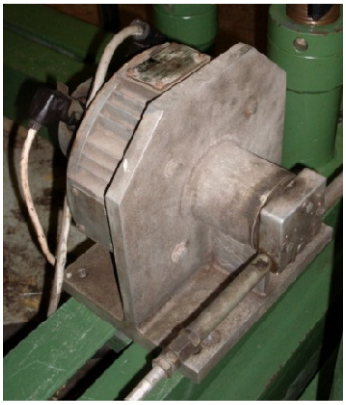

Figure 31: Throttle actuator

b) Engine coolant controller

On the engine coolant control system a stand-alone controller was installed. The input to the controller is the engine water outlet temperature while its output is a 4-20 mA signal to the three way valve actuator. The controller is capable of using PID control which enables excellent stability of the coolant temperature. Values for P, I and D were set by running the built in auto tune function of the controller while the engine was running.

c) Engine control unit

For the project an ECU as well as a wiring loom was sponsored by *Bosch South Africa.* This ECU receives input from a throttle position sensor, lambda sensor, coolant temperature sensor, a MAP and intake air temperature sensor, a knock sensor, a crankshaft speed sensor as well as a camshaft position sensor, all of which were supplied with the engine.

The ECU (as well as the starter solenoid) needs a supply voltage of 12 V which is achieved in vehicles using the ignition switch and the battery. For simulating the ignition switch two relays were installed; one for switching on the ECU (also used for switching on the fuel rail pump and lambda scanner) and one for switching on the starter solenoid. These two relays are connected to the PLC which allows the user to switch on the ECU and operate the starter motor from the control room.

d) PLC

To allow user control of the dynamometer speed set point and the throttle actuator position as well as monitor the various parameters measured, an *Allen Bradley* PLC was installed. Initially a new PLC product from *Allen Bradley* namely the *Micro830* connected to a *PanelView* touch screen was installed, both of which were donated for the project. In Figure 32 the PLC and the touch screen is shown. The touch screen serves as the user interface.

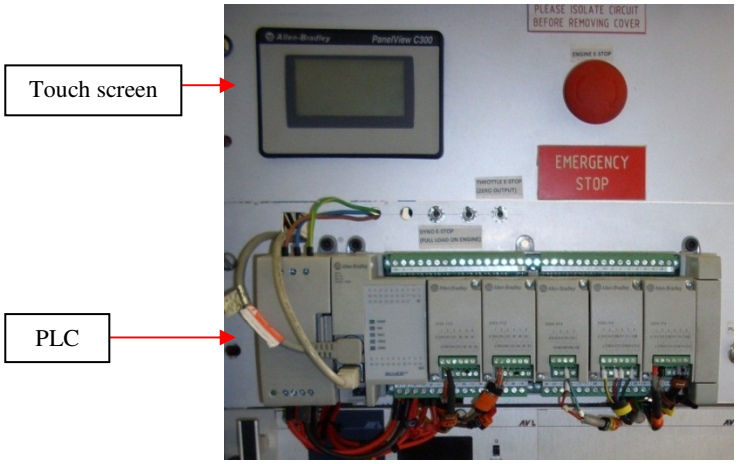

Figure 32: Micro830 PLC and Panelview touch screen

Although this PLC setup worked very well, the screen was too small and slow to program. It was therefore decided to change the user interface to a more user friendly package namely *ETA* (*Engine Test Automation*) which was obtained from *Cape Advanced Engineering*. This software package however would not communicate with the *Micro830* and therefore it was decided to use a *MicroLogix1200* PLC which is capable of communicating with ETA. The *MicroLogix1200* can be seen in Figure 30 and Figure 33.

It consists of the following:

1. Base unit containing 16 relay outputs and 24 AC digital inputs,
2. Two analogue input modules,
3. Two thermocouple input modules,
4. One analogue output module, and
5. One DC digital input module.

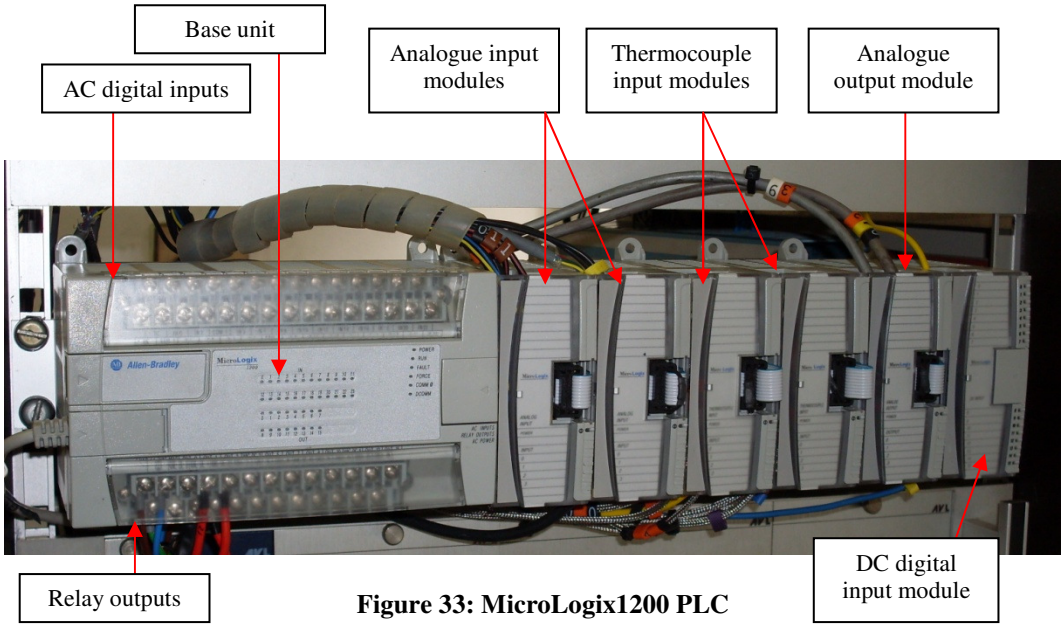

Figure 33: MicroLogix1200 PLC

The connections that were made to the base unit are at the relay outputs only. Channel 1 was used for the ignition relay while channel 2 was used for the starter solenoid relay. These relays are supplied with 24 V DC using an external power supply located in the 19" cabinet. The negative terminals of both relays are wired to the emergency stops shown in section 3.6.1 which de-energizes the relays when pressed and therefore shuts down the engine.

The analogue input modules were used to measure oil pressure, the fuel mass in the *AVL* measuring vessel, relative humidity, atmospheric pressure, speed, torque, lambda and fuel pressure. Input to the modules can be either 0-10 V or 4-20 mA which has to be set in the programming software.

To enable easy replacement of the thermocouples and aid with fault finding, a junction box was installed on the test bed. A junction box was also installed for the relays. From the thermocouple junction box extension wires were run to the 19" cabinet and wired into the thermocouple modules of PLC. The type of thermocouple used can be specified for each channel of the module using the software package (see section 3.7.2) for the PLC.

The analogue output module was used to send the command values to the dynamometer controller as well as the throttle actuator controller. The module is capable of providing both current and voltage outputs which also has to be set in the programming software.

The last module in the PLC namely the digital input module was used to hard wire an override button. This button can be used to prevent the software program from de-energizing the ignition relay and therefore shutting down the engine. Shut down occurs when one of the measured parameters exceeds the set points for the low or high limit.

3.7 System Control Software and User Interface

A layout of and the communication channels between the hardware and software packages that were used is shown in Figure 34. The *Allen Bradley* driver is used by *ETA* to communicate with the PLC through the *RsLinx* software package. The PLC is programed in *RsLogix* and is connected to the PC using RS232 communication protocol.

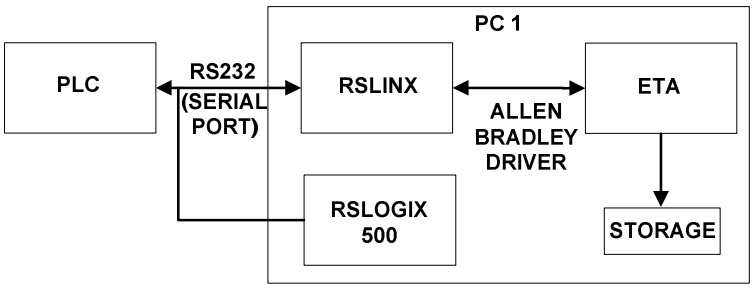

Figure 34: Software layout

3.7.1 Control user interface

For the engine test setup *ETA* is used as the supervisory control and data acquisition (SCADA) interface. Using *ETA*, the engine can be controlled, parameters can be monitored (temperatures, pressures, flows, torque, speed etc.), alarms and emergency shutdowns can be programmed, sensors can be calibrated and data can be logged. Furthermore, automated test sequences can also be programmed. The interface that was developed for the project is shown in Figure 35.

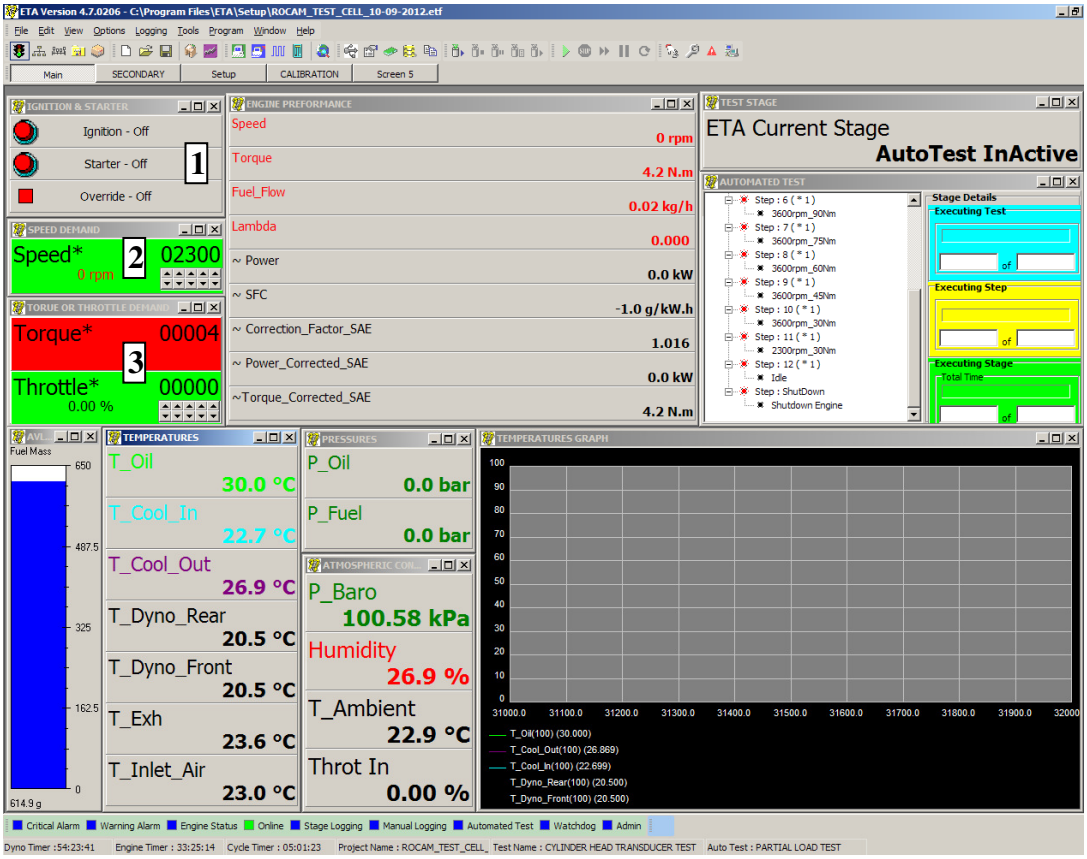

Figure 35: ETA user interface

The interface developed provides the user with the control functions labelled 1 to 3 in the figure. These controls are as follows:

1. Ignition and Starter buttons for controlling the ignition and starter solenoid relays respectively.
2. Desired speed setting control panel.
3. Control panel for throttle or torque setting. The user can choose between one of the two by simply clicking on the appropriate block.

Data is exchanged between the PLC and *ETA* in the form of raw registry values between 0 and 32767 using the *RsLinx* software package and the *Allen Bradley* driver. In the case of a voltage input or output a 0 register value corresponds to 0 V while a 32767 register value corresponds to 10 V. A signal of 4-20 mA will be sent as 6241 for 4 mA and 32767 for 20 mA.

Each of the analogue input and output channels of the PLC can be calibrated in *ETA* using the channel calibration screens. In the calibration screens the registry values can be captured and the corresponding physical quantity assigned to that registry value. This is done for several consecutive points after which the program calculates a linear fit for the points. The calibration screens of the channels are given in appendix D.3.

Due to the large amount of information present on the user interface, it is difficult for the operator to constantly monitor all the parameters. Alarms were therefore set up on all the important channels in *ETA*. These channels include speed, torque, oil and fuel pressure, fuel mass in the *AVL* as well as all temperatures excluding ambient and air inlet temperature. The alarm system allows *ETA* to shut down the engine in case one of the parameters exceeds the set low or high limits.

3.7.2 Ladder logic program

Although *ETA* supplies the user interface, the PLC still has to be programmed using the ladder logic programming software package *RsLogix 500*.

The ladder program that was compiled consists of one main routine and several subroutines. These routines are shown in appendix D.1. The main ladder routine is used only to monitor the watch dog timer and to jump to the different subroutines. The watch dog timer is used to monitor whether the PLC is connected or not. When power to the PLC is cut off or the serial connection between the PLC and the PC is disturbed, the watch dog timer will stop and an error will be shown in the user interface.

The subroutines that were programmed include:

1. Digital inputs,
2. Digital outputs,
3. Torque PID control,
4. Fuel flow calculation, and
5. Sending of values between PLC and *ETA*.

Registry values are exchanged between *ETA* and the PLC using integer buffers located in the PLC memory. All analogue inputs are written (by the PLC) to the N10 buffer while all the analogue outputs are written (by *ETA*) to the N14 buffer.

The dynamometer control unit has built in functions to control the throttle setting of the engine and the current to the dynamometer. The operator inputs a desired speed and torque and the controller then adjusts the current to the dynamometer and the position of the throttle until the desired speed and load set points are achieved. It was found however that when using this function, the controller moved the throttle to the wide open position for any speed and load set point. It was therefore assumed that the throttle control function of the controller was faulty. The throttle therefore had to be controlled by the PLC and a *torque PID control* routine was therefore written. The speed control function of the controller was functional and could therefore be used to control the current to the dynamometer.

When the user selects the torque setting mode in *ETA* it activates the automatic throttle control function of the *torque PID control* routine. This PID controller adjusts the throttle until the desired torque is achieved.

It also maintains this setting until the user changes the desired torque set point. The torque set point desired by the user is read from N14:2 and a voltage output is then written to channel 1 of the analogue output module. The Values for the P, I and D constants were set while running the engine.

The user is also provided with the option to manually adjust the throttle in *ETA*. In this mode the PLC reads the user input from N14:3 and directly outputs a voltage to channel 1 of the analogue output module. The same is done for the speed setting were the user input is read from N14:1 and the output is written to channel 0 of the analogue output module.

The digital inputs subroutine is used to send the digital input values to ETA and to monitor the override button. When the override button is pressed, this rung prevents *ETA* from turning off the ignition. The digital outputs subroutine is used to control the ignition and starter and prevents engagement of the starter motor once the engine is running. All digital input values are written to N10:99 while all digital output values are written to N14:99.

3.7.3 Calibration of instrumentation

The oil and fuel pressure transmitters were calibrated using a hand held pressure pump connected to the transmitter as well as a pressure gauge. The output from the transmitters as well as the pressure reading from the gauge was recorded using the *ETA* calibration screens. The atmospheric pressure and relative humidity channels were calibrated by setting the maximum and minimum output from the transmitters equal to the maximum and minimum registry values of the PLC.

To enable proper control of the engine's throttle, the throttle actuator's zero point and range had to be adjusted. This was done using the potentiometers on the front face of the actuator controller. The zero point was adjusted until the throttle valve was at the idle position. Thereafter the range was set by adjusting the corresponding potentiometer to a certain setting and then applying an input in *ETA*, corresponding to full throttle, to the controller. This was repeated until a full throttle input command resulted in the throttle valve being fully open

Calibration of the load cell (and therefore torque measurement) was done using calibration arms and a range of calibration weights as shown in Figure 36. The weights are loaded into a tray, located at a distance of exactly 1021 mm from the dynamometer centre, on the load cell side calibration arm. At this distance a weight of 1 kg results in a torque of 10 Nm exactly.

Figure 36: Load cell calibration

3.8 In-cylinder Pressure Measurement System

To measure and capture the pressure in the cylinder during combustion, very accurate and sensitive equipment is needed. The equipment that was purchased or sourced and the software program that was written are described in this section.

3.8.1 Components

The setup consists of the following:

- Two miniature AutoPSI-TC *Optrand* fibre optic pressure transducers
- A *NGK* TR15B-13 spark plug which was modified to allow installation of the *Optrand* transducers in the spark plug
- An uncooled *Kistler* 6117B piezoelectric transducer with a matching installation spark plug.
- An *AVL* Micro-IFEM charge amplifier.
- A *Kübler* 5020 incremental shaft encoder.
- A modified cylinder head to allow installation of the *Optrand* transducers directly in the combustion chamber.
- A *National Instruments* USB-6351 DAQ device with the appropriate software.

Full specifications of the pressure transducers, the shaft encoder and DAQ device (shown in Figure 37) are given in appendix C.3. All of the transducers were calibrated using a dead weight tester. The results from the calibration can be found in appendix C.1.

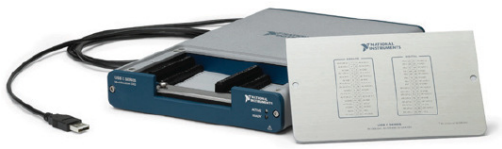

Figure 37: Data acquisition device (National Instruments, 2012)

a) *Optrand* pressure transducers

The *Optrand* fibre optic transducers (shown in Figure 38) that were purchased both have the same specifications. One of the transducers is installed in the modified spark plug and the other into the modified cylinder head. This allowed a comparison of the performance of the transducers in different measuring positions.

Figure 38: Optrand miniature pressure transducer

The spark plug used to install the *Optrand* transducers is a standard *NGK* TR15B-13 which was modified by *Optrand Inc.* A hole was firstly machined through the side of plug. This hole formed an indicating channel which was then fitted with an adaptor to allow installation of the *Optrand* transducers. The spark plug with the installed transducer is shown in Figure 39.

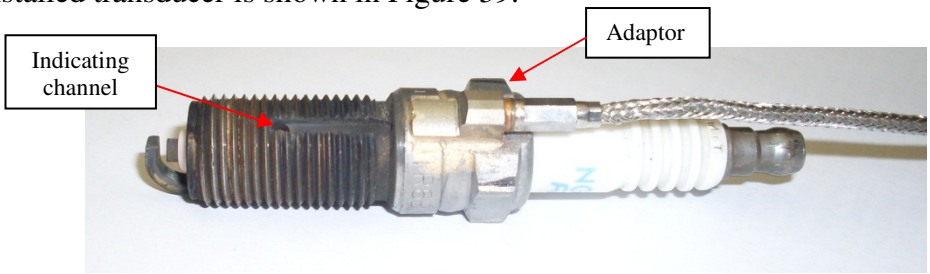

Figure 39: NGK modified spark plug with installed pressure transducer

b) *Kistler* pressure transducer

The uncooled *Kistler* pressure transducer that was used was installed in a purposely manufactured (by *Kistler*) spark plug. The spark plug with the installed transducer is shown in Figure 40. This transducer was connected to an *AVL* Micro-IFEM charge amplifier which converts the charge output from the transducer to a voltage.

According to the specifications of the *Kistler* and *Optrand* transducers, they should have similar performance during combustion pressure measurement. An in detail comparison of the actual performance of the transducers is however made in section 5.2.2.

Figure 40: Kistler spark plug with installed pressure transducer (Kistler, [S.a.])

c) Shaft encoder

The shaft encoder used in the project enables measurement of in-cylinder pressure every 0,1 ° of crankshaft rotation. The shaft encoder has six output channels namely A, B, Z and the inverse of each of these channels.

To enable coupling of the encoder to the engine's crankshaft, a hub was designed and manufactured. This hub bolts onto a modified crankshaft pulley. The alignment of the hub and crankshaft axis was adjusted using a dial gauge until the total run-out of the hub was less than 30 microns. Although this run-out was within the required specifications of the shaft encoder, a bellows coupling was used to connect the shaft encoder to the hub. This allowed for a larger tolerance of run-out between the hub and crankshaft axis as well as reduced vibration transfer to the encoder. The installed shaft encoder setup is shown in Figure 41.

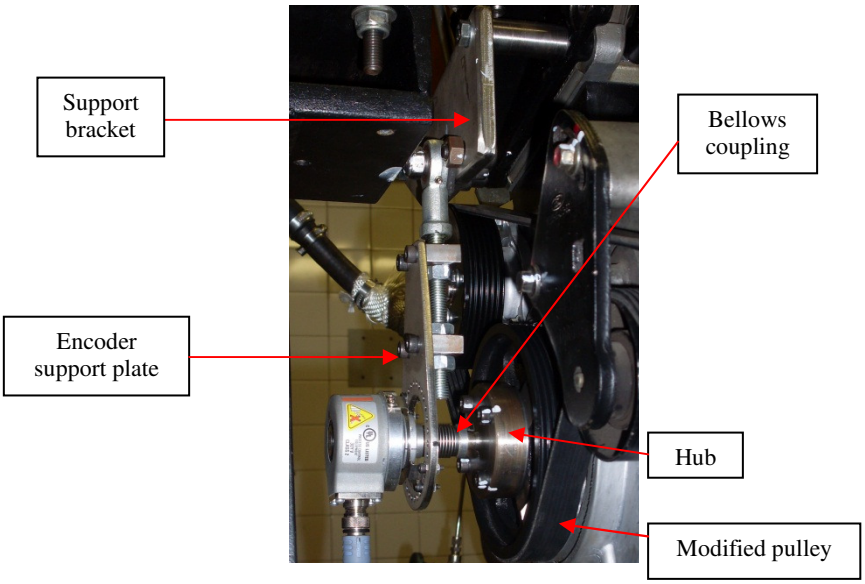

Figure 41: Shaft encoder setup

The shaft encoder is suspended by the *encoder support plate* shown in Figure 41 and Figure 42. This plate has two interface blocks bolted to it which are used to attach the plate to the support bracket using a threaded bar and a rod end. The rod end allows the shaft encoder to float to and fro (without rotation of the casing) while the engine is running and vibrating. This reduces both the load on the encoder bearings as well as the vibration transfer during engine operation.

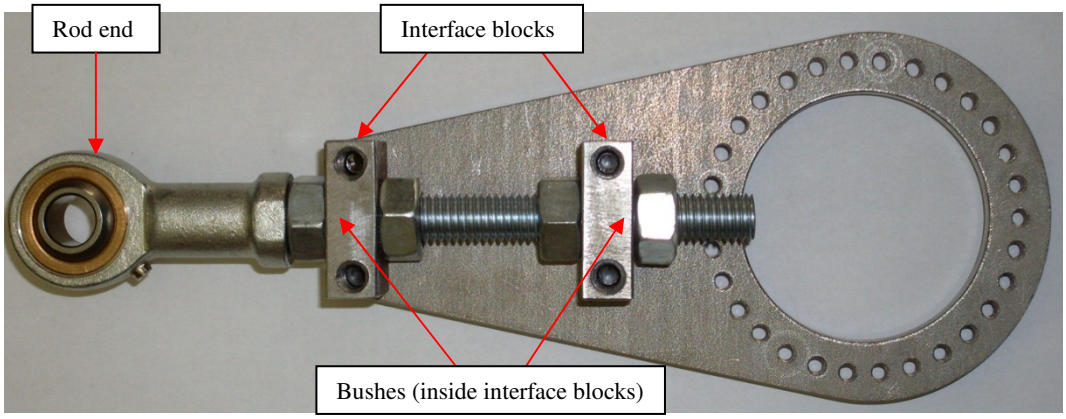

Figure 42: Encoder support plate rear view

A simple frequency analysis was done on the support plate and bracket assembly to determine whether any of its natural frequencies are within the speed range of the engine. The procedure that was used is described in appendix C.2. The analysis showed that none of the harmonics of the assembly are within the speed range of the engine.

d) Modified cylinder head

For installing one of the *Optrand* transducers in the combustion chamber of the engine, the final year project done by Kenny (2010) was used. The cylinder head from that project is shown in Figure 43 next to the standard cylinder head from this project.

In the figure it can be seen that a sleeve was installed in the cylinder head into which the transducer is then installed. The sleeve protrudes through oil and water galleries which were sealed off from each other using a *Loctite* sealant (Kenny, 2010). The transducer is installed in a threaded hole in the combustion chamber as can be seen in Figure 44.

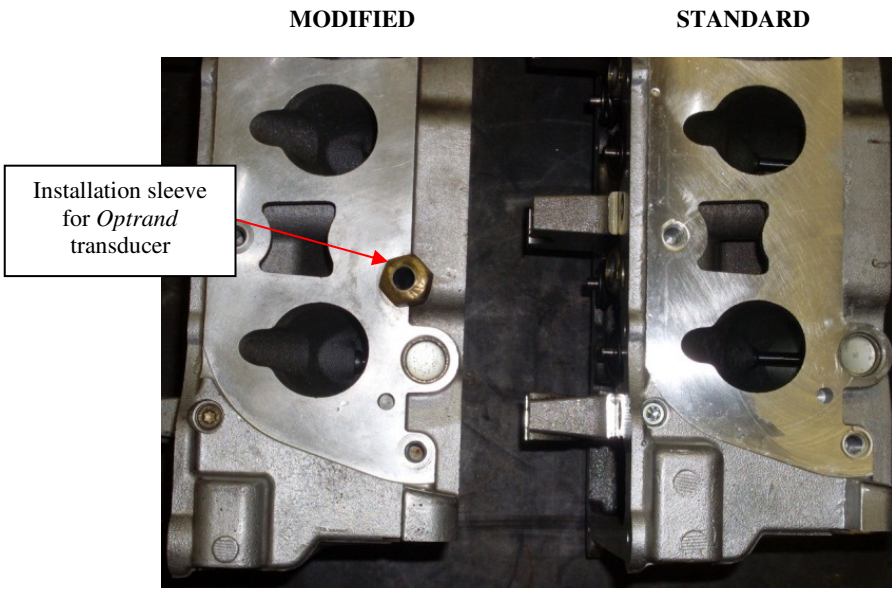

Figure 43: Side-by-side photograph of modified and standard cylinder head

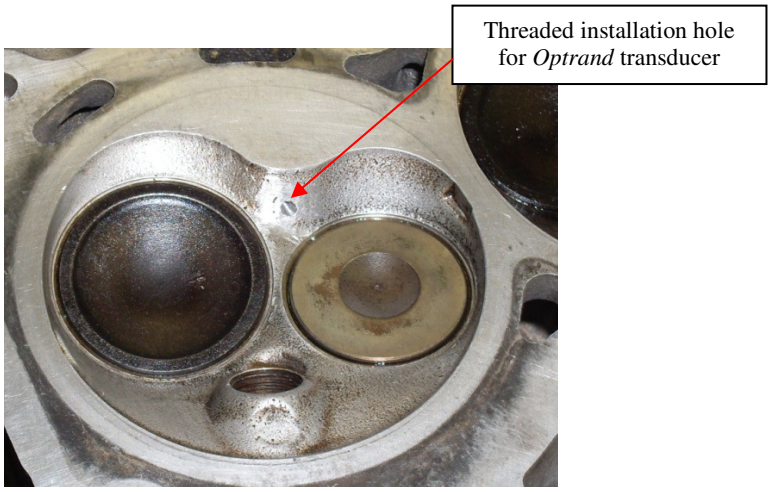

Figure 44: Combustion chamber of modified cylinder head

3.8.2 System wiring

The wiring of the shaft encoder and *Optrand* pressure transducers to the DAQ is shown in Figure 45. For clarity, wires that are white on the equipment is shown in yellow on the diagram. All the channel output wires from the shaft encoder were connected to allow access to all the channels during use.

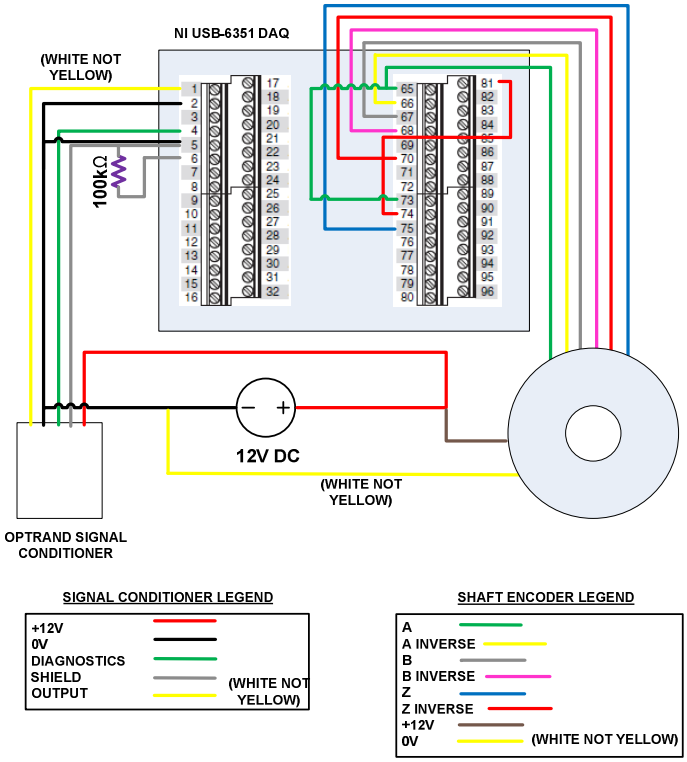

Figure 45: Indicating setup wiring

3.8.3 User interface

The software package that was used with the *National Instruments* DAQ is called *LabView*. Programming in *LabView* is done in two parts. Firstly, the main program is compiled by using a block diagram and secondly the user interface is developed. In the block diagram there are numerous functions that can be implemented. These functions can be interconnected to build a program called a virtual instrument that is user/task specific. The block diagram that was created for data capturing is shown in appendix D.2. while the user interface is shown in Figure 46.

When the program is switched to run mode, the DAQ starts reading the data from the pressure transducer every 0,1 ° of crankshaft rotation. The pressure trace that is captured is then showed on the graph on the front panel. The pulse on channel Z of the encoder is used as the starting point for data capturing. When the encoder was installed on the engine, this trigger pulse was tuned to coincide as closely as possible with TDC of cylinder number one of the engine.

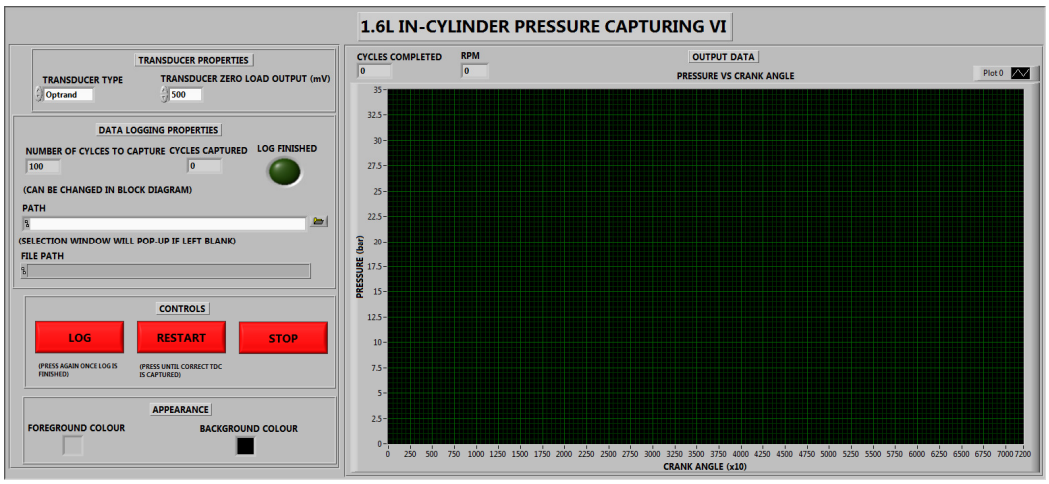

Figure 46: Indicating setup user interface

Due to two trigger pulses occurring in one full four stroke cycle, the pressure measurement may start at the incorrect TDC point. For the project the intake stroke TDC point was used as the starting point and therefore a method was needed to ensure that the correct TDC is picked up. To achieve this, a *RESTART* button was placed on the front panel which will restart the measurement at the other TDC point when it is activated. The *STOP* button will abort the virtual instrument once it is pressed.

Once the correct TDC signal has been captured, the data can be logged for a specified number of cycles using the *LOG* button where one cycle is equal to two crankshaft revolutions. Once all the cycles have been logged a window is provided allowing the user to select the file for saving the data. The number of cycles that are logged can be selected as per the user requirements.

3.9 Emissions Equipment and Measurement

When comparing the performance of different fuels, comparisons between the emissions from the fuels are very important. For this purpose a *Bosch* ETT 855 exhaust gas analyser (shown in Figure 47) was purchased and installed on the test setup. This analyser uses an infrared absorption technique to (within 1 % accuracy) measure the following:

1. Volume percentage O_2 present in the sample,
2. Volume percentage CO present in the sample,
3. Volume percentage CO_2 present in the sample, and
4. The parts per million (ppm) of HCs present in the sample.

Figure 47: Bosch ETT 855 exhaust gas analyser

From measurement 1 to 4 the analyser is able to calculate a lambda value for the exhaust gas sample.

The analyser requires two gas samples namely exhaust gas and fresh air. Fresh air is supplied to the analyser from another test cell to ensure that no exhaust gas enters this line. The exhaust gas sampling point is located directly in the engine's exhaust system just before the first noise damper (silencer).

Condensation which forms in the exhaust gas supply line to the analyser can damage the analyser. It was therefore decided to install a chiller unit in the line as recommended by *Bosch*. This unit cools down the gas and then separates the condensate before it can reach the analyser. It was however recognised that cooling of the exhaust gas sample could cause some of the HCs to condense before they reach the analyser. For this reason it is recommended that a heated line be installed from the engine's exhaust to the gas analyser. This line should typically be kept at temperatures higher than 100 °C. (Williams, 1997)

4. System Fault Finding

Before the system could be commissioned it had to be tested for reliability, accuracy and repeatability. During these tests any major issues in the setup could be identified and rectified. In this section these issues and their solutions will be discussed.

Issues that were identified during installation of the equipment and initial repeatability testing included:

- Faulty or incorrect controllers
- *AVL* fuel flow unit calibration problems
- Vibrations of the shaft encoder
- Drive shaft imbalance
- Leaking pressure transducer spark plug
- Insufficient dynamometer cooling
- Excessive noise on thermocouple readings
- Low air-fuel ratios at high loads

The most significant of these issues were the calibration problems of the *AVL* fuel flow unit, the excessive drift of the *Kistler* pressure transducer and the insufficient dynamometer cooling.

4.1 Fuel Flow Meter Calibration

Initial calibration of the *AVL* flow meter did not result in an accuracy of 0,1 g as prescribed by the manufacturer. The calibration procedure is done by lowering a 100 g weight onto the measuring vessel and then lifting off. Once the weight is lifted completely off the vessel the display on the control unit should indicate a change in mass of exactly 100 ± 0,1 g. If this is not the case, potentiometers on the circuit board in the *AVL* unit can be adjusted until the correct tolerance is achieved. This has to be done with the vessel empty, full and half full.

With the initial calibration the following values could be achieved for an empty, half full and full vessel:

- Empty = 100 g
- Half full = 100,1 g
- Full = 89 g

The calibration value with a full vessel could not be adjusted to within the range as specified. It was assumed that the fault was mechanical and not electrical as accurate values could be obtained for two of the points. The *AVL* unit was therefore examined for any problems which could have an effect on the calibration.

It was found that the flexible pipes which supply the vessel with fuel were distorted. These pipes flex when the vessel is displaced and can therefore have an effect on the calibration. An attempt was made to straighten the pipes which improved the calibration only by a small percentage.

Another issue that was identified was that the damping oil level in the unit was lower than specified by the manufacturer. This oil fills the damping cylinder which is attached to the opposite end of the beam which supports the measuring vessel. The function of the cylinder is to prevent the vessel from oscillating excessively and causing an error in the fuel flow reading. The oil was therefore filled to the specified level which solved the calibration issue. The following values were recorded:

- Empty = 100,1 g
- Half full = 100,1 g
- Full = 100 g

4.2 Kistler Pressure Transducer Drift

During calibration of the *Kistler* pressure transducer, excessive drift was observed on the signal from the charge amplifier. Another charge amplifier of the same type (*Kistler* model 5001) was then used which gave similar results. The transducer cable was then removed from the transducer located in the spark plug.

An oil build-up was found in the installation socket in the spark plug. This oil was removed and the connections cleaned. The transducer and cable were then baked in an oven for 10 hours at 65 °C. When the transducer was then retested the drift appeared to be less, but still not sufficiently reduced to obtain a calibration curve.

It was then decided to use a different model charge amplifier, namely an *AVL* Micro-IFEM charge amplifier, which significantly reduced the drift of the transducer. A calibration curve could then be obtained and the sensitivity of the transducer calculated. The *Kistler* amplifier is an older model and it was therefore suspected that it is not compatible with the newer model pressure transducer.

4.3 Dynamometer Cooling

The engine that was used for the project was new and it therefore had to undergo a break-in test. During this test it was found that the dynamometer cooling water outlet temperature, from the front loss plate, exceeded 60 °C when running at 40 kW or higher. This was a concern as the rated engine power is 70 kW and the dynamometer cooling water temperature may not exceed 60 °C. The flow rate through each side of the dynamometer was then measured and it was found that the flow rate through the rear cooling chamber was more than double that of the front cooling chamber.

To improve the flow rate (and therefore the convective heat transfer coefficient) the dynamometer was flushed with a 3.5 pH acid solution in order to break down an assumed scale build-up in the cooling chambers. The acid that was used is hydrochloric acid which was mixed with water on a volumetric basis. A special funnel and outlet pipes had to be manufactured to enable flushing of the dynamometer. The funnel and outlet pipes are shown in Figure 48.

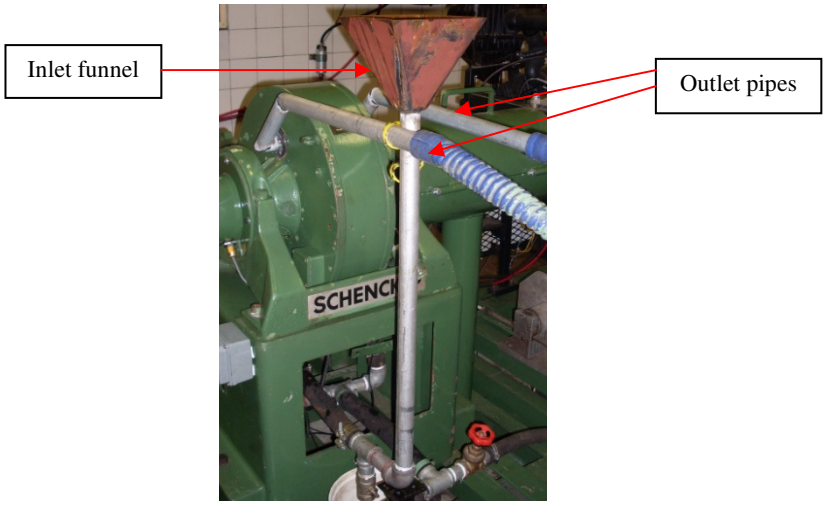

Figure 48: Adaptors for flushing dynamometer

The flushing process did not sufficiently clear the blockage and it was therefore decided to disassemble the dynamometer and manually clean the cooling chambers. Photographs of one of the loss plates, before and after cleaning, are shown in Figure 49.

BEFORE **AFTER**

Figure 49: Loss plates before and after cleaning

After reassembly the rotor and bearing clearance of the dynamometer had to be adjusted to within the tolerance specified by the manufacturer. This was done by using the adjustment nuts/sleeves on the dynamometer and a dial gauge. The rotor was set to a distance exactly half way between the two loss plates while the bearing clamping sleeve was set to a clearance of 0,1 mm. The full assembly procedure can be found in the *Schenck* dynamometer manual.

The dynamometer was then re-installed and run-in on the test setup. Running-in the dynamometer had to be done to allow the bearings to displace excess grease into galleries which ensured that the bearings did not overheat and seize. During the run-in the bearing temperatures were monitored using an infrared thermometer. The maximum bearing temperatures that were measured in the bearing housing was 41 °C.

Once the run-in was completed and the bearings settled, the engine was brought up to 40 kW. At this load point the dynamometer water outlet temperatures were below 25 °C and it was therefore concluded that cleaning of the cooling chambers improved the flow rate (and therefore heat transfer coefficient).

After the run-in procedure the engine was run at wide-open-throttle to determine the maximum torque and rated power of the engine. Maximum uncorrected torque and power that was measured is 132 N·m and 70 kW respectively which meets the performance requirements of the manufacturer (see appendix A.2.). After the test was completed a torque curve for the engine was plotted, which is shown in Figure 50.

5. Testing and Results

The main objective of the project was to develop a repeatable fuel testing facility. This was therefore the main focus during the test phase of the project. Repeatability of the engine and dynamometer setup as well as the in-cylinder pressure measurement setup was examined.

Apart from developing a repeatable test facility the project also investigated the effect on the measured in-cylinder pressures when using different measuring positions in the combustion chamber. Furthermore, a comparison was also made between different in-cylinder pressure transducers.

The details and results of the above mentioned tests are described in this chapter. All of the instrumentation was checked for calibration before the tests were done to ensure the best possible accuracy.

5.1 Repeatability Testing

For the project a set of partial load testing points were selected according to the performance of the selected engine in a motor vehicle. Estimated performance of the engine while driving at 60 km/h and 120 km/h in different gears was calculated using the procedure given in appendix B.1. At 60 km/h it was calculated that the engine produces approximately 30 N·m at a speed of 2300 rpm in 4th gear and at 120 km/h (in 5th gear) an approximate load and speed of 75 N·m and 3600 rpm was calculated.

An array of partial load test points, shown graphically in Figure 50, was then selected starting and ending at a load and speed of 30 N·m and 2300 rpm. The specific points were chosen to allow a repeatability analysis of the system over a range of engine operating conditions.

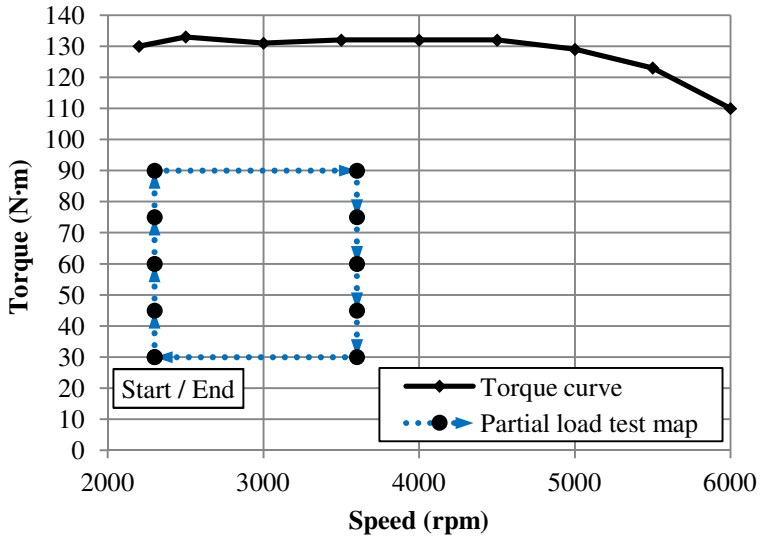

Figure 50: Partial load testing points

The partial load points were then used to program an automated test sequence in *ETA*. Initially data was logged for a duration of 3 minutes which was found to be insufficient time for the exhaust gas temperature to stabilize. Logging time was then increased to 8 minutes which resulted in steady-state exhaust gas temperatures.

5.1.1 Engine and dynamometer setup

Parameters that were used to measure the repeatability of the engine and dynamometer system were BSFC, exhaust gas temperature and lambda. The repeatability curves are shown in Figure 51 to Figure 53. In the figures it can be seen that minimal differences in the results were obtained for test 1 and 2 (see appendix G for test results). The average percentage differences that were obtained for BSFC and lambda are 0,8 % and 0,35 % respectively. Exhaust gas temperature results showed a difference of 1,2 °C (on average) between the two tests.

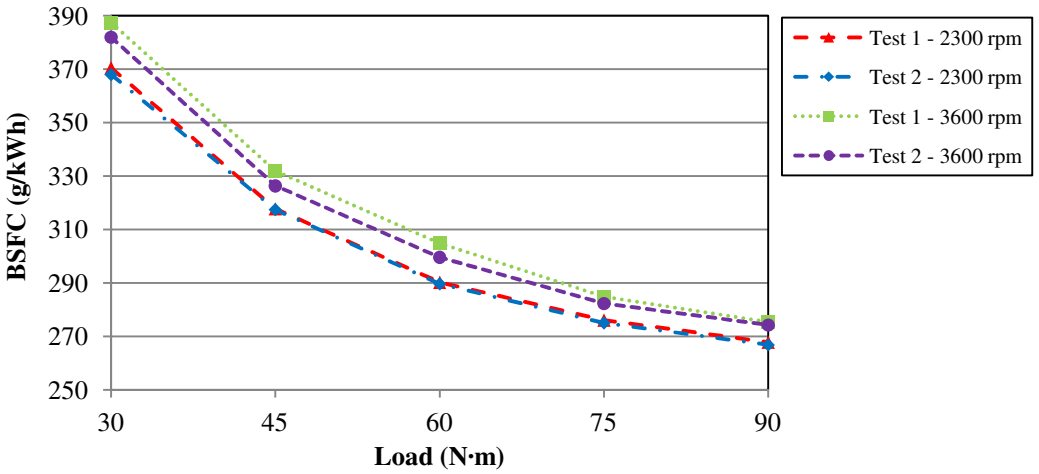

Figure 51: BSFC repeatability

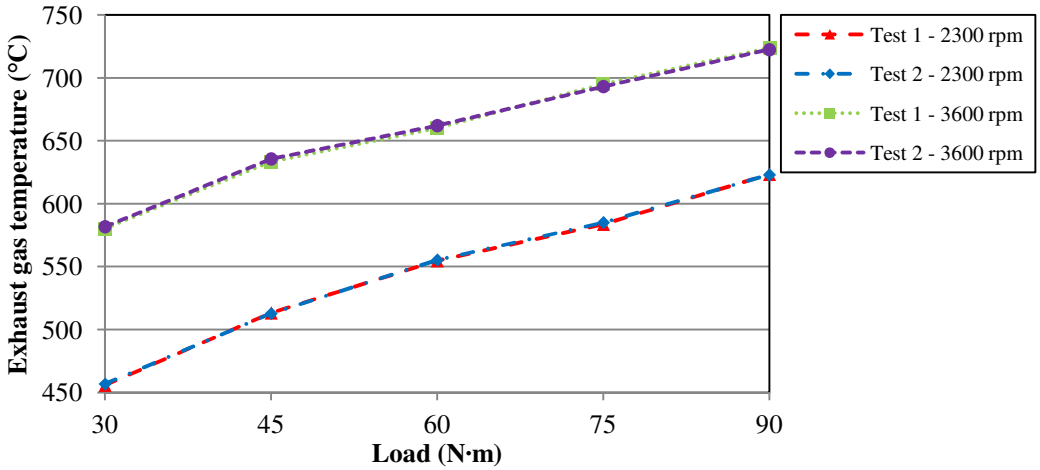

Figure 52: Exhaust gas temperature repeatability

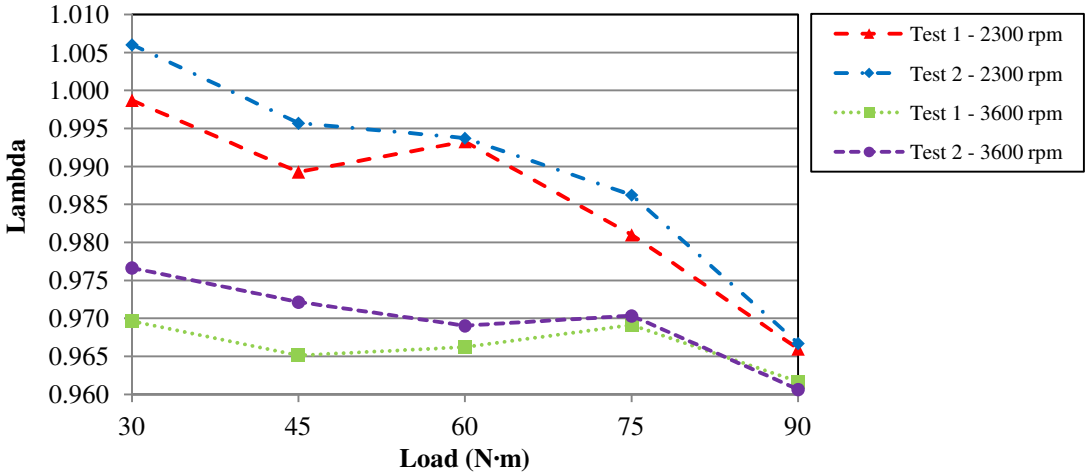

Figure 53: Lambda repeatability

Although the engine is fitted with a lambda sensor to enable closed loop lambda control, the engine did not run at the stoichiometric point of lambda equal to 1 (as can be seen in Figure 53). It was therefore concluded that the engine was run with the ECU in open loop control mode. This was confirmed and monitored using an *Autel* Autolink AL309 OBD-II code reader.

5.1.2 In-cylinder pressure measurement setup

For in-cylinder pressure measurements, cylinder number 1 of the engine was used for reasons described in section 2.5.2. Before the pressure curves could be plotted, the pressure values had to be properly phased and referenced. This was done by plotting hot motoring log P - log V curves and then adjusting the phasing until the conditions described in section 2.5.4 were met.

Referencing was done using the measured intake MAP at IVC. Absolute intake manifold pressure was measured using an engine diagnostics device which displays the reading from the MAP sensor. The accuracy of the MAP sensor was tested using a *WIKA* reference pressure gauge. It was found that the MAP sensor is sufficiently accurate for referencing of the in-cylinder pressure values.

The indicating setup was tested for repeatability using an *Optrand* pressure transducer and the modified spark plug by capturing 100 consecutive engine cycles at each test point. This large amount of cycles was needed in order to reduce the noise on the pressure curve by taking an average over all the captured cycles. The amount of cycles typically captured for in-cylinder pressure measurement is 100 or more cycles.

Note that pressure is given in bar to be consistent with curves found in the literature. Furthermore, for comparison purposes, the pressure in Figure 54 was referenced to 0,3 bar gauge pressure at 30 ° crank angle after TDC (ATDC) during the intake stroke.

For the tests that were done in this section, the 2300 rpm at 30 N·m and 3600 rpm at 90 N·m were used as these were the lowest and highest loads tested during the project. The curves obtained for in-cylinder pressure vs. crank angle are shown Figure 54. The figure shows no significant difference in the results from test 1 and 2 and therefore indicates good repeatability of the system.

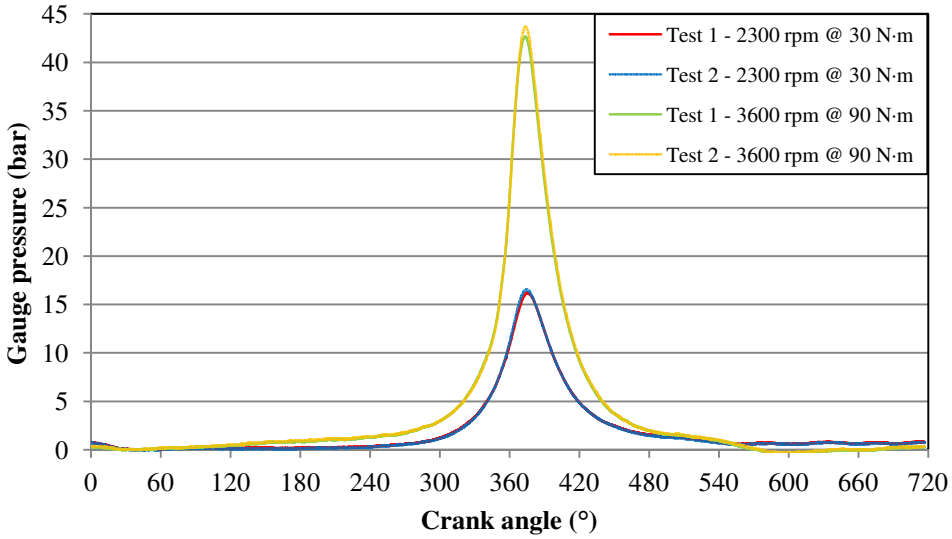

Figure 54: Optrand: In-cylinder pressure vs. crank angle

The pressure vs. volume curves that were obtained are shown in Figure 55 and Figure 56. To determine the repeatability of these curves, calculation of the net IMEP values were used. However, to ensure accurate IMEP calculations the clearance volume of the engine in cylinder number 1 first had to be measured. This was done by measuring the volume of the combustion chamber in the cylinder head as well as the volume on top of the piston at TDC using a digital burette. A number of measurements were made after which an average was calculated for the clearance volume. The results from the measurement (as well as other engine specifications) can be found in appendix A.2.

The results from the net IMEP calculations are given in Table 1.

Table 1: Optrand net IMEP repeatability

		Net IMEP (bar)		
Speed (rpm)	**Load (N·m)**	**Test 1**	**Test 2**	**% difference**
2300	30	2,69	2,74	1,8
3600	90	6,46	6,63	2,6

The difference between the load points at 2300 rpm indicated better repeatability than the load points at 3600 rpm. This is due to thermal effects on the transducer at high load points which will be discussed in more detail in section 5.2.2. Similar results were obtained with the other available *Optrand* transducer.

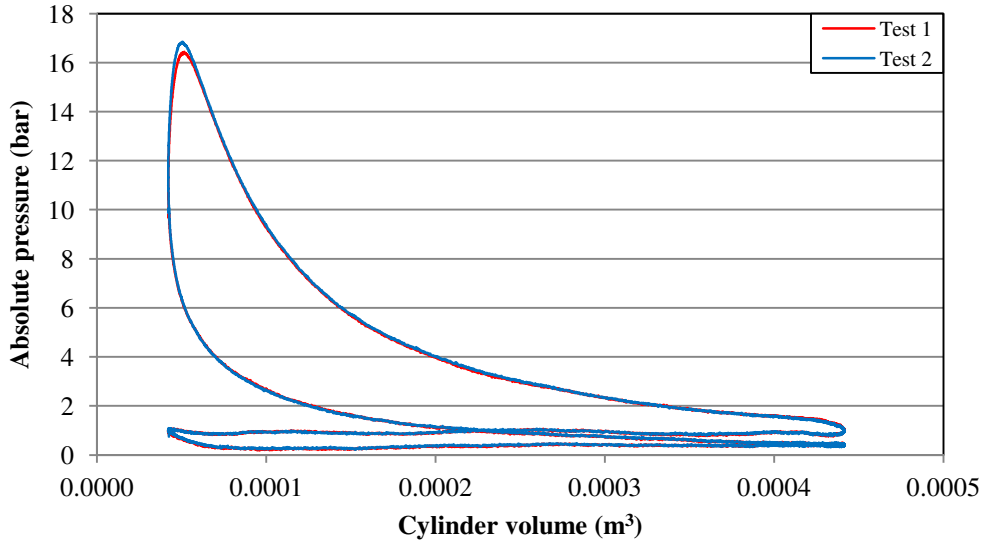

Figure 55: Optrand: In-cylinder pressure vs. volume (2300 rpm @ 30 N·m)

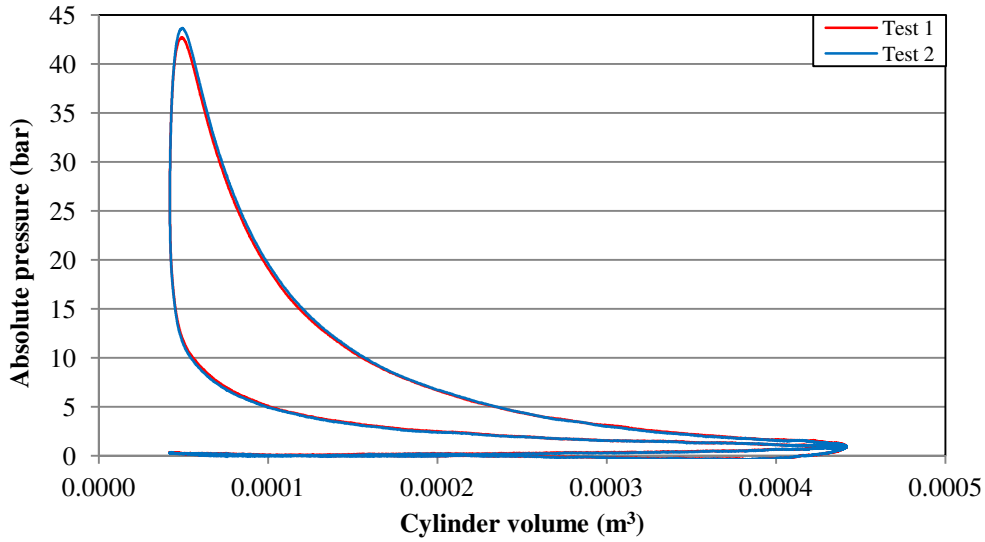

Figure 56: Optrand: In-cylinder pressure vs. volume (3600 rpm @ 90 N·m)

The *Kistler* transducer was then installed in an attempt to increase repeatability of the indicating setup at high load points. The pressure versus volume curves that were obtained for 3600 rpm @ 90 N·m are shown in Figure 57. From the curves a net IMEP of 8,04 bar and 7,96 bar was calculated for test 1 and 2 respectively. This translates into a percentage difference of 1,0 % which is a significant improvement over the *Optrand* transducers.

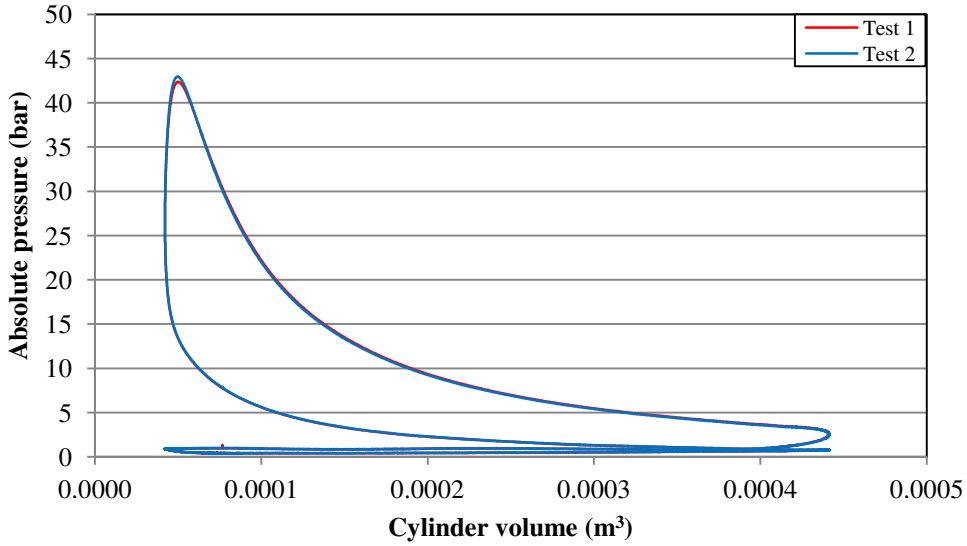

Figure 57: Kistler: In-cylinder pressure vs. volume (3600 rpm @ 90 N·m)

5.2 In-cylinder Pressure Measurement Comparisons

The effect of using different in-cylinder pressure measuring positions on the measured pressures was studied using the modified spark plug and the modified cylinder head. An *Optrand* transducer was installed in each of these positions and not removed for all the pressure comparison testing that was done. This ensured that the compression ratio remained the same for each pressure trace captured.

Furthermore, the performance of the *Optrand* transducers was compared to that of the *Kistler* transducer. For these tests the modified spark plug (with the attached *Optrand* transducer) was removed from the engine and the *Kistler* spark plug (with the attached *Kistler* transducer) installed.

The captured pressure values were again referenced and phased using a hot motoring curve. However, for comparison purposes, the pressure in Figures 58, 62 and 64 was referenced to 0,3 bar gauge pressure at 30 ° ATDC during the intake stroke.

5.2.1 Measuring position comparison: Optrand vs. Optrand

When using the modified spark plug, the in-cylinder pressures are measured in an indicating channel (see section 3.8.1). This is expected to cause more acoustic noise than when the measuring position in the modified cylinder head is used where the measuring position is directly in the combustion chamber.

The measuring position in the modified cylinder is however closer to the combustion and directly over the piston bowl. This will cause higher heat flux on the pressure transducer than with the spark plug measuring position. It is therefore expected that thermal effects on the transducer will be more significant when using the measuring position in the cylinder head. (AVL, 2002)

a) In-cylinder pressures and IMEP

According to AVL (2002), pressure in the combustion chamber is not uniform and therefore the use of different measuring positions should produce different measured pressures. The pressure vs. crank angle curves that were obtained at the two measuring positions used, for 2300 rpm @ 30 N·m as well as 3600 rpm @ 90 N·m, are shown in Figure 58. As can be seen from the figures, the spark plug mounted transducer measured a lower combustion and expansion pressure than the cylinder head installed transducer. The differences in pressure readings therefore corresponded to the literature. These differences can be seen more clearly in Figure 59 and Figure 60.

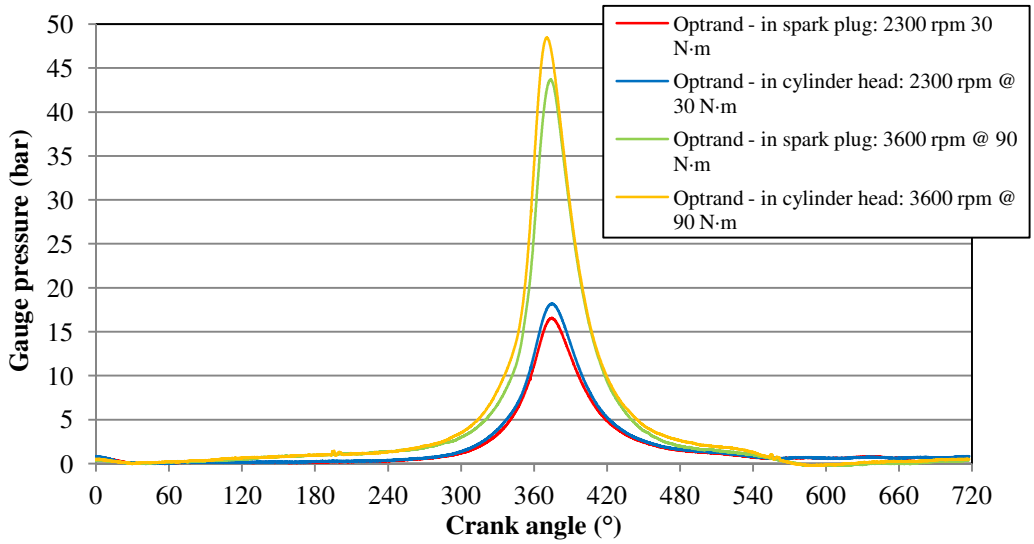

Figure 58: Position comparison: Pressure vs. crank angle

The mean effective pressures obtained at the different measuring positions are given in Table 2.

Table 2: Mean effective pressures obtained with Optrand transducers

			$IMEP_{net}$ (bar)		$IMEP_{gross}$ (bar)		FMEP (bar)	
Speed (rpm)	**Load (N·m)**	**BMEP (bar)**	**Spark plug**	**Head**	**Spark plug**	**Head**	**Spark plug**	**Head**
2300	30	2,36	2,74	2,95	3,19	3,44	0,38	0,59
3600	90	7,08	6,63	6,71	6,31	6,50	-0,45	-0,37

The effect that the difference in measured pressure, between the two measuring positions, had on the net IMEP calculation was significant. The net IMEP, for the 2300 rpm point, calculated from the cylinder pressures obtained with the spark plug installed transducer was 7,4 % lower than the cylinder head installed transducer.

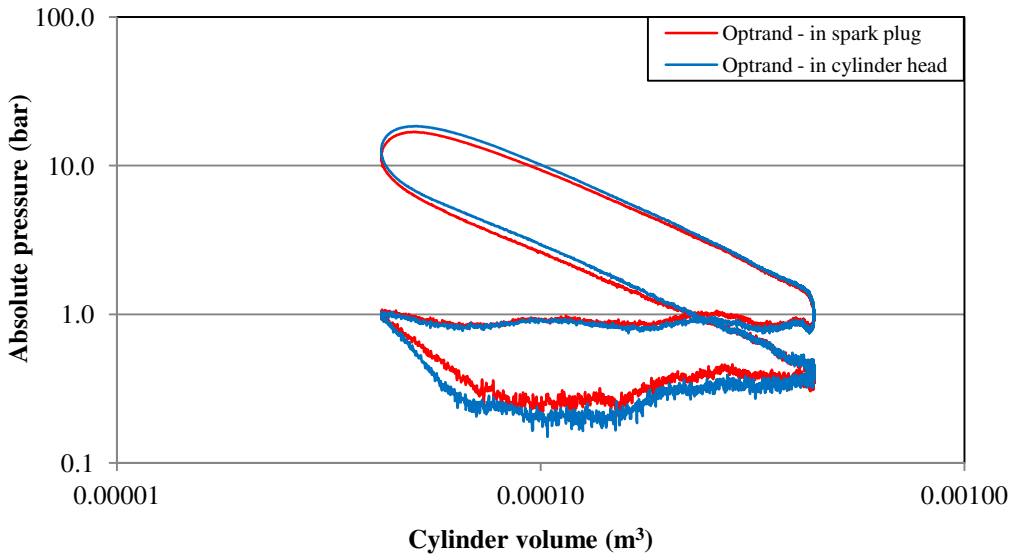

Figure 59: Position comparison: log P - log V (2300 rpm @ 30 N·m)

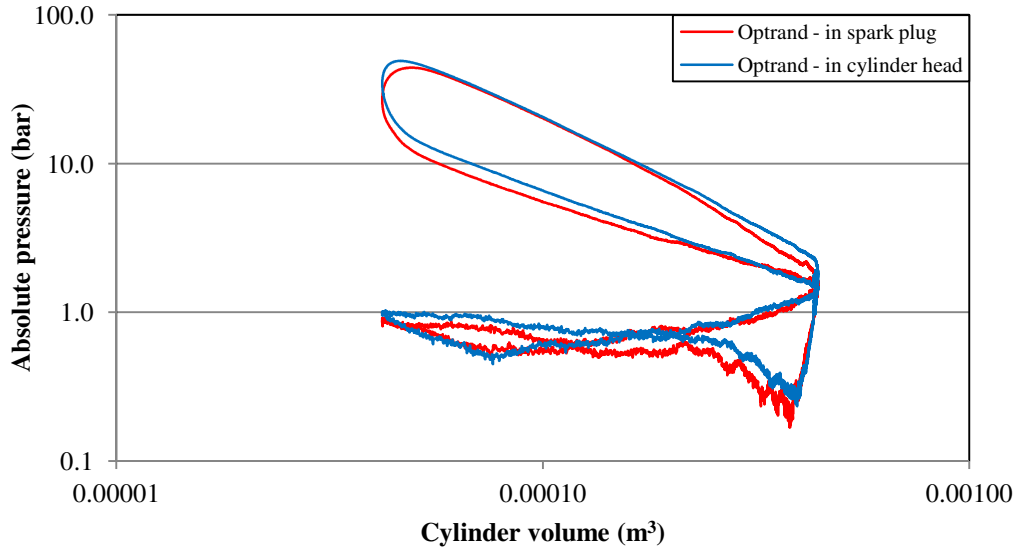

Figure 60: Position comparison: log P - log V (3600 rpm @ 90 N·m)

An anomaly was however found with the calculated net IMEP values for the 3600 rpm point at both measuring positions. The net IMEP values were found to be lower than the corresponding BMEP values for both measuring positions. This results in a negative FMEP which is not possible.

The gross IMEP values were also found to be lower than the net IMEP values implying negative pumping work which is also not possible for a naturally aspirated engine. It was therefore suspected that the *Optrand* transducers are not sufficiently accurate under the influence of high heat flux.

b) Noise on pressure curve

Due to the indicating channel (in the spark plug) acting as an acoustic resonator, it was expected that more noise would be present on the pressure curve measured using the spark plug installed transducer than for the cylinder head installed transducer. One captured cycle at each position was therefore plotted to enable comparison of the noise levels. These curves are shown in Figure 61 and they indicate slightly higher amplitudes in noise when using the spark plug installation position.

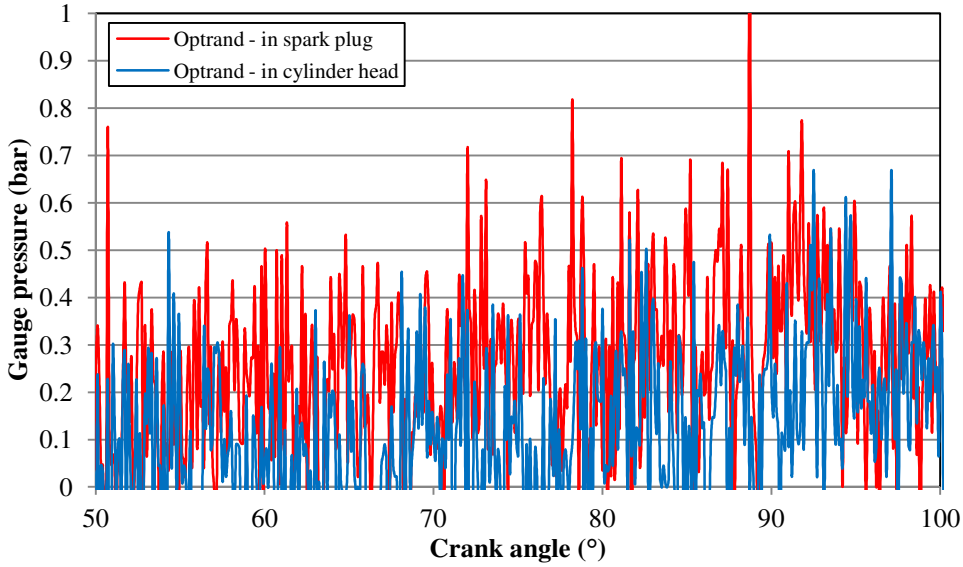

Figure 61: Position comparison: Noise (3600 rpm @ 90 N·m)

c) Effect of high heat flux

Analysis of the effect of the heat flow load on the transducers at the different measuring positions could be done by plotting pressure versus volume on a log scale. For this purpose the 3600 rpm @ 90 N·m point was used. The curves that were obtained are shown in Figure 60 where a cross over between the intake and exhaust stroke pressure can be seen for both measuring positions. This is incorrect as the exhaust stroke pressures should be higher than the intake stroke pressures for naturally aspirated engines. This phenomenon is known as the bow tie effect and it is caused by thermal processes on the transducers (Lancaster et al., 1975).

The effects of high heat flow loads at points greater than 20 kW could also be seen on the real-time pressure curves while running the engine. At these points the pressure curve continuously shifted vertically between each individual cycle. It was therefore suspected that the *Optrand* pressure transducers were not sufficiently accurate for high load testing.

5.2.2 Transducer comparison: Optrand vs Kistler

The same analysis that was described in section 5.1.1 was repeated for comparing the performance of the *Kistler* to that of the *Optrand* transducers. The *Kistler* transducer was also installed in cylinder number 1 of the engine and the same testing points were used.

a) In-cylinder pressures and IMEP

The pressure vs. crank angle curves that were obtained (for 2300 rpm @ 30 N·m) with the *Kistler* transducer are shown in Figure 62 along with those obtained from the *Optrand* transducers. From the figure it can be seen that the *Kistler* and the spark plug installed *Optrand* transducer corresponds closely during the full 720 ° cycle due to the similarity of the measuring positions of the two. In comparison to the cylinder head installed transducer the *Kistler* measured a lower peak pressure. The difference in measured pressures can also be seen on the pressure vs. volume curves (on log scales) shown in Figure 63.

The values and positions of peak pressures obtained with the *Optrand* and *Kistler* transducers are given in Table 3 while the calculated IMEP and FMEP values are given in Table 4.

Table 3: Comparison of peak pressure values and positions

		***Optrand* - spark plug**	***Optrand* - in head**	***Kistler***
Speed (rpm)	**Load (N·m)**	**Peak pressure values (gauge pressure in bar)**		
2300	30	16,54	18,19	16,08
3600	90	43,64	48,38	41,94
		Positions of peak pressures		
2300	30	14,6 ° ATDC	14,8 ° ATDC	17 ° ATDC
3600	90	13,6 ° ATDC	10,4 ° ATDC	14,3 ° ATDC

Table 4: Mean effective pressures obtained with Kistler transducer

Speed (rpm)	**Load (N·m)**	**$IMEP_{net}$ (bar)**	**$IMEP_{gross}$ (bar)**	**PMEP (bar)**	**FMEP (bar)**
2300	30	2,94	3,41	0,47	0,58
3600	90	8,05	8,46	0,41	0,97

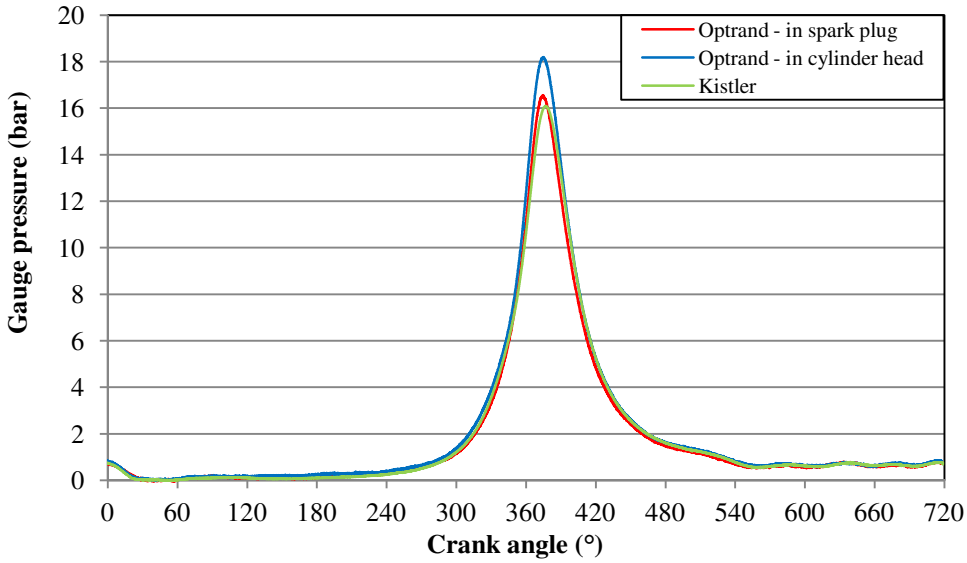

Figure 62: Transducer comparison: Pressure vs. crank angle (2300 rpm @ 30 N·m)

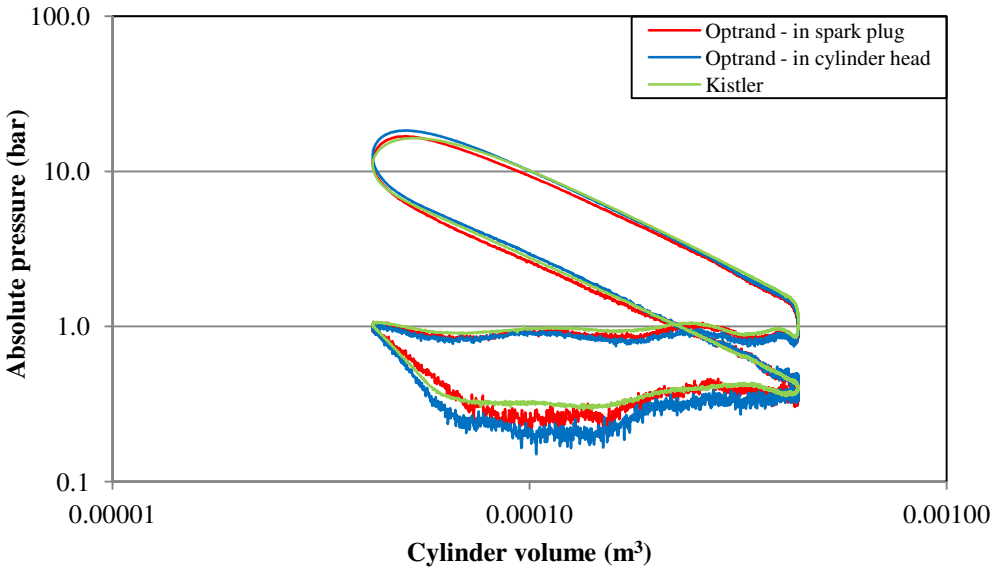

Figure 63: Transducer comparison: log P - log V (2300 rpm @ 30 N·m)

At the higher load conditions however the *Kistler* outperformed the *Optrand* transducers as is shown in Figure 64 and Figure 65. From these curves it could be seen that the *Kistler* did not measure lower exhaust stroke than intake stroke pressures as was found with the *Optrand* transducers. Calculation of IMEP values with the *Kistler* also gave better results and repeatability (see section 5.1.2) than its fibre optic counterparts. As can be seen from Table 4, positive FMEP and PMEP values were obtained using the pressure measurements from the *Kistler* transducer.

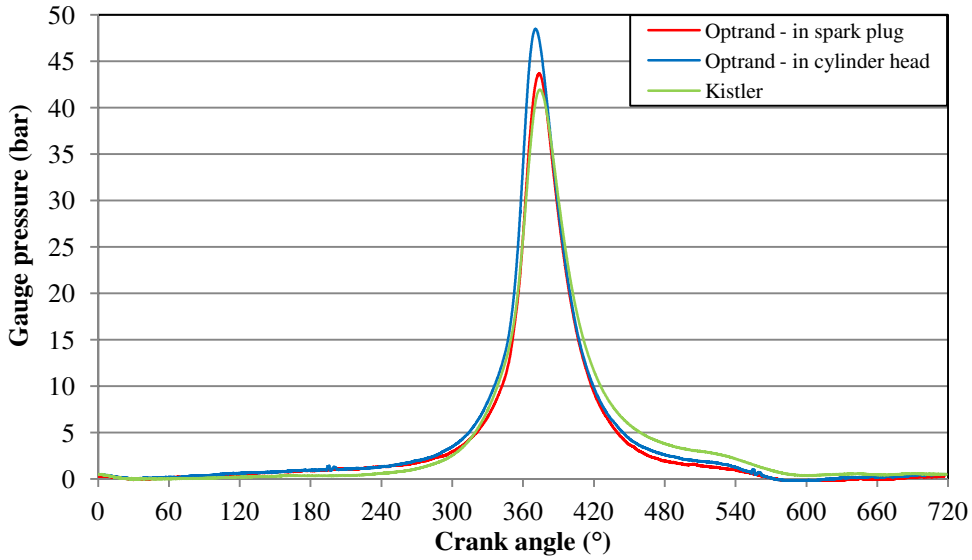

Figure 64: Transducer comparison: Pressure vs. crank angle (3600 rpm @ 90 N·m)

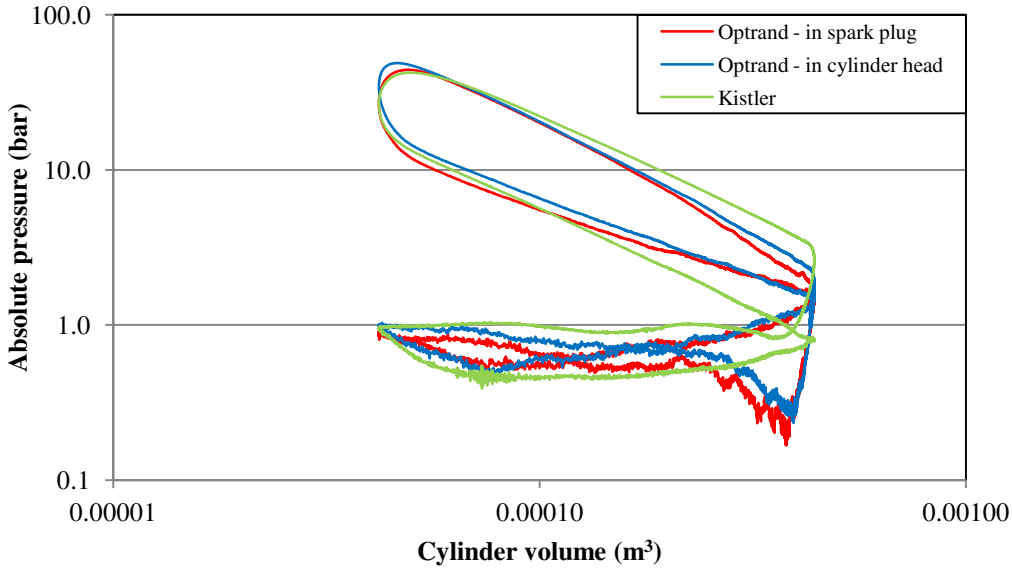

Figure 65: Transducer comparison: log P - log V (3600 rpm @ 90 N·m)

b) Noise on pressure curve

Another improvement of the pressure curves obtained with the *Kistler* transducer over the *Optrand* transducers is less amplitude in noise. This is due to the higher sensitivity of the *Kistler* transducer. The sensitivities of the transducers are:

- *Kistler* = 49 mV/bar
- *Optrand* = 14 mV/bar

In Figure 66 the differences in noise captured by the transducers can be seen.

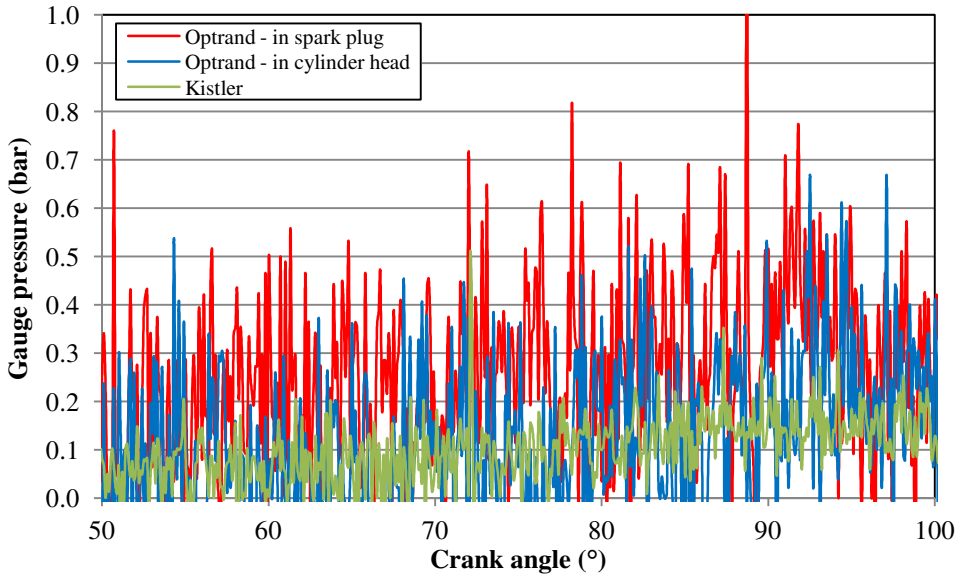

Figure 66: Transducer comparison: Noise (3600 rpm @ 90 N·m)

c) Effect of heat flux

The possible reason for the better performance of the *Kistler* at the higher load points is that the thermal effects are less than with the *Optrand* transducers. This can be seen in Figure 65 which shows the log P - log V curves for the three transducers. In the figure it can be seen that the bow tie effect does not occur when using the *Kistler* transducer.

Furthermore, the figure shows that the compression and expansion lines are linear with the *Kistler* transducer which is not the case with the *Optrand* transducers. The compression and expansion strokes can be approximated as a polytropic process and straight lines are therefore expected when plotted on log scales. Deviations from straight lines is frequently due to thermal effects on the transducers (Lancaster et al., 1975).

The polytropic exponent that was obtained for the expansion stroke, using the *Kistler* pressure data, is 1,3. This is consistent with literature which recommends a value of 1,3 [± 0,05] (Heywood, 1988).

5.2.3 Summary of findings

In summary the following differences were found between the two measuring positions using the *Optrand* transducers:

1. The position in the cylinder head produced higher combustion and expansion pressure readings than the spark plug position,
2. The calculated IMEP is higher when calculated using the pressure measured directly in the combustion chamber,

3. The amplitude in noise present on the pressure traces captured through the spark plug were slightly higher than through the cylinder head, and
4. Cross over of exhaust stroke and intake stroke pressures occurring due to thermal effects on the transducer are experienced at both measuring positions.

The comparison between the *Kistler* and *Optrand* pressure transducers showed the following:

1. The *Kistler* transducer is not severely affected by high heat flux as is the case with the *Optrand* transducers,
2. The pressure traces from the *Optrand* transducers did not produce straight lines (on the log P- log V curves) for the compression and expansion strokes whereas the *Kistler* transducer did, and
3. The noise on the pressure trace was less with the *Kistler* transducer than with the *Optrand* transducers.

5.3 Petrol and Petrol-Ethanol Blend Testing

To complete one of the project objectives, the engine had to be run on a petrol-ethanol blend. For the tests a blend, by volume, of 90 % unleaded petrol 95 RON (ULP 95) and 10 % ethanol was used. This blend is referred to as E10 in the automotive industry. The same automated partial load test procedure described in section 5.1 was used to study the effect of the ethanol addition. This test was executed twice for the E10 blend to check for repeatability.

Before and after the E10 blends were tested, a test was done with pump ULP. These tests are referred to as the bracket tests and they were done to check whether any change in the system occurred during the E10 tests. The results from the bracket tests were also used to plot the repeatability curves in section 5.1.1. Samples of the fuels that were used in the project were analysed by *Intertek South Africa.* The results from these tests and details of the ethanol are given in appendix F.

5.3.1 Engine performance comparison

For the project the engine was only tested under partial load conditions and therefore the effect on maximum torque and power when using E10 could not be evaluated. However, the lower energy content of the ethanol implied that a difference should be seen in the fuel consumption (and therefore BSFC) between ULP and E10 during partial load testing. When the ECU is using closed looped control it is expected that the fuelling will increase when the fuel is switched from ULP to a blend of petrol and ethanol.

It was however found that during the bracket and the E10 tests the ECU used open loop control implying that it determines the amount of fuelling according to set values in its *map*.

This implied that if the throttle setting (set by the PLC) at the different test points were the same for both fuels, the fuel flow rate will not change. The throttle set point (and therefore fuel consumption) did however increase slightly for the E10 blend.

The results that were obtained for BSFC and exhaust gas temperatures using E10 are shown in Figure 67 and Figure 68 along with the average results obtained during the bracket tests. The figures show a slight increase in BSFC for the E10 and similar exhaust gas temperatures for both fuels. Furthermore, the figures also show that good repeatability was obtained during the E10 tests.

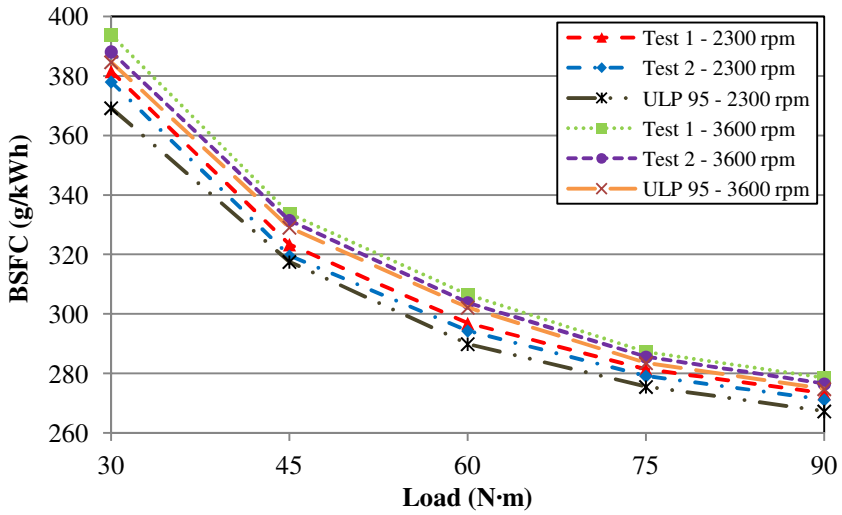

Figure 67: E10 BSFC results

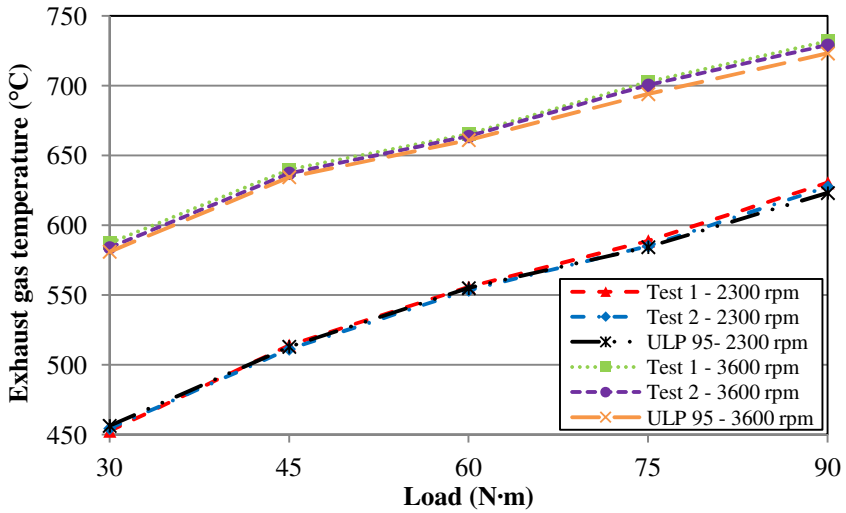

Figure 68: E10 exhaust gas temperature results

5.3.2 Emissions comparison

In comparison to ULP, ethanol has a 34,7 % higher oxygen content by weight (Koc et al., 2009). Due to this, the oxygen content of E10 is also higher than with ULP, which implies that an increase in air-fuel ratio should be observed when switching from ULP to E10. This effect was observed during the E10 testing through higher measured lambda values with the E10 blend than with ULP.

The increased oxygen content also caused a decrease in CO and an increase in CO_2 present in the exhaust gas due to more complete combustion taking place (Koc et al., 2009). The change in lambda, CO_2 and CO can be seen in Figure 69, Figure 70 and Figure 71 respectively.

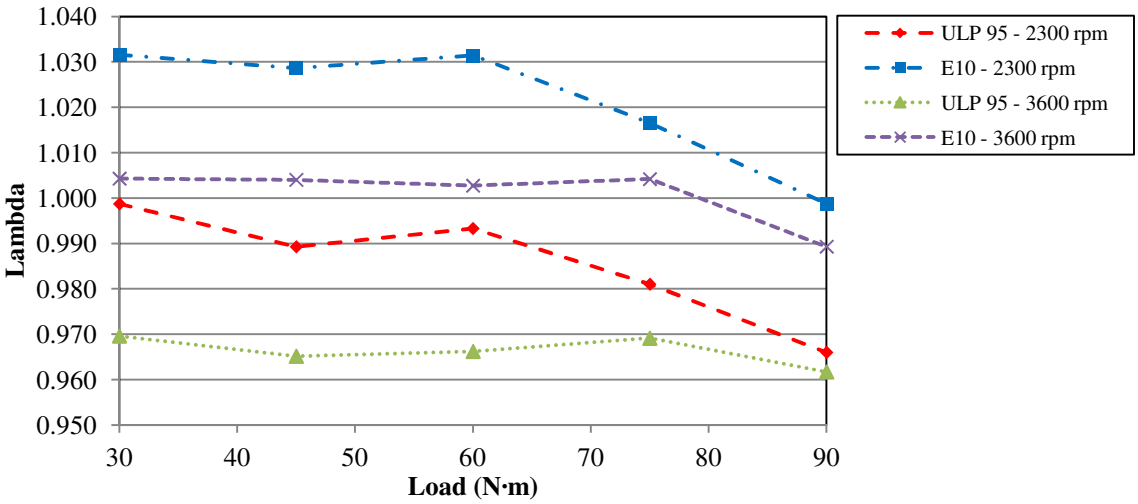

Figure 69: Lambda values obtained with ULP 95 and E10

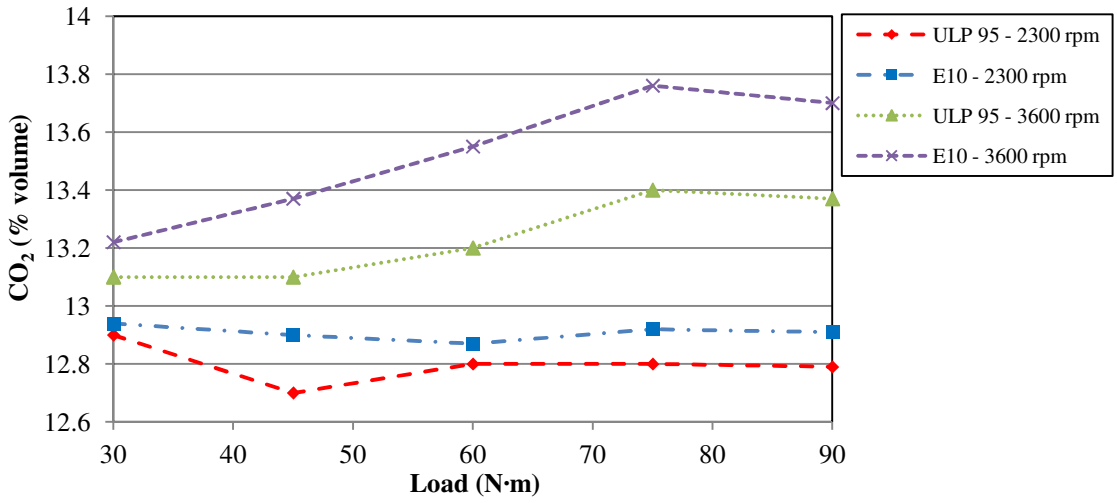

Figure 70: CO2 produced with ULP 95 and E10

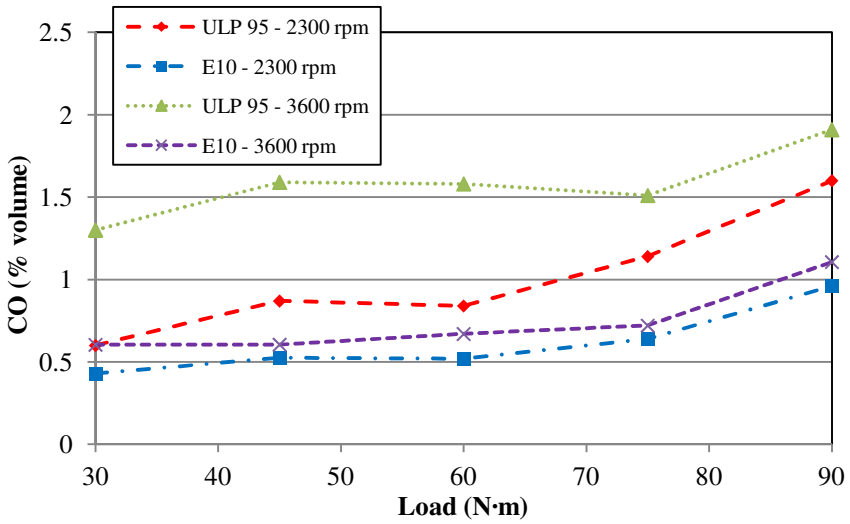

Figure 71: CO produced with ULP 95 and E10

5.3.3 Combustion comparison

For the analysis that was done in this section the 3600 rpm at 90 N·m and 2300 rpm at 30 N·m test points were used. This allowed for a comparison of the combustion of the fuels at a high speed and load condition as well as a low speed and load condition. In-cylinder pressure was measured using the *Kistler* transducer for the tests discussed in this section.

Before the comparison was made, the pressure data was phased and referenced. The hot motoring log P - log V curves that were obtained for bracket test 1 after phasing and referencing is shown in Figure 72. Similar curves were obtained with the results from bracket test 2 as well as both of the E10 tests.

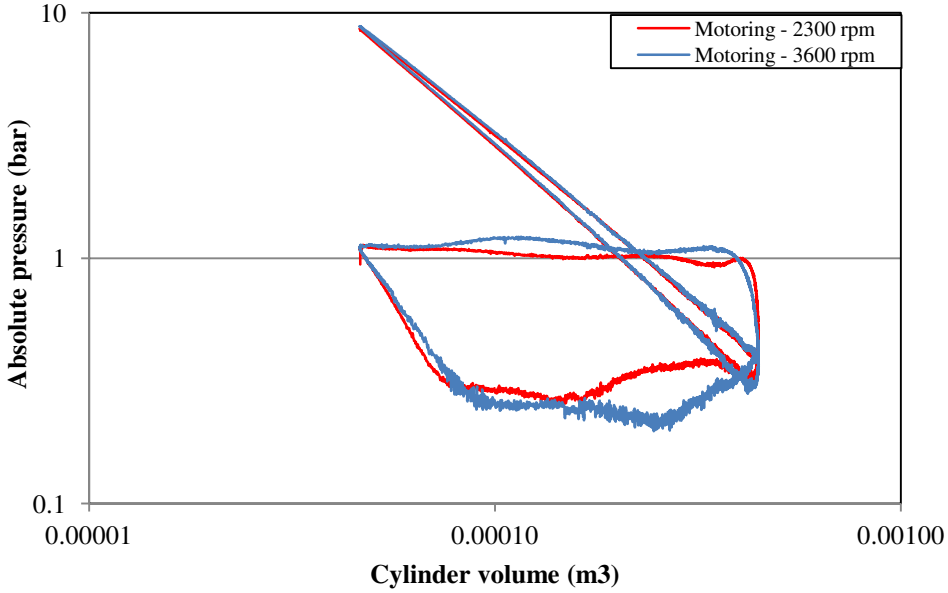

Figure 72: Phased and referenced log P - log V motoring curve (bracket test 1)

a) In-cylinder pressures

The peak in-cylinder pressures as well as IMEP values for both fuels did not show significant differences. The results that were obtained are given in Table 5.

Table 5: ULP 95 and E10 combustion pressure comparison

		Peak gauge pressure (bar)		Peak pressure position (° ATDC)		$IMEP_{net}$ (bar)	
Speed (rpm)	**Load (N·m)**	**ULP 95**	**E10**	**ULP 95**	**E10**	**ULP 95**	**E10**
2300	30	16,08	16,10	16,7	16,6	2,94	2,96
3600	90	41,89	41,27	12,8	13,6	8,05	8,03

b) Heat release rate and mass fraction burnt

According to (Rodrigo & Sodré, 2010) the combustion of ethanol is faster and therefore the burn rate should increase when ethanol is added to petrol. However, they tested an ethanol-petrol blend under advanced timing conditions and with a higher percentage of ethanol than 10 % by volume. According to Srinivasan & Saravanan (2010) the heat release rate as well as burn rate decreases with increasing ethanol content due to flame quenching. During their testing a fixed ignition timing was used, as was the case with the testing done in this project. However, they also used blends with an ethanol content higher than 10 %. Schifter et al. (2011) found marginal effects on the combustion rate when adding 10 % ethanol to petrol.

The heat release model that was used for the project is a simple zero dimensional, single-zone model using a second order polynomial for calculation of γ (see section 2.5.3) and the heat transfer coefficient proposed by Eichelberg. For the calculation of bulk gas temperatures the reference temperature at IVC was assumed to be 340 K (Klein, 2007). An assumption had to be made seeing as air flow measurements made during testing did not give accurate results. Accurate air flow rate measurements are needed in the calculation, using the ideal gas law, of the reference temperature. Cylinder wall temperature was assumed to be constant at 440 K (Klein, 2007).

The results that were obtained for the heat release rate are shown in Figure 73 and Figure 74. The curves did not show a major difference between the fuels. A slight decrease in the peak heat release rate was however observed with the E10 blend at the 3600 rpm point due to a lower peak pressure than the petrol fuel.

As can be seen in the heat release curves there is a dip below zero during the compression stroke. This is due to evaporation of the injected fuel i.e. latent heat transfer from the charge air to the fuel (Shehata, 2010). During the expansion stroke it can be seen that the heat release rate only reaches zero at 516 ° crank angle.

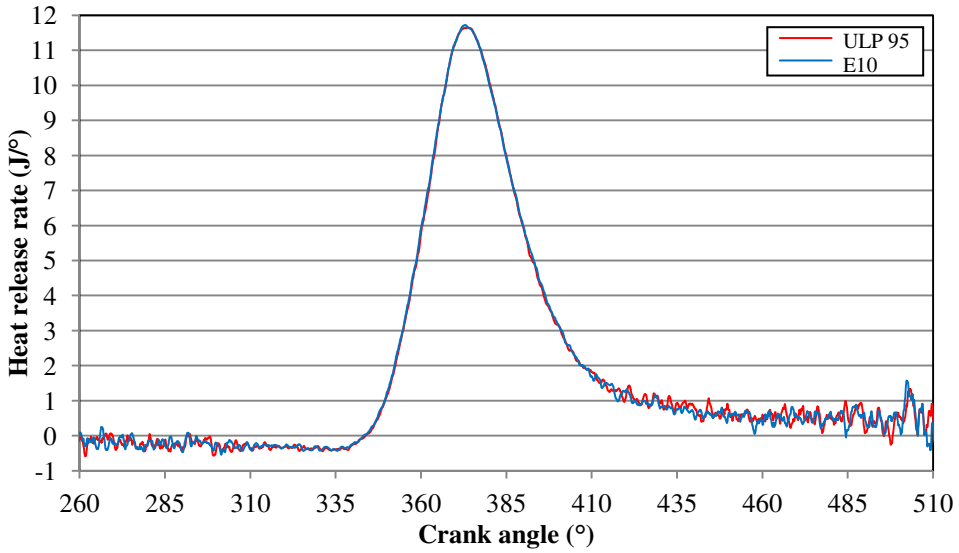

Figure 73: Heat release rate curves (2300 rpm @ 30 N·m)

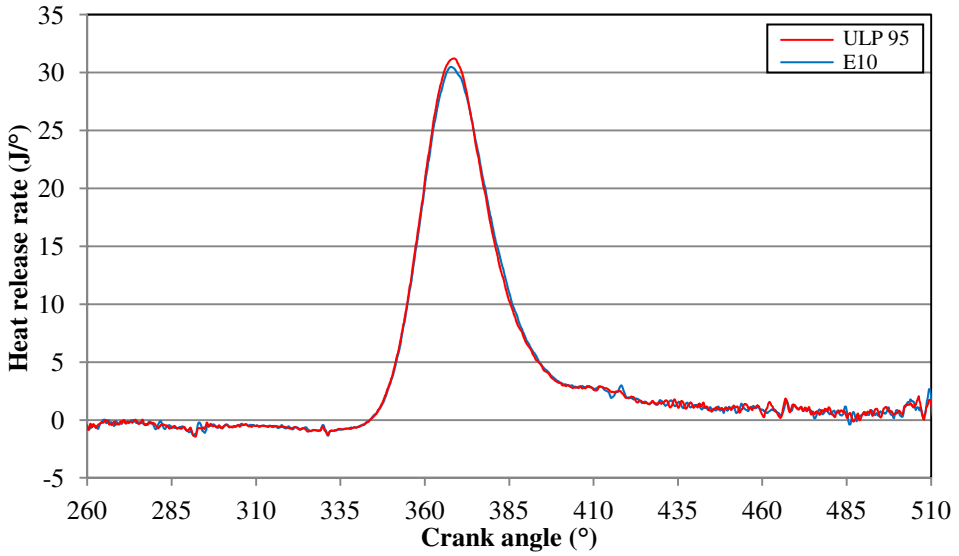

Figure 74: Heat release rate curves (3600 rpm @ 90 N·m)

The curves that were obtained for mass fraction fuel burnt are shown in Figure 75. These curves are plotted against degrees after spark delivery in the literature. However, they have been plotted against crank angle in this report to allow comparison of the effect of engine load change. The curves did not show a significant difference in combustion of the two fuels. A higher burn rate was observed at the higher load point with both fuels, in comparison to the lower load point.

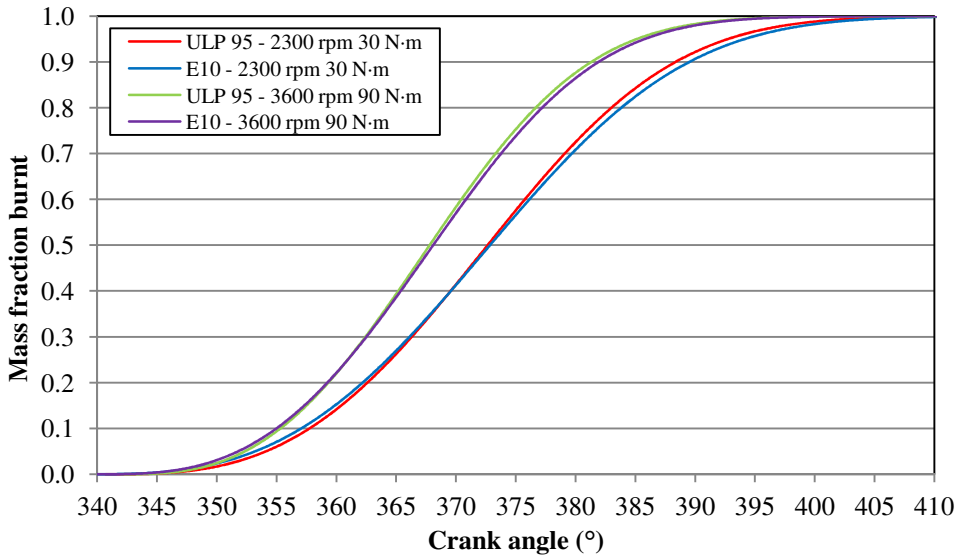

Figure 75: Mass fraction of fuel burnt curves

The crank angle at which a MFB of 10 % and 90 % was obtained, for the different fuels, are given in Table 6. From the table it can be seen that the combustion duration for E10 and ULP during partial load is very similar with E10 burning slightly slower.

Table 6: Mass fraction of fuel burnt results for ULP 95 and E10 tests

			Crank angle (°)		Rapid burning angle (°)	
Speed (rpm)	**Load (N·m)**	**MFB (%)**	**ULP 95**	**E10**	**ULP 95**	**E10**
2300	30	10	2,2 BTDC*	2,9 BTDC	20,6	22,4
		90	18,4 ATDC	19,5 ATDC		
3600	90	10	4,6 BTDC	5 BTDC	16	17
		90	11,4 ATDC	12 ATDC		

* Note: BTDC = Before top dead centre.

6. Conclusions and Recommendations

An engine and dynamometer setup with monitoring and control capabilities was developed. The setup was developed to allow Stellenbosch University to do SI engine fuels testing, using a standard passenger vehicle engine. The engine that was used was chosen due its proven reliability and widespread use locally and overseas with neat petrol as well as blends of ethanol and petrol.

The repeatability testing of the setup showed excellent results and the main objective of the project was therefore achieved. Testing was done in the partial load operating range of the engine, representing typical freeway driving conditions.

For comparing the combustion characteristics of different fuels, an in-cylinder pressure measurement setup was also developed. The setup includes fibre optic as well as a piezoelectric pressure transducer, an optical shaft encoder, a modified cylinder head and a high speed DAQ device. Testing of this setup also showed good repeatability. The setup is able to measure combustion pressures at 0,1 ° crankshaft angle intervals with a sensitivity of either 14 mV/bar or 49 mV/bar, depending on the transducer used.

The indicating setup allowed for the comparison of different locations for in-cylinder pressure measurement. Measurements could be made by installing the fibre optic transducers into a modified spark plug or directly into the combustion chamber using the modified cylinder head. It was found that installing the transducer directly into the combustion chamber caused higher readings of peak pressure. Noise present on the pressure signals was found to be similar at both positions.

The indicating setup also allowed a comparison between the performance of piezoelectric and fibre optic pressure transducers during combustion. It was found that at low loads the performance of the transducers are similar. However, at high load conditions the fibre optic transducers showed high sensitivity to thermal effects whereas the piezoelectric did not. Furthermore, the pressure curves obtained with the piezoelectric transducer included less noise than the fibre optic transducers due to a higher sensitivity.

The effects on engine performance of mixing 10 % ethanol and 90 % petrol, compared to neat petrol, were also studied. It was found that the fuel consumption increased slightly when using the E10 blend. This is due to the lower energy content of ethanol. The addition of the ethanol also increased the oxygen content of the charge supplied to the combustion chamber. This could be seen in the obtained lambda values which were higher than with neat petrol. The increase in oxygen content also caused a decrease in CO and an increase in CO_2 emissions in comparison to neat petrol. This is due to the improved combustion when using the E10 blend.

Analysis of the combustion parameters when using neat petrol and E10 did not indicate any significant differences between the fuels. A slight decrease in peak heat release rate was observed for E10 at a speed and load of 3600 rpm and 90 N·m due to a slight decrease in peak pressure. Furthermore, a slight increase in combustion duration was observed with the E10 blend.

Recommendations for future work are:

- Modification of a standard cylinder head for in-cylinder pressure measurement using a miniature piezoelectric pressure transducer.
- Testing of the effect of different ethanol blends at partial and full load conditions.
- Installation of an aftermarket ECU to enable control of injection and ignition timing as well as closed loop lambda control.
- Installation of highly accurate emissions equipment for fuel comparison testing.

Appendix A: Engine, Dynamometer and Drive Shaft Specifications

For future reference and as additional supporting information for the project, the drive shaft design and drawings, the specifications of the engine and the specifications of the dynamometer are given in this appendix.

A.1. Drive Shaft

In Figure 76 an exploded view of the designed drive shaft is shown. The figure shows the locating spigot (spherical plain bearing) that was installed to keep the shaft aligned with the dynamometer. The drawings for the custom designed and manufactured flanges can be found in Figure 77 and Figure 78. It has been included to illustrate the thickness of each flange and therefore their appropriateness for the application.

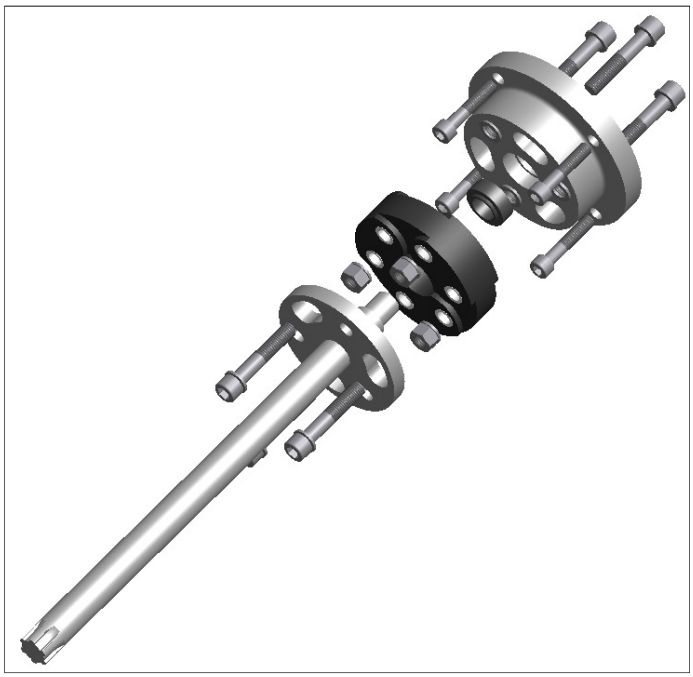

Figure 76: Drive shaft exploded CAD model

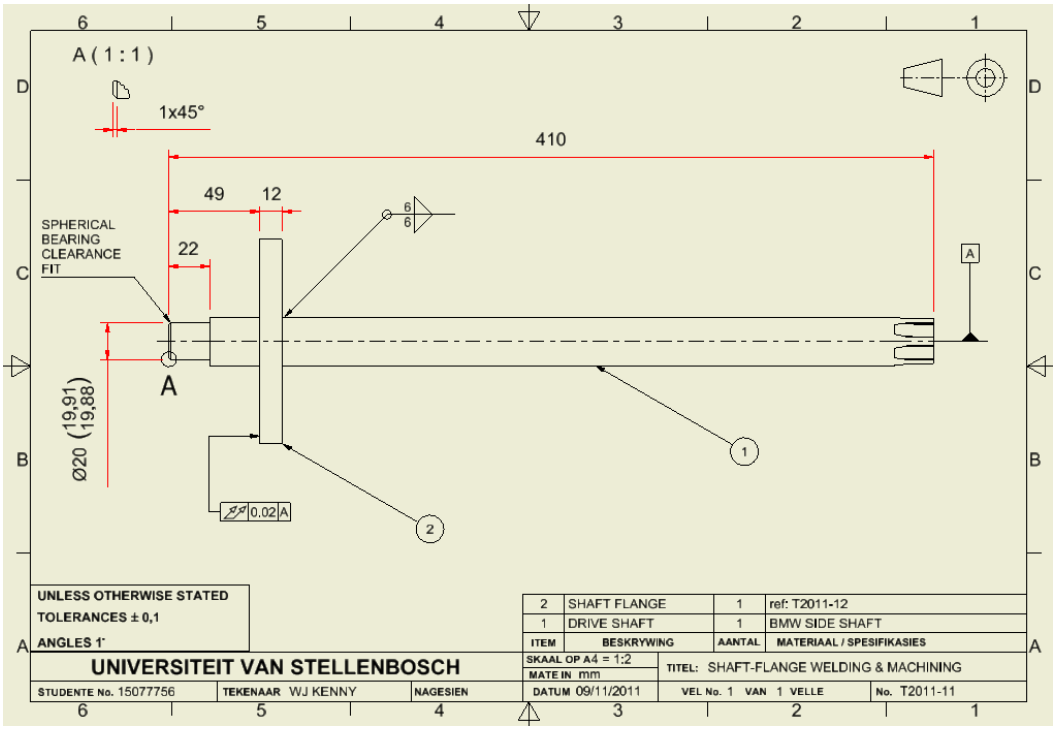

Figure 77: Side shaft and flange welding and machining

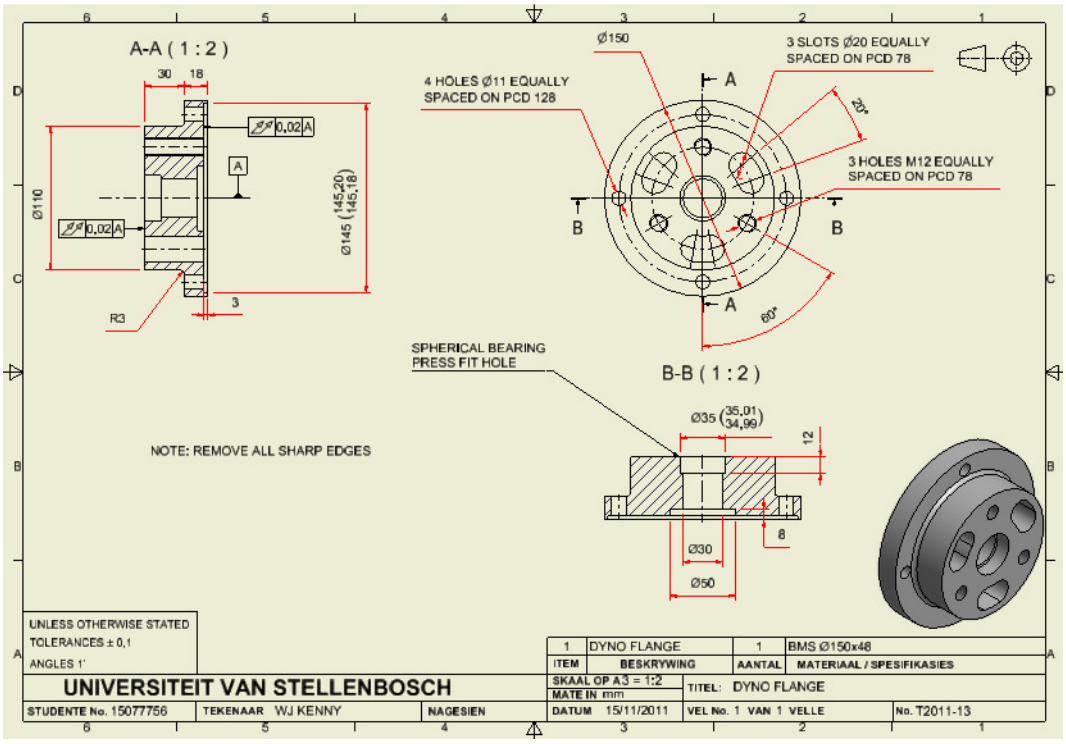

Figure 78: Dynamometer flange

A.2. Engine

In order to implement heat release and mass faction burnt models as well as to calculate IMEP and BMEP values, certain geometrical constants and specifications of the engine are needed. This includes the clearance volume, connecting rod length, cylinder bore diameter, piston stroke and displaced volume. All of these except the connecting rod length as well as clearance volume were readily available.

Connecting rod length was measured by removing one from a spare engine available in the testing facility. Clearance volume was measured on the modified as well as a standard cylinder head using a digital burette. It was found that the difference in clearance volume between the two cylinder heads is negligible. The clearance could also be estimated using the given compression ratio and swept volume of the engine. However, for more accurate calculation results the clearance volume was measured. In Table 7 the clearance volume and all the other engine specifications that were needed for the project are given.

Table 7: Engine specifications

4 cylinder, 1.6 L SI engine	
Maximum torque	137 N·m @ 2500 rpm
Maximum power	70 kW @ 5500 rpm
Bore diameter	82,07 mm
Stroke	75,48 mm
Connecting rod length	129 mm
Displaced volume	0,001597 m^3
Clearance volume	0,00004647 m^3
Compression ratio	9,5
Intake valve opening	12 ° BTDC
Intake valve closing	24 ° after bottom dead centre (ABDC)
Exhaust valve opening	24 ° before BDC (BBDC)
Exhaust valve closing	12 ° ATDC
Ignition timing at 2300 rpm and 30 N·m	36 ° BTDC *
Ignition timing at 3600 rpm and 90 N·m	29 ° BTDC *

* Note: Timing and intake MAP was monitored using an *Autel* Autolink AL309 OBD-II code reader.

A.3. Dynamometer

In Table 8 the specifications of the *Schenck* W130 dynamometer that was used in the project are given. The torque vs. speed curve is highlighted in red in Figure 79.

Table 8: Dynamometer specifications (Schenck Pegasus GmbH, 1997)

***Schenck* W130 eddy current dynamometer**	
Nominal torque	400 N
Speed	10000 rpm
Nominal power	130 kW
Maximum coupling weight at maximum speed	2 kg
Mass of inertia	0,14 kg·m^2
Weight	270 kg
Torsion spring constant up to centre of dynamometer	0,0535 N·m/rad

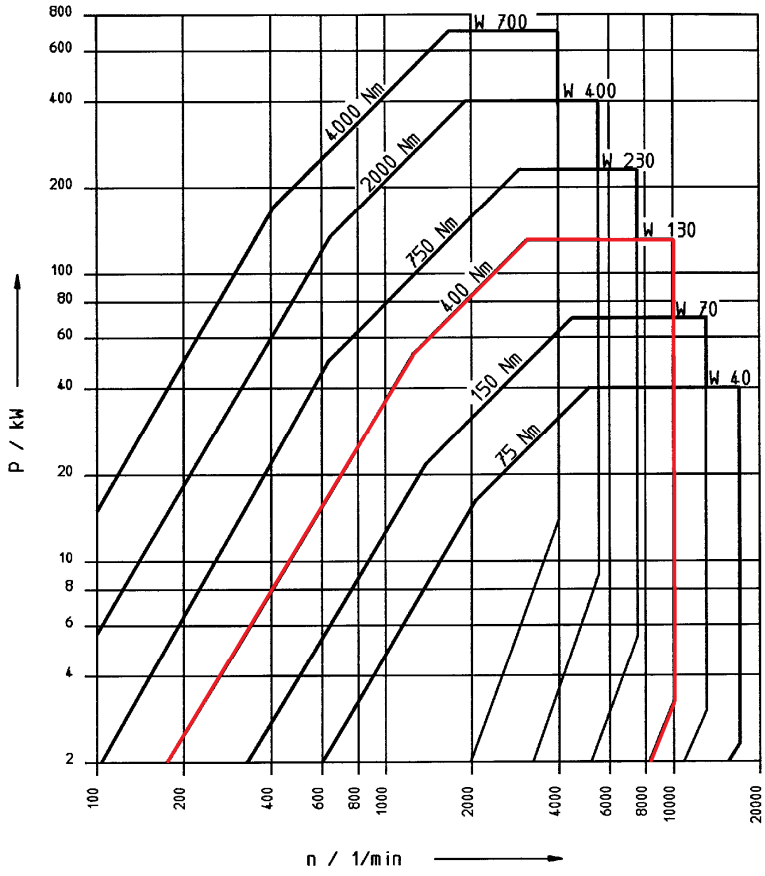

Figure 79: Dynamometer torque vs. speed curve (Schenck Pegasus GmbH, 1997)

Appendix B: Calculations and Derivations

The procedure that was used to calculate the partial load testing points for the project and the derivation of a zero dimensional apparent heat release model are given in this appendix.

B.1. Load Point Calculation Procedure

To determine the partial load test points the total running resistance of a motor vehicle fitted with the engine used in the project had to be approximated using the procedure set out in Bosch (2000). The total running resistance (F_w) comprises of the rolling resistance (F_{Ro}), aerodynamic drag (F_L) and climbing resistance (F_{St}), all of which are illustrated in Figure 80. Climbing resistance was omitted in the load point calculations as it was assumed that the vehicle is driving on a flat road.

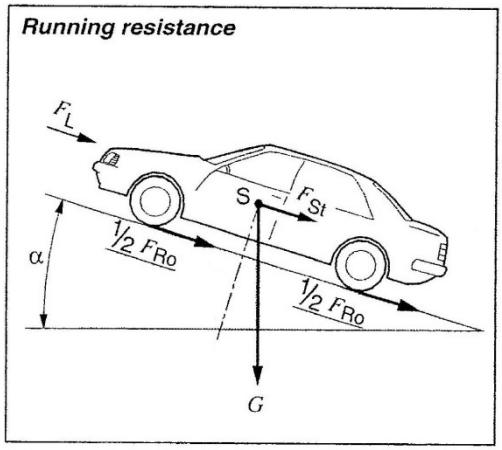

Figure 80: Resistive forces on motor vehicles (Bosch, 2000)

For calculating the rolling resistance the following formula can be used:

$$F_{Ro} = f\, m_v\, g \tag{13}$$

where f is the dynamic friction coefficient, m_v is the vehicle mass and g is gravitational acceleration. Aerodynamic drag can be calculated as follows:

$$F_L = 0{,}5\rho\, c_d\, A_f\, (v + v_0)^2 \tag{14}$$

where ρ is the density of air, c_d is the drag coefficient of the vehicle, A_f is the frontal area of the vehicle, v is the vehicle speed and v_0 is the headwind speed. The frontal area can be calculated by multiplying the product of the vehicle height and track width by 0,9 (as recommended by Bosch (2000)).

The total running resistance can then be converted to required power at the wheels of the vehicle as follows:

$$P_w = F_w\, v \tag{15}$$

The required engine power can then be calculated using the following formula:

$$P_{engine} = \frac{F_w\, v}{\eta} \tag{16}$$

where η is the drive train efficiency, which lies in the range of 88-92 % for the type of vehicle.

Once the power has been calculated the required brake torque and engine speed can be determined as follows:

$$T_b = \frac{P_{engine}\, r_w\, i}{v} \tag{17}$$

$$n = \frac{n_{wheel}}{i} \tag{18}$$

where r_w is the wheel diameter, i is the gear ratio between the engine and the wheels and n is the engine speed.

The constants that were used for calculating the engine load and speed at 60 km/h and 120 km/h, in 4th and 5th gear respectively, are given in Table 9 below.

Table 9: Constants used during load point calculations

Constant	
f	0,013
m_v	1635 kg
g	9.81 m/s^2
c_d	0.47
A_f	2.154 m^2
v_0	0 m/s
η	0,9
i - 4th gear	0,259
i - 5th gear	0,324

B.2. Apparent Heat Release Derivation

The equation for a simple zero dimensional, single-zone, apparent heat release model (on a crank angle basis) is derived in this section. For this model the combustion chamber is modelled as an open boundary system as shown in Figure 81.

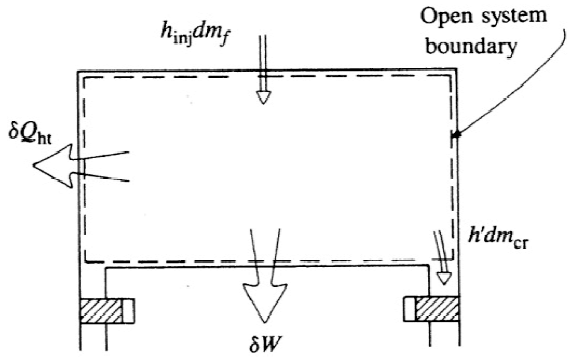

Figure 81: Heat release analysis system boundary (Heywood, 1988)

The energy balance for this open system is:

$$\frac{dQ_{ch}}{d\theta} = \frac{dU_s}{d\theta} + \frac{dQ_{ht}}{d\theta} + \frac{dW}{d\theta} + \sum h_i \, dm_i \qquad (19)$$

where dQ_{ch} is the gross heat release rate, dQ_{ht} is the heat transfer to the walls, dW (which is equal to pdV) is the work done on the piston and dU_s is the change of sensible energy of the cylinder contents. The last term represents the flow across the system boundaries. With PFI and DISI engines the only flow that occurs is gas flow into and out of the crevices as well as blow-by while with stratifed DISI engines the flow includes the injected fuel. The effects of blow by can usually be ignored. (Heywood, 1988)

If it is assumed that U_s is given by $mu(T)$, where m is the mass within the system boundary, u is the internal energy (per kg) of the cylinder contents and T is the mean bulk gas temperature, dU_s can be written as:

$$dU_s = m \, c_v(T) \, dT + u(T) \, dm \qquad (20)$$

where c_v is the specific heat of the gas. Assuming that the only flow across the boundary is due to crevices (dm_{cr}) and substituting equation 20 into equation 19 yields the following equation:

$$dQ_{ch} = m \, c_v(T) \, dT + (h' - u) \, dm_{cr} + p \, dV + dQ_{ht} \qquad (21)$$

where h' is the enthalpy of the gases flowing into or out of the crevices.

Using the ideal gas law and assuming a constant value for the gas constant *R*, the following equation can obtained:

$$dT = \frac{V\,dp}{m\,R} + \frac{p\,dV}{m\,R} - \frac{p\,V\,dm}{m^2\,R}$$

$$= \frac{V\,dp}{m\,R}\left(\frac{p}{p}\right) + \frac{p\,dV}{m\,R}\left(\frac{V}{V}\right) - \frac{p\,V\,dm}{m^2\,R}$$

$$= \frac{T\,dp}{p} + \frac{T\,dV}{V} - \frac{T\,dm}{m} \tag{22}$$

Therefore:

$$\frac{dT}{T} = \frac{dp}{p} + \frac{dV}{V} - \frac{dm}{m} \tag{23}$$

Using equation 22, equation 21 can be written as:

$$\frac{dQ_{ch}}{d\theta} = \frac{c_v}{R}\,V\,\frac{dp}{d\theta} + \left(\frac{c_v}{R} + 1\right)p\,\frac{dV}{d\theta} + (h' - u + c_vT)\,\frac{dm_{cr}}{d\theta} + \frac{dQ_{ht}}{d\theta} \tag{24}$$

Defining the specific heat ratio as $\gamma = \left(1 + \frac{R}{c_v}\right)$, equation 24 can be written as:

$$\frac{dQ_{ch}}{d\theta} = \frac{V}{\gamma - 1}\,\frac{dp}{d\theta} + \frac{\gamma}{\gamma - 1}\,p\,\frac{dV}{d\theta} + (h' - u + c_vT)\,\frac{dm_{cr}}{d\theta} + \frac{dQ_{ht}}{d\theta} \tag{25}$$

Depending on the required accuracy of the model, equation 25 can be simplified by ignoring the effects of crevices.

The heat transfer to the combustion chamber walls can be calculated using Newton's law of cooling. The area that is required in this equation is described by the following:

$$A = A_{ch} + A_p + \pi\,B\,(l + a - s) \tag{26}$$

where A_{ch} and A_p are the cylinder head and piston crown surface areas respectively.

Calculation of the rate of change of the cylinder volume can be done, on a numerical basis, using a central differencing scheme. To calculate the rate of change of pressure with respect to crank angle 2nd order central differencing can be used as described by:

$$\frac{dp_i}{d\theta} = \frac{p_{i-2} - 8\,p_{i-1} + 8\,p_{i+1} - p_{i+2}}{12\,\Delta\theta} \tag{27}$$

where p_i is the pressure at the analysed point and $\Delta\theta$ is crank angle interval.

Cylinder volume at each crank angle position can be calculated using the following equation:

$$V = V_c + \frac{\pi B^2}{4}(l + a - s) \tag{28}$$

where V_c is the clearance volume of the cylinder, B is the cylinder bore, l is the connecting rod length, a is the crank radius and s is the distance between the crank axis and the piston pin. These parameters are shown in Figure 82. The figure illustrates the geometry of a cylinder, piston, connecting rod and crankshaft assembly.

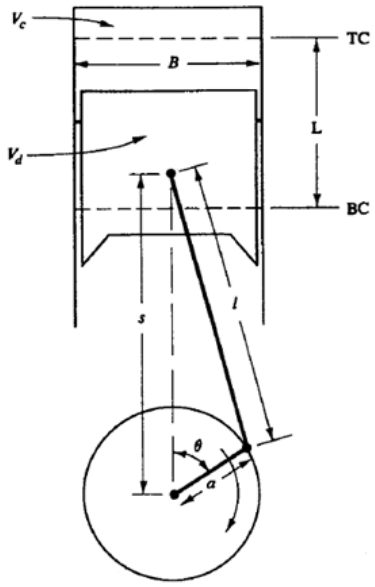

Figure 82: Engine cylinder geometry parameters (Heywood, 1988)

This distance s can be calculated using equation 29.

$$s = a\cos\theta + (l^2 - a^2\sin^2\theta)^{0,5} \tag{29}$$

Appendix C: In-cylinder Pressure Measurement Setup

In this appendix the calibration of the *Kistler* and *Optrand* pressure transducers, the design of the shaft encoder support as well as the pin assignments of the connectors that were used are given. The specifications of each transducers, shaft encoder and DAQ device are also given.

C.1. Pressure Transducers Calibration

The sensitivity (in mV/psi) of the *Optrand* transducers is determined by the manufacturer and is printed on the signal conditioner connected to the transducers. The sensitivity of the *Kistler* transducer depends on the charge amplifier used. The sensitivities were checked using a dead weight tester, calibration weights and a reference transducer namely an *HBM* electronic pressure transducer. Firstly the *HBM* was used to measure the pressure for a specific sequence of weights. These pressures were then recorded and used during calculation of the sensitivity for each of the other transducers.

The calibration curves of the transducers as well as their sensitivities are shown in Figure 83. All of the transducers showed excellent linearity under the static loadings from the weights.

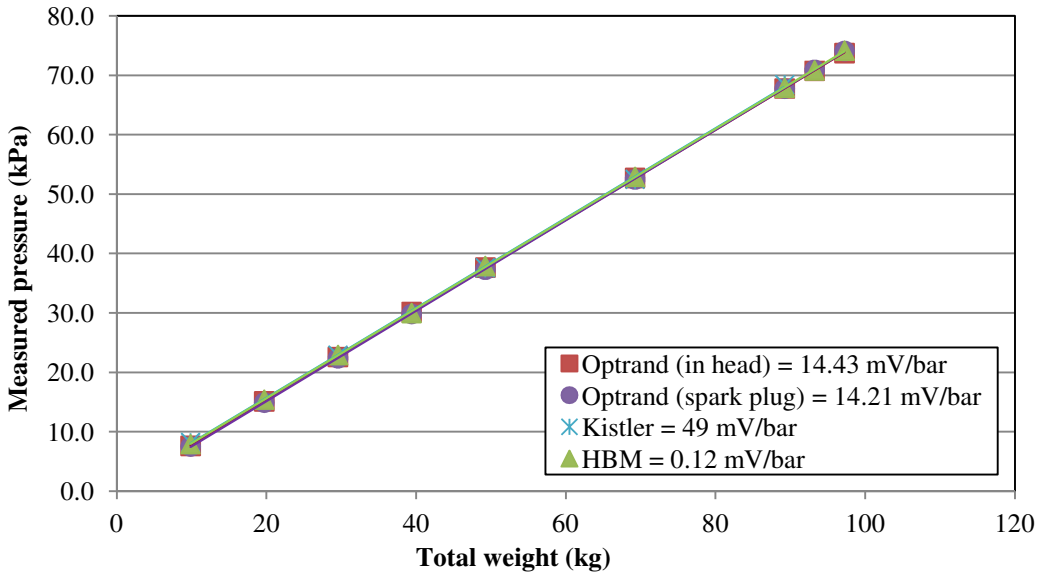

Figure 83: In-cylinder pressure transducers calibration curves

Although the pressure transducers are able to measure pressures in excess of 100 bar, the dead weight tester was not able to handle the amount of mass needed to reach pressures in excess of 74 bar. The linearity of the transducers in the range above 74 bar could therefore not be checked. This was however not an issue seeing as the test points used in the project all resulted in combustion pressures less than 74 bar.

C.2. Shaft Encoder Support Frequency Analysis

During the design of the shaft encoder support a simple frequency analysis was done to determine whether the support will be excited at its natural frequency while running the engine in the range of 800-6000 rpm. It was found that the natural frequencies of the support where all in excess of 6000 rpm engine speed with a first harmonic at 6900 rpm. This first harmonic is shown in Figure 84.

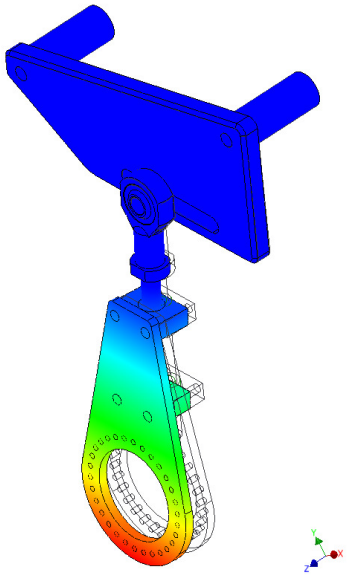

Figure 84: Shaft encoder support modal analysis

Although the analysis that was done was very simplified, it was only used to gain an understanding of the behaviour of the support bracket setup. A more accurate model was not done due to the unknown properties of the rod end. A worst case scenario was implemented where the rod end was seen as a fixed support which cannot rotate.

C.3. Component Specifications and Pin Assignments

Specifications for the pressure transducers, shaft encoder (and bellows) as well as the DAQ device can be found in Table 10, Table 11 and Table 12 respectively.

Table 10: Transducer specifications (Optrand Incoporated, [S.a.]) (Kistler, [S.a.])

	***Kistler* model 6117B**	***Optrand* AutoPSI-TC**
Major diameter	4,4 mm	4 mm
Measuring range	0-200 bar	0-250 bar
Sensitivity	49 mV/bar (with charge amp)	14 mV/bar
Operating temperature	350 °C max	380 °C max
Temperature sensitivity	±1.5 % @ 250 °C	±1.9 % @ 250 °C
Non-linearity	<±0.6 % FSO	±1.5 % FSO

Table 11: Shaft encoder and bellows specifications (Fritz Kübler GmbH, 2012)

Shaft encoder model number	**Kübler 8.5020.D312.3600**
Maximum speed	6000 rpm
Number of pulses per revolution	3600
Vibration resistance	100 m/s^2
Shock resistance	2500 m/s^2
Working temperature range	-40-80 °C
Output circuit	RS422
Supply voltage	5-30 V DC
Number of output channels	6
Bellows model number	**Kübler 8.0000.1101.1010**
Bellows: • Maximum radial displacement • Maximum axial displacement • Maximum angular displacement	 ± 0,2 mm ± 0,7 mm ± 1,5 °
Shaft diameter	10 mm

Table 12: Data acquisition device specifications (National Instruments, 2012)

***National Instruments* USB-6351**	
Analogue input channels	8 differential or 16 single ended
Digital input channels	24
Sampling rate	1 MS/s for multi-channel inputs
Analogue input range	± 10 V DC

The pin assignments for the 15 pin D-connectors used in the project are given in Table 13 while in Figure 85 a layout of the connector pin numbers are shown. Connectors were used for connecting the transducer as well as the shaft encoder to the DAQ device. Note that the *Optrand* transducer and the shaft encoder is connected to the same power supply.

Table 13: Connector pin assignments

Pin #	Description	Colour	Connector for:
1	Supply voltage	Brown	Shaft encoder
2	Ground	White	
3	A	Green	
4	A inverse	Yellow	
5	B	Gray	
6	B inverse	Pink	
7	Z	Blue	
8	Z inverse	Red	
9	Shield	Shield	
1	Supply voltage	Red	*Optrand* transducer
2	Ground	Black	
3	Diagnostics	Green	
4	Shield	Shield	
5	Output signal	White	
2	Ground	Green	*Kistler* transducer
4	Shield	Shield	
5	Output signal	Red	

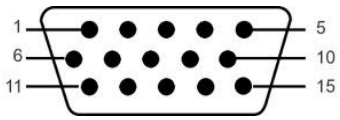

Figure 85: 15 pin D-connector layout

Appendix D: Software Programming

The ladder logic routines that were developed are shown Figure 86 to Figure 91 while the *LabView* block diagram is shown in Figure 92.

D.1. PLC Ladder Routines

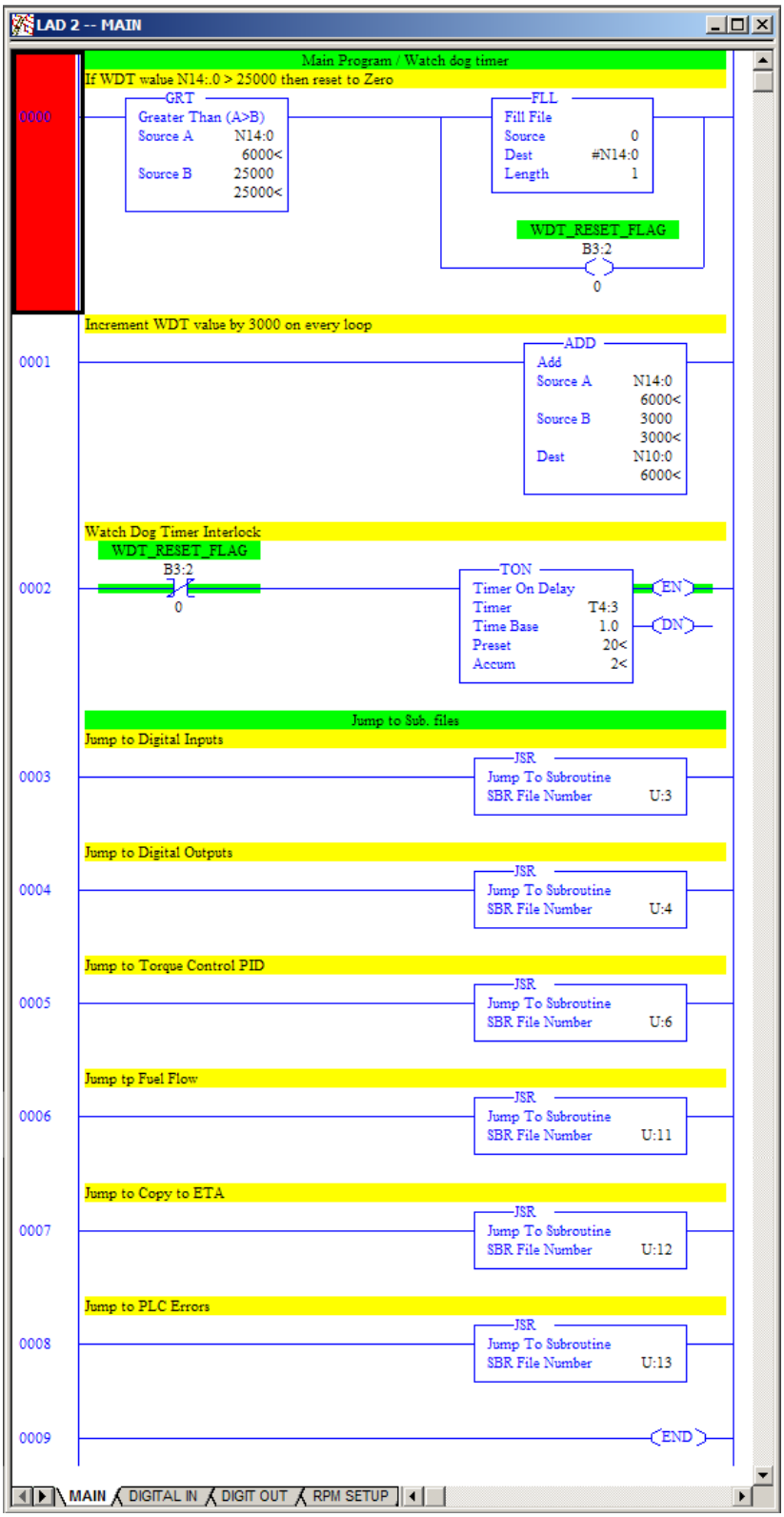

Figure 86: Main ladder routine

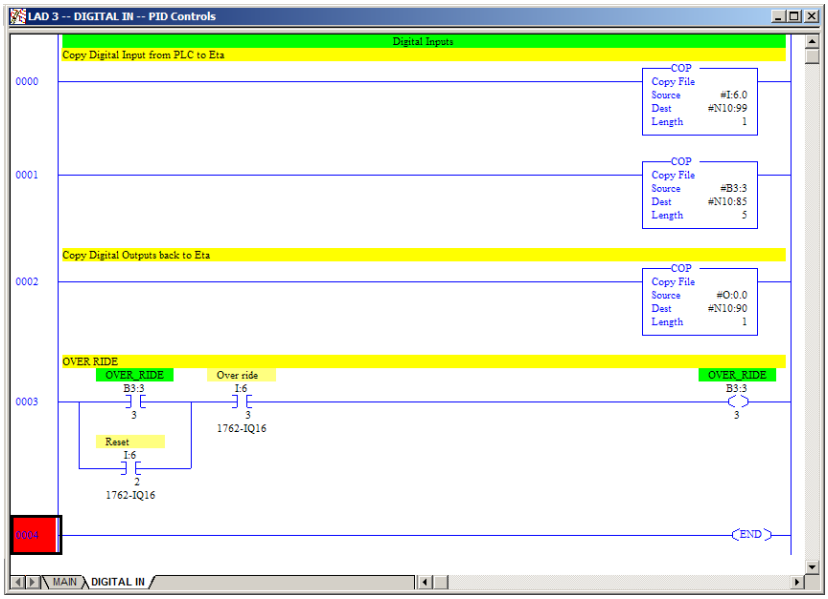

Figure 87: Digital input and output data exchange routine

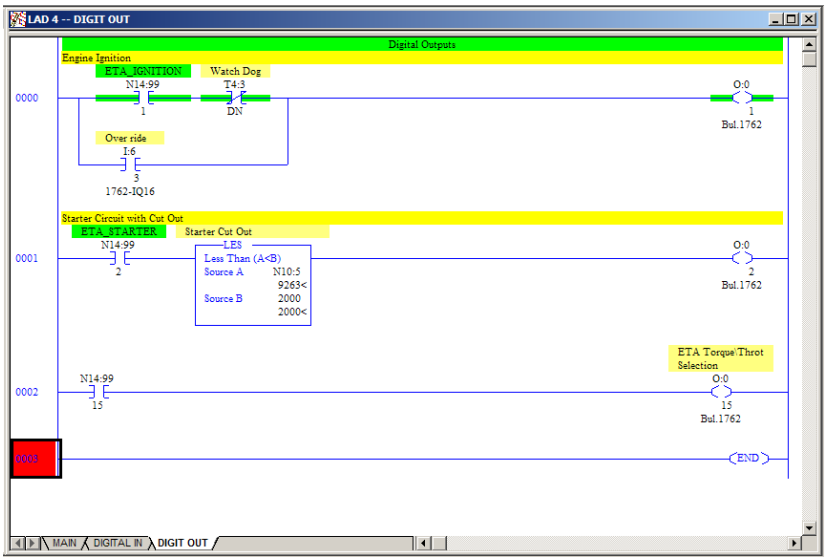

Figure 88: Digital output control routine

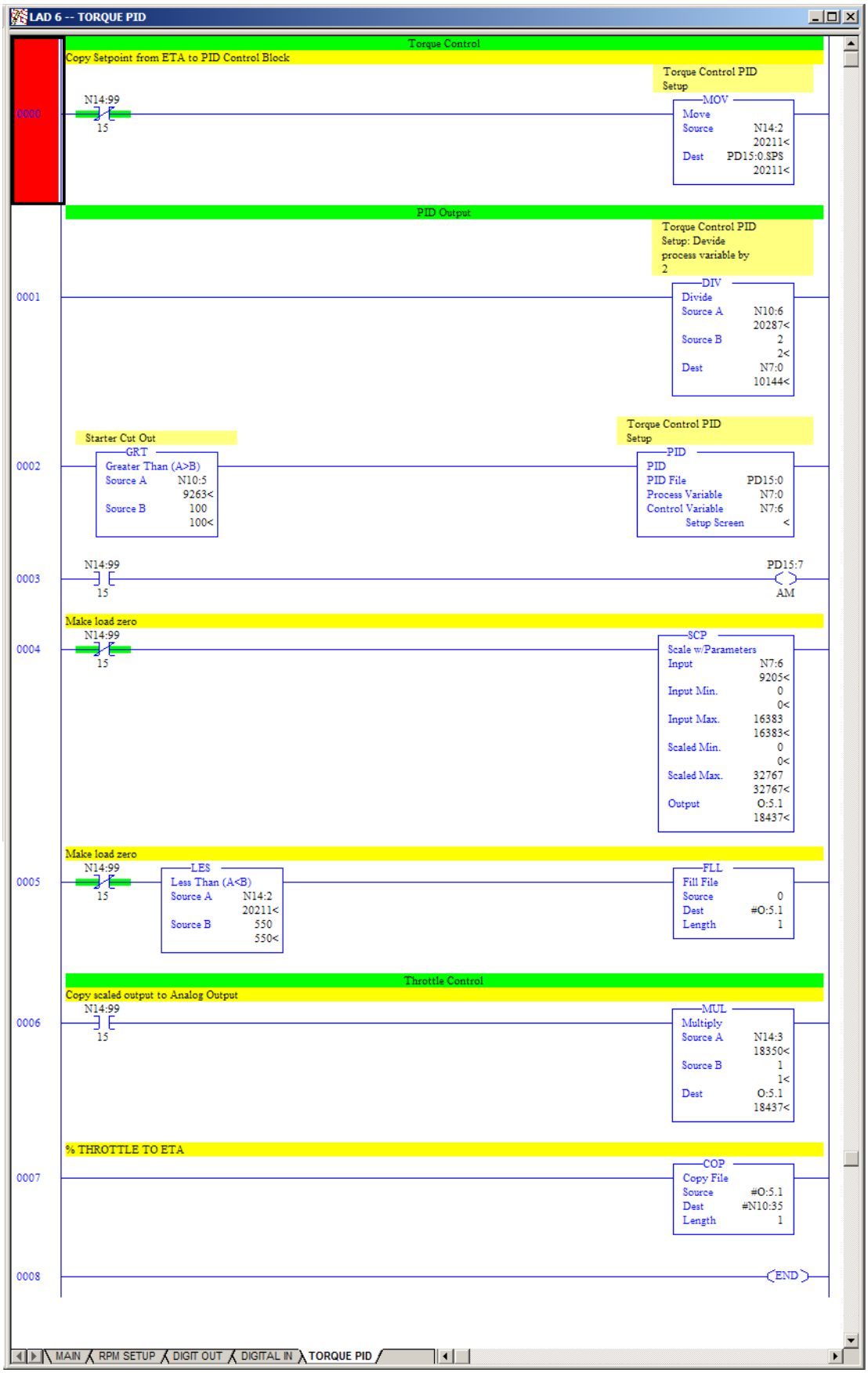

Figure 89: Torque PID control routine

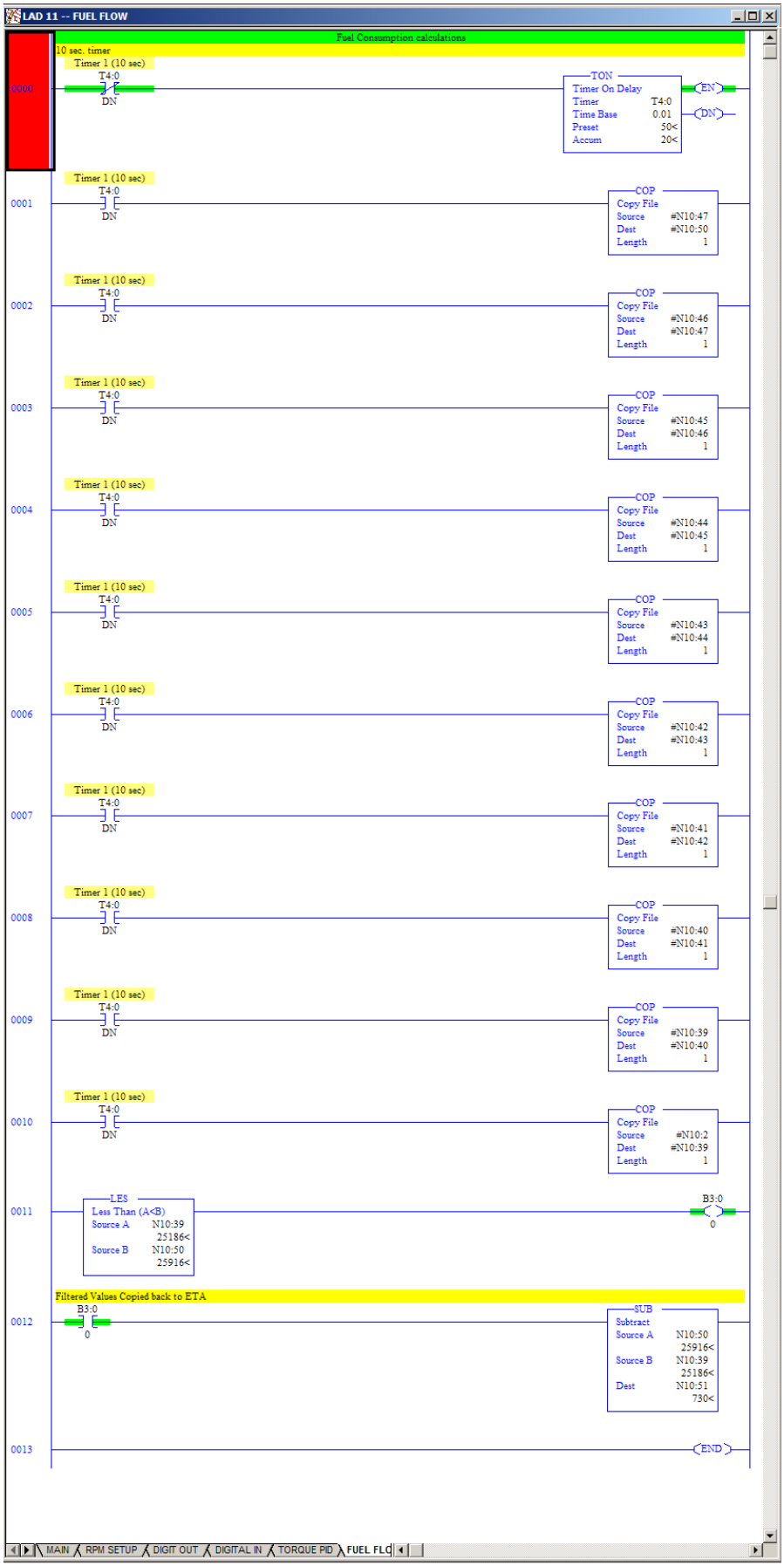

Figure 90: Fuel flow calculation subroutine

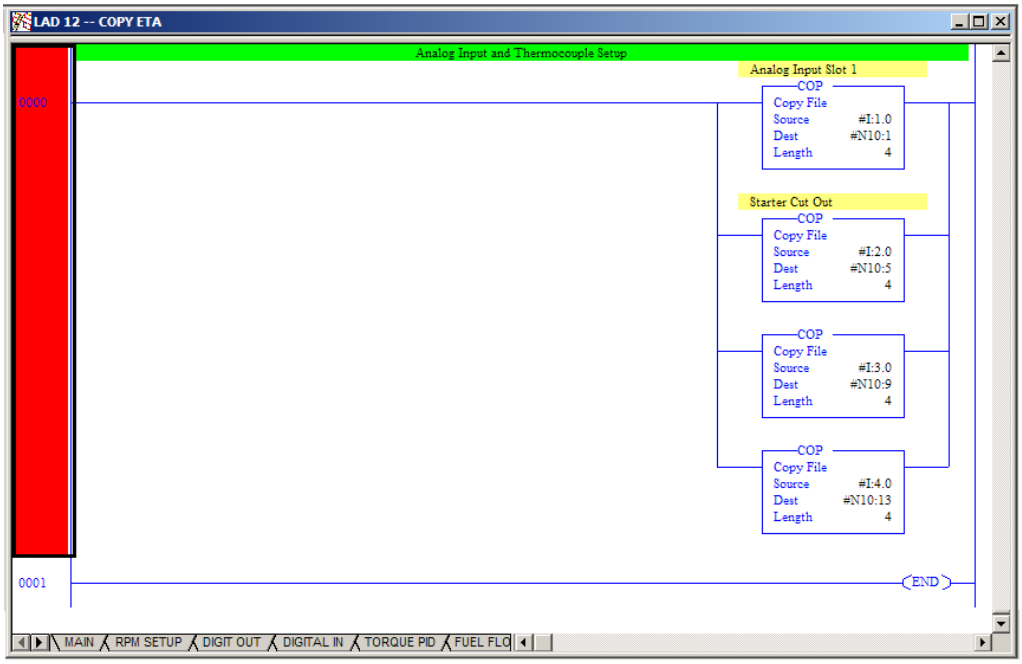

Figure 91: Analogue input and thermocouple data exchange routine

D.2. LabView Block Diagram

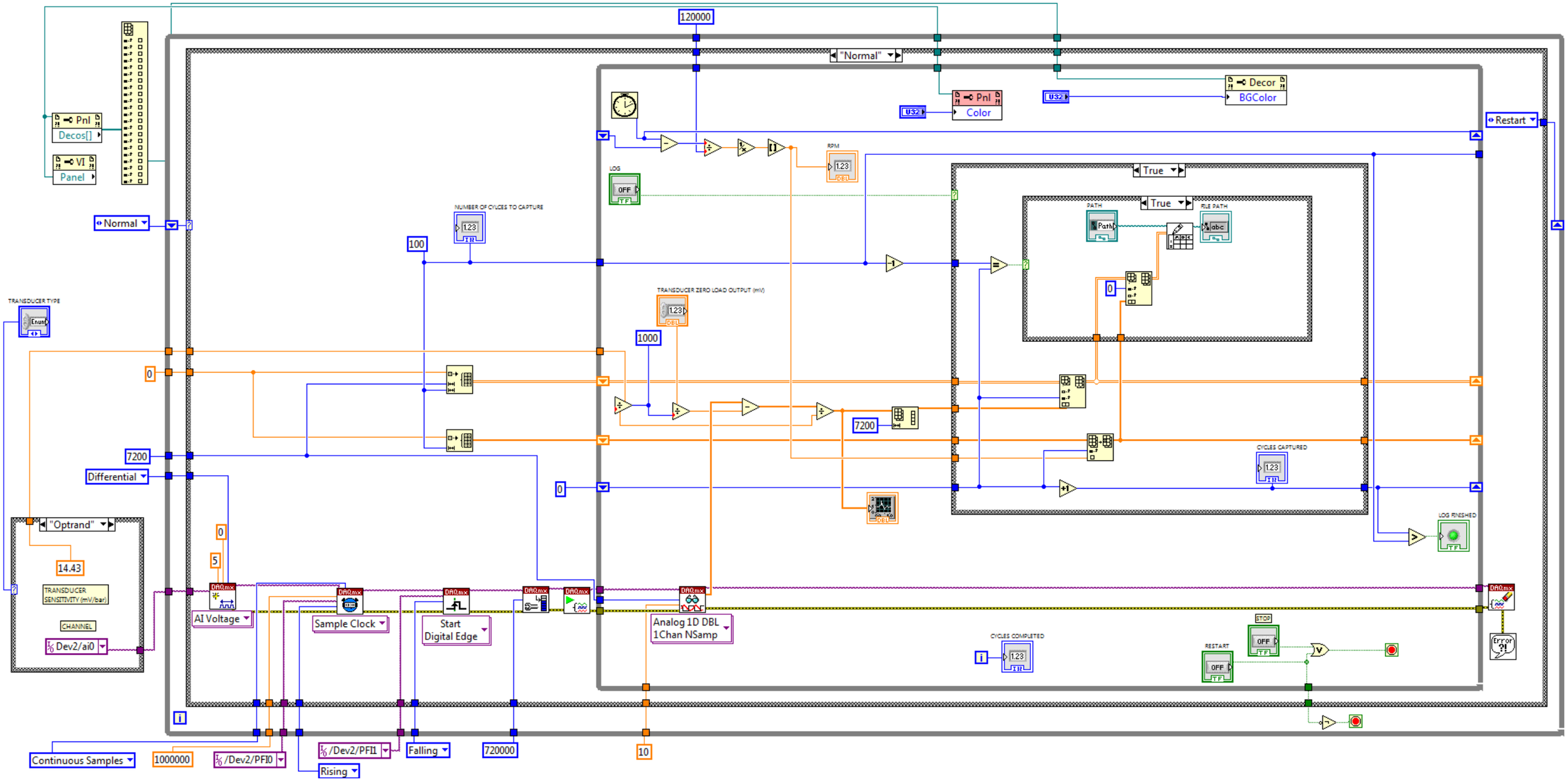

Figure 92: LabView block diagram

D.3. ETA Calibration Screens

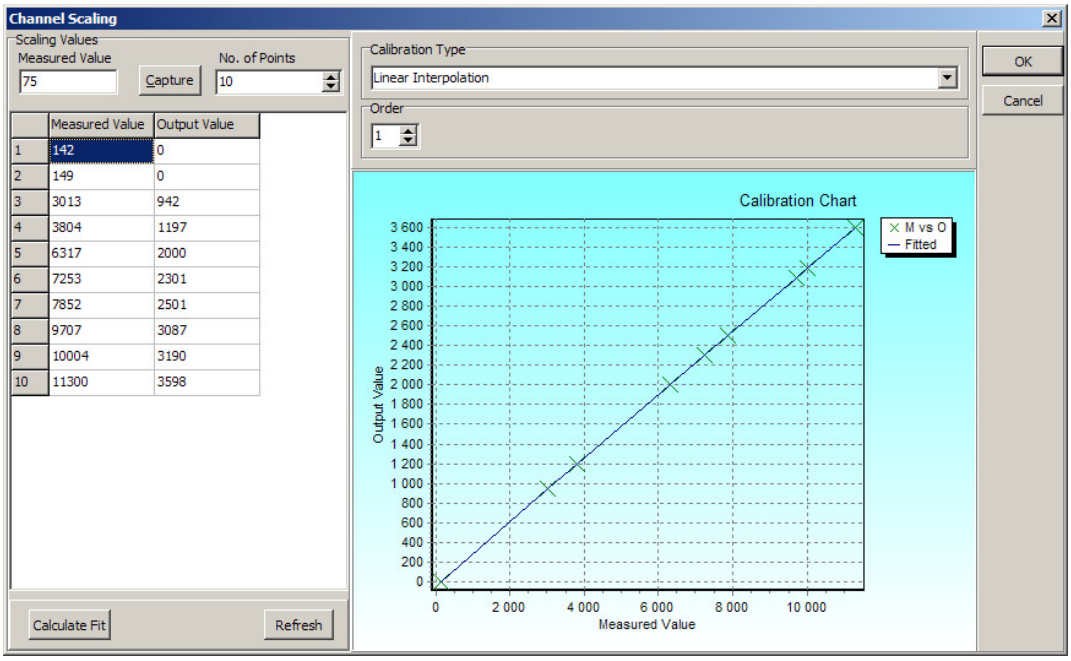

Figure 93: Speed input calibration screen

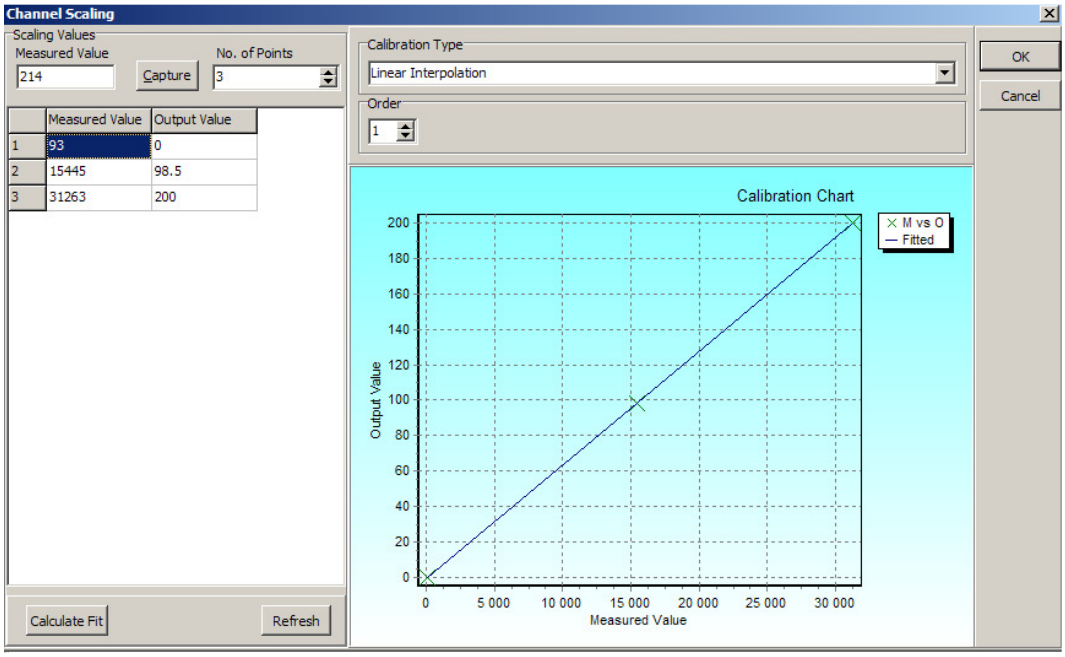

Figure 94: Torque input calibration screen

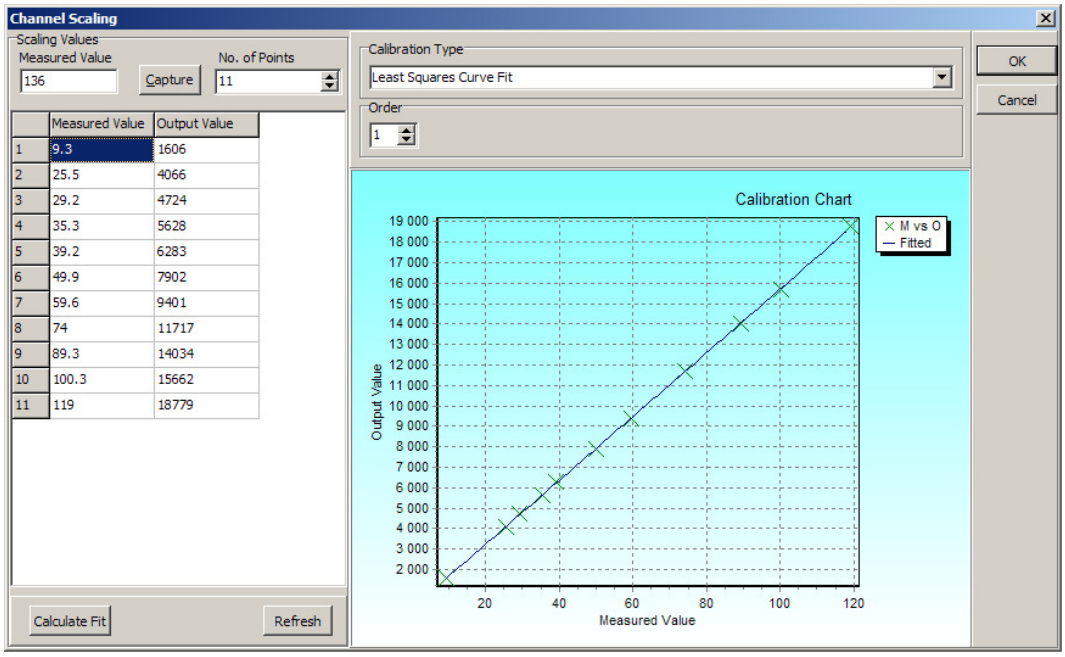

Figure 95: Torque output calibration screen

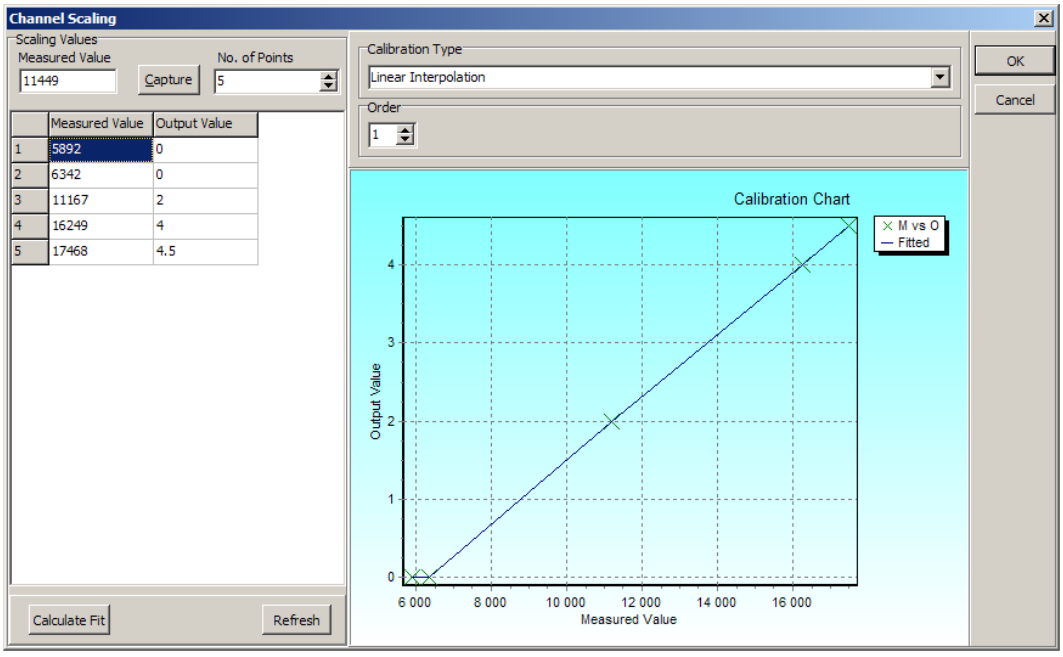

Figure 96: Fuel pressure calibration screen

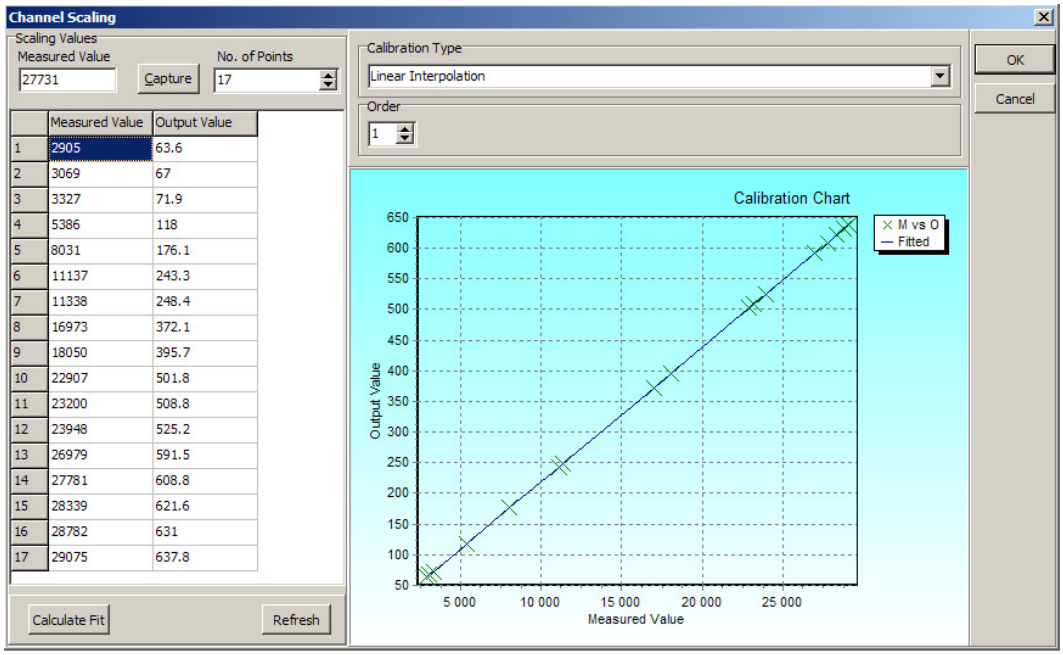

Figure 97: AVL fuel mass calibration screen

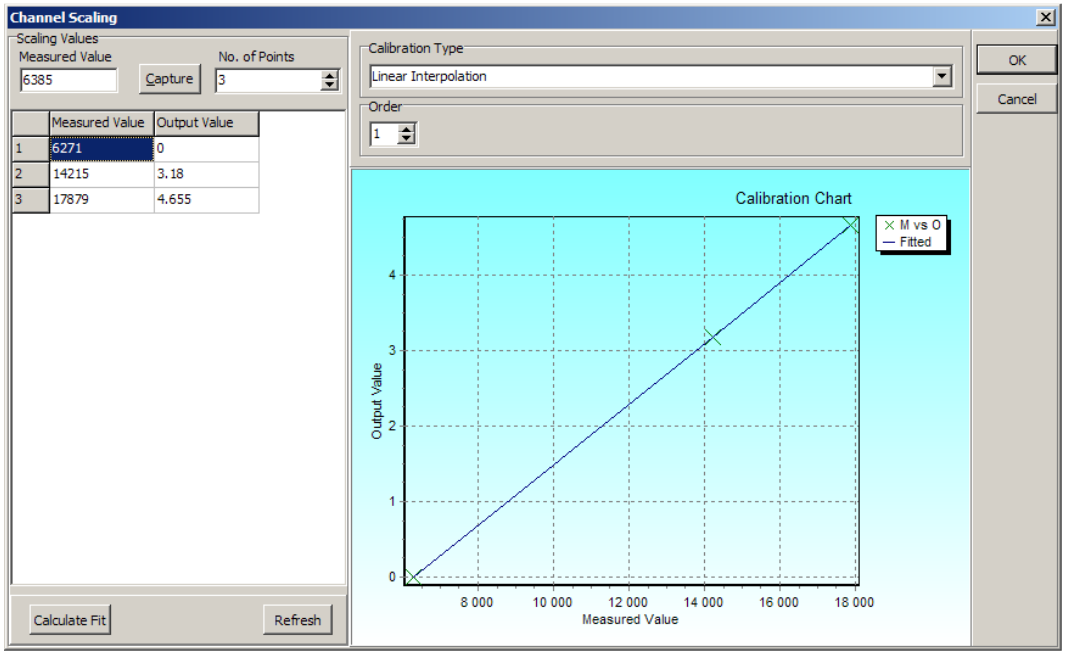

Figure 98: Oil pressure calibration screen

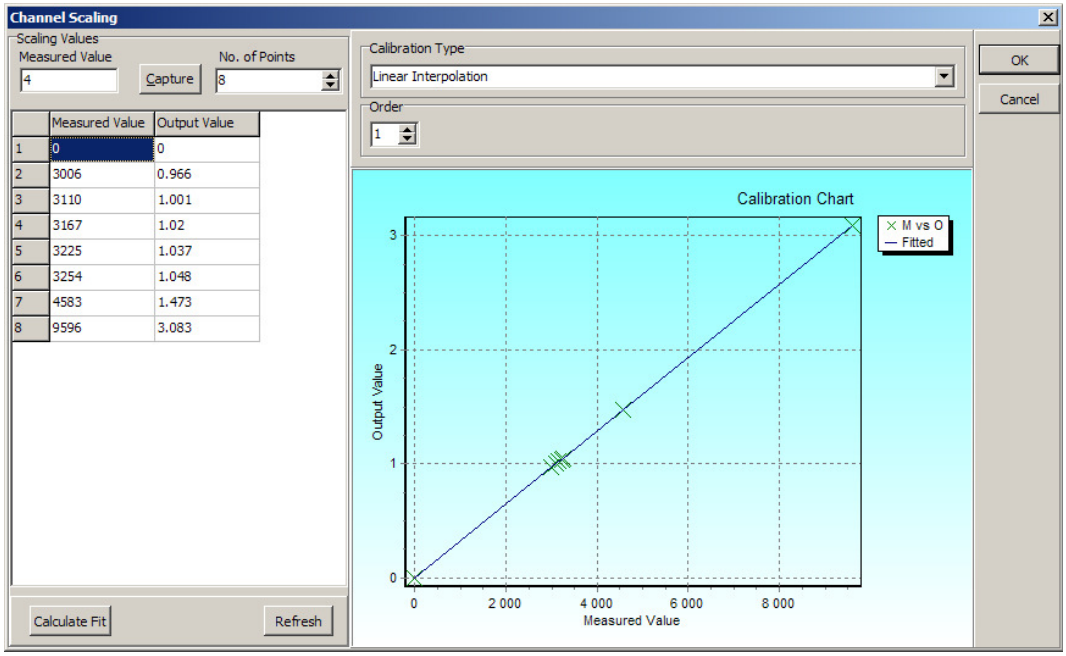

Figure 99: Lambda calibration screen

Appendix E: Wiring Diagrams

The layout of the wiring between the controllers, controlled devices (specimens) and the computer is shown in Figure 100. Specific wiring diagrams are shown in Figure 101 to Figure 107.

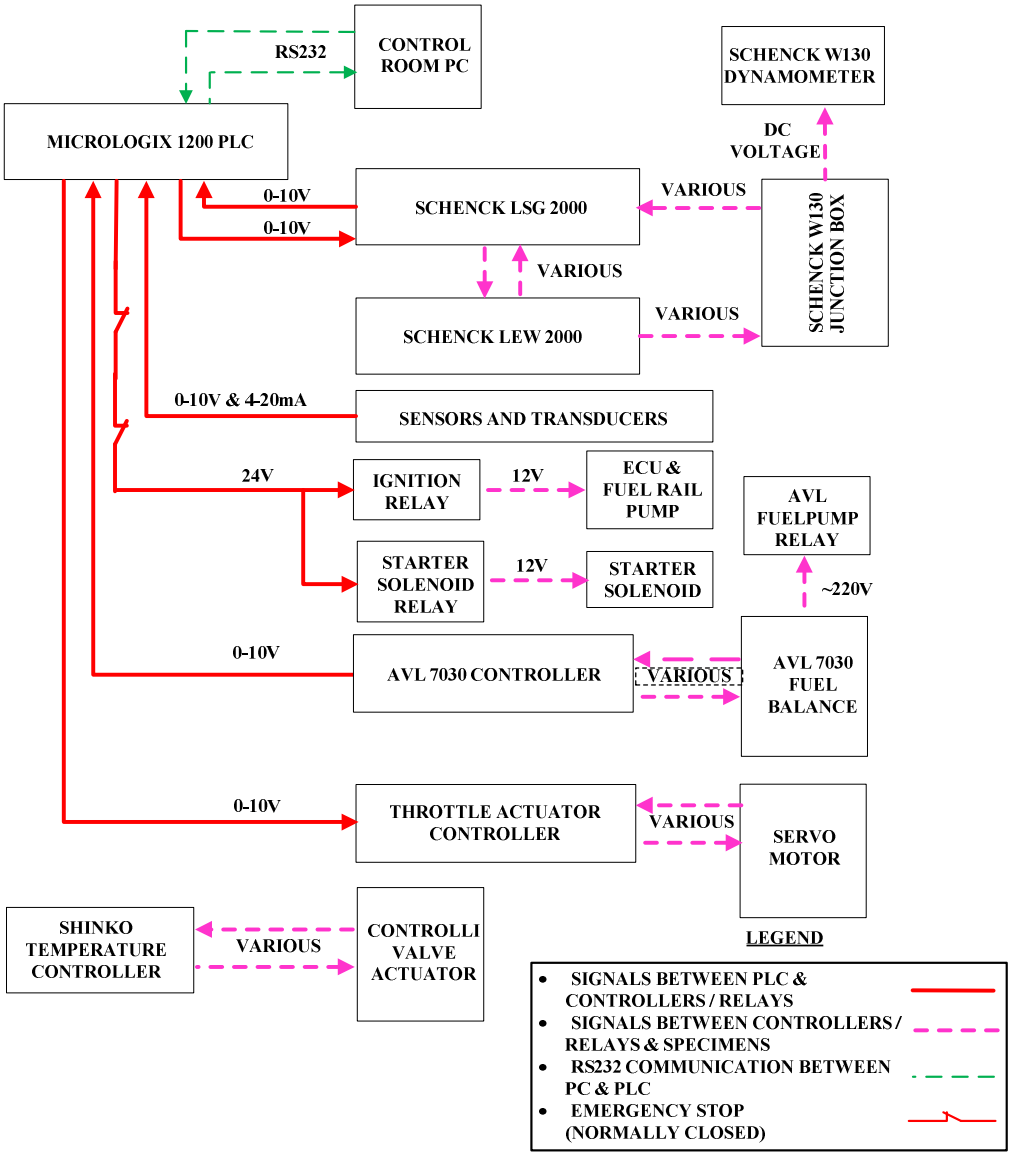

Figure 100: System wiring layout

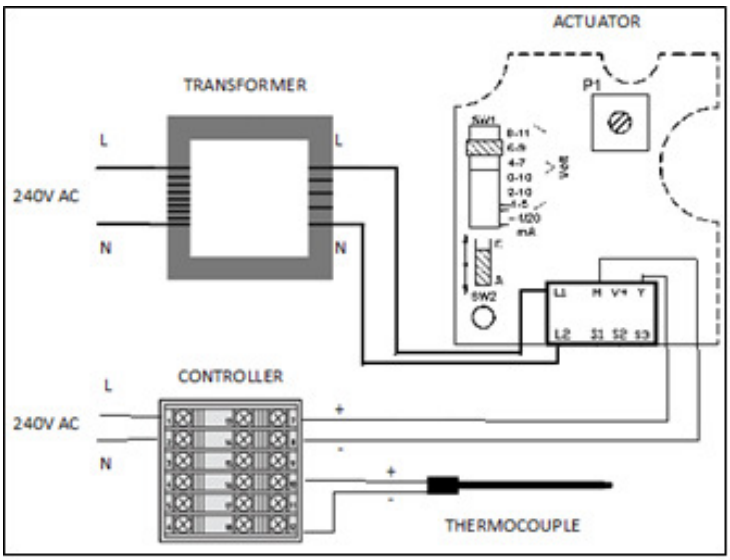

Figure 101: Cooling system wiring

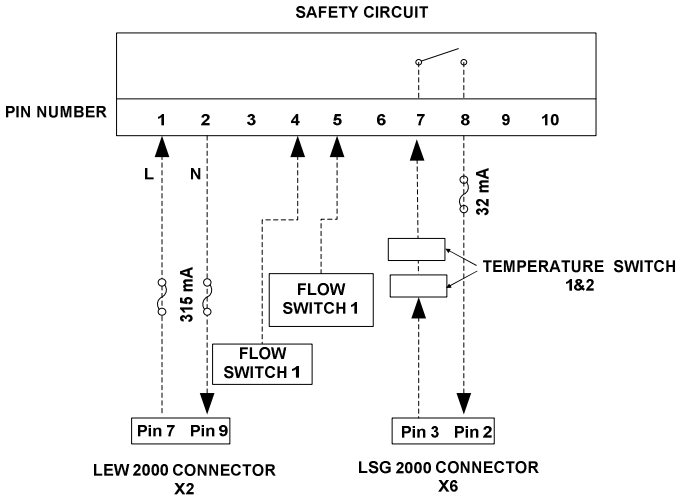

Figure 102: Dynamometer safety circuit wiring

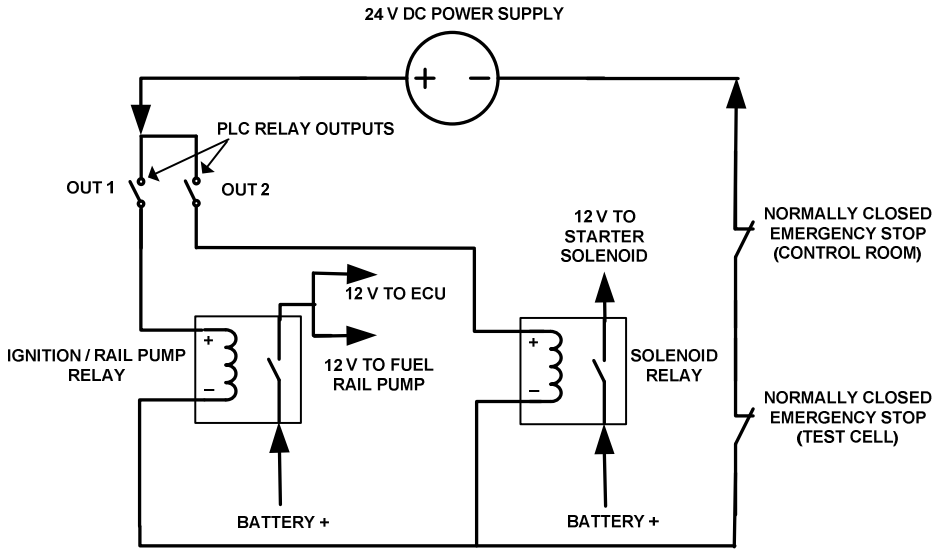

Figure 103: Relay wiring

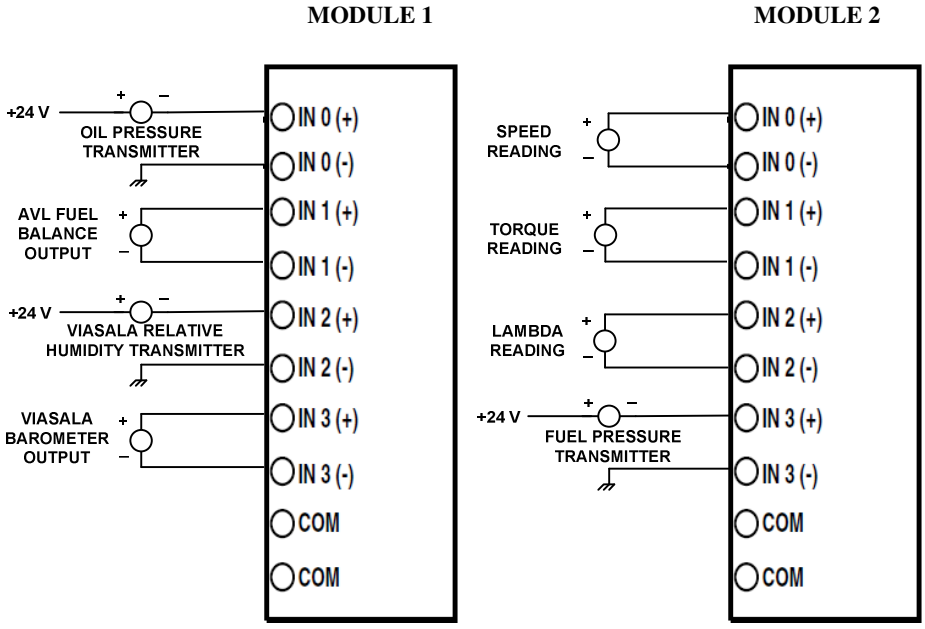

Figure 104: Analogue input module wiring

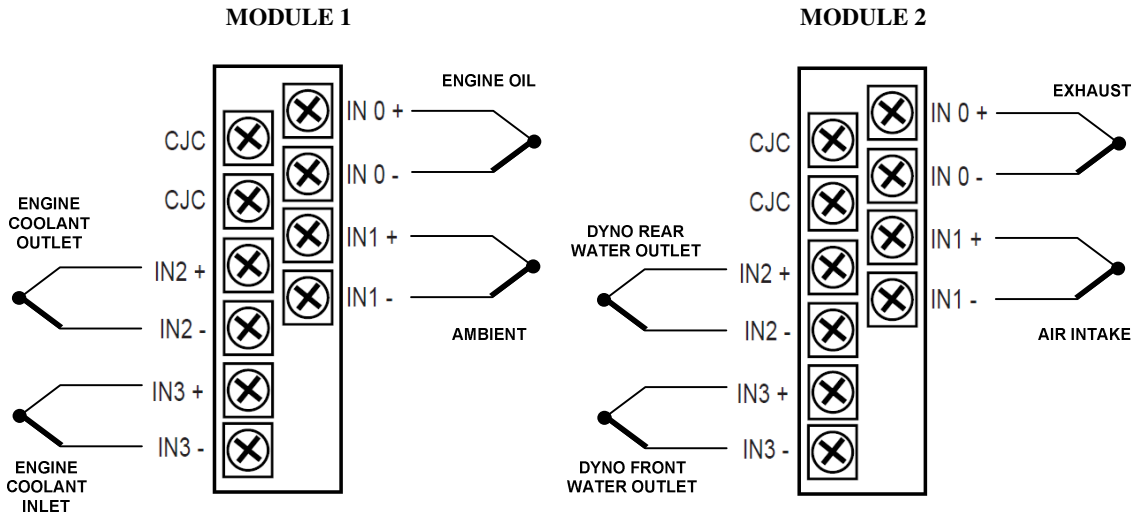

Figure 105: Thermocouple module wiring

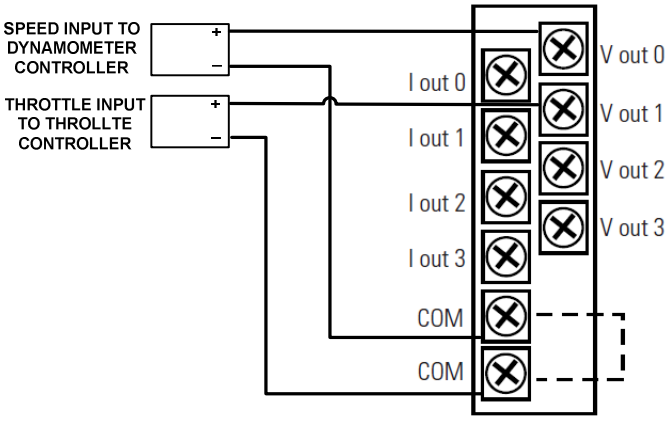

Figure 106: Analogue output module wiring

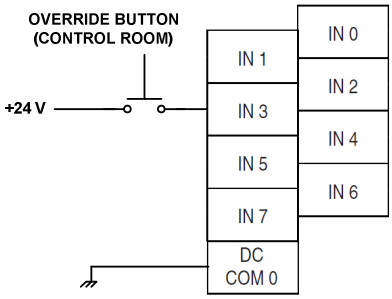

Figure 107: Digital input module wiring

Appendix F: Fuel Analysis Results

The ULP 95 and E10 fuels were analysed by *Intertek South Africa.* The results from their tests are given in Table 14. The results show good correspondence with the WWFC guidelines except for the sulphur content. An increase in RON was also found with the E10 blend which was expected due to the higher octane rating of ethanol.

The ethanol (obtained from *Servochem (Pty) Ltd)* that was used, is anhydrous ethanol with a purity of 99,9 %.

Table 14: Fuel analysis results

Test	Method	100 % ULP 95	90 % ULP 95 & 10 % Ethanol
RON	ASTM D2699	96.5	98.5
MON	ASTM D2700	86.8	86.6
Sulphur (mg/kg)	ASTM D5453	188	177
Density @ 20 ^{0}C (kg/l)	ASTM D4052	0.7399	0.744
Dry vapour pressure equivalent	ASTM D5191	62	68.5
Existent Gum:	ASTM D381		
Unwashed (mg/100ml)		80	83
Washed (mg/100ml)		<1	<1
Manganese (ppm)	ASTM D3831	<1.0	<1.0
Distillation (^{0}C):	ASTM D86		
Initial boiling point		35.1	36.2
10 % volume recovery		50.6	48.5
50 % volume recovery		96	70.4
70 % volume recovery		126.4	122.4
90 % volume recovery		157.7	156.7
Final boiling point		200.7	201.6
Residue/Loss (% volume)		1.0/1.0	1.0/1.0
Evaporation @ 70 ^{0}C (% volume)		29	49
Aromatics (% volume)	ASTM D1319	37	36.4

Appendix G: Test Results

The values that were obtained during the bracket and E10 tests are given in this appendix.

Table 15: Bracket test 1 results

	Torque (N·m)	Speed (rpm)	Power (kW)	BSFC (g/kWh)	Fuel flow (kg/h)	Exhaust gas temperature (°C)	Lambda	Inlet air temperature (°C)	Coolant outlet temperature (°C)	Coolant inlet temperature (°C)
Bracket test 1: 09/11/2012	30	2300	7.3	370.3	2.7	455.4	0.999	23.1	83.0	75.9
	45	2300	10.9	313.3	3.4	513.3	0.989	23.4	82.6	74.7
	60	2300	14.5	290.2	4.2	554.8	0.993	25.5	82.5	74.3
	75	2300	18.1	276.1	5.0	583.9	0.981	26.2	82.2	73.5
	90	2300	21.8	264.0	5.7	623.3	0.966	26.6	81.9	73.0
	30	3600	11.4	387.4	4.4	580.3	0.970	27.2	81.4	75.9
	45	3600	17.1	332.4	5.7	633.3	0.965	27.4	81.3	75.3
	60	3600	22.7	296.7	6.7	660.1	0.966	27.6	81.3	74.2
	75	3600	28.4	268.4	7.6	694.9	0.969	27.7	81.3	73.6
	90	3600	34.1	269.4	9.2	723.7	0.962	27.3	81.9	73.9

Table 16: Bracket test 2 results

	Torque (N·m)	Speed (rpm)	Power (kW)	BSFC (g/kWh)	Fuel flow (kg/h)	Exhaust gas temperature (°C)	Lambda	Inlet air temperature (°C)	Coolant outlet temperature (°C)	Coolant inlet temperature (°C)
Bracket test 2: 14/11/2012	30.0	2300.0	7.3	367.6	2.7	456.6	1.006	25.4	82.4	75.9
	45.0	2300.0	10.9	317.0	3.5	512.6	0.995	26.7	81.9	74.5
	60.0	2300.0	14.5	279.7	4.1	555.2	0.994	27.3	81.8	73.8
	75.0	2300.0	18.2	270.4	4.9	585.0	0.985	28.0	81.6	73.2
	90.0	2300.0	21.8	258.0	5.6	623.0	0.967	28.8	81.3	72.5
	30.0	3600.0	11.4	368.5	4.2	581.8	0.977	30.4	81.0	75.5
	45.0	3600.0	17.1	326.3	5.6	635.6	0.972	30.7	80.7	74.4
	60.0	3600.0	22.8	299.5	6.8	662.0	0.969	30.6	80.8	74.1
	75.0	3600.0	28.5	280.2	8.0	693.0	0.968	30.3	81.0	73.8
	90.0	3600.0	34.1	266.5	9.1	722.4	0.961	29.5	81.4	73.9

Table 17: E10 test 1 results

	Torque (N·m)	Speed (rpm)	Power (kW)	BSFC (g/kWh)	Fuel flow (kg/h)	Exhaust gas temperature (°C)	Lambda	Inlet air temperature (°C)	Coolant outlet temperature (°C)	Coolant inlet temperature (°C)
E10 test 1: 12/11/2012	30.0	2300.0	7.3	381.6	2.8	452.6	1.016	23.3	82.5	76.0
	45.0	2300.0	10.9	323.4	3.5	514.1	1.012	24.0	82.1	74.8
	60.0	2300.0	14.5	296.9	4.3	555.8	1.017	24.7	81.9	74.2
	75.0	2300.0	18.2	281.5	5.1	588.8	1.006	25.2	81.8	73.7
	90.0	2300.0	21.8	273.3	5.9	630.5	0.991	25.6	81.8	73.0
	30.0	3600.0	11.4	393.9	4.5	587.2	1.004	25.6	81.3	75.4
	45.0	3600.0	17.1	334.4	5.7	640.2	1.004	26.1	81.4	75.2
	60.0	3600.0	22.8	297.7	6.8	665.4	1.003	26.3	81.1	74.4
	75.0	3600.0	28.4	278.0	7.9	702.6	1.004	26.6	81.5	74.4
	90.0	3600.0	34.1	278.6	9.5	731.9	0.989	26.0	81.7	74.3

Table 18: E10 test 2 results

	Torque (N·m)	Speed (rpm)	Power (kW)	BSFC (g/kWh)	Fuel flow (kg/h)	Exhaust gas temperature (°C)	Lambda	Inlet air temperature (°C)	Coolant outlet temperature (°C)	Coolant inlet temperature (°C)
E10 test 2: 13/11/2012	30.0	2300.0	7.3	377.8	2.8	454.2	1.032	22.9	82.7	76.2
	45.0	2300.0	10.9	319.2	3.5	511.2	1.029	24.2	82.1	74.9
	60.0	2300.0	14.5	294.1	4.3	553.5	1.032	24.9	82.0	74.3
	75.0	2300.0	18.1	279.1	5.1	585.1	1.017	25.4	82.0	73.9
	90.0	2300.0	21.8	271.2	5.9	627.5	0.999	26.1	81.8	73.2
	30.0	3600.0	11.4	388.2	4.4	583.9	1.009	27.5	81.1	75.6
	45.0	3600.0	17.1	328.2	5.6	637.4	1.003	27.7	81.1	74.9
	60.0	3600.0	22.7	303.9	6.9	663.7	1.002	27.8	81.1	74.5
	75.0	3600.0	28.4	285.6	8.1	700.4	1.011	27.3	81.1	73.9
	90.0	3600.0	34.1	260.9	8.9	728.4	0.992	26.5	81.7	74.3

References

Additive Technical Committee, [S.a.]. *Fuel additives and the environment*. [Online] Available at: http://www.atc-europe.org/public/doc52.pdf [Accessed 29 November 2012].

Al-Hasan, M., 2003. Effect of ethanol-unleaded gasoline blends on engine performance and exhaust emissions. *Elsevier: Energy Conversion & Management*, 44: 1547-1561.

Australian Historical Motoring Federation, 2010. [Online] Available at: http://www.ahmf.org.au/PDF_Docs/Ethanol%20in%20Petrol%20final.pdf [Accessed 29 January 2013].

AVL, 1984. *Operating manual: Dynamic fuel consumption measuring equipment 730*. Graz: AVL.

AVL, 2002. *Engine indicating: User handbook*. Graz: AVL.

Blair, G.P., 1999. *Design and simulation of four-stroke engines*. Warrendale: SAE.

Bosch, 1995. *Automotive electric/electronic systems*. Stuttgart: Robert Bosch GmbH.

Bosch, 2000. *Automotive handbook*. Stuttgart: Robert Bosch GmbH.

California Environmental Protection Agency, 1998. *An overview of the use of oxygenates in gasoline*. [Online] Available at: http://www.arb.ca.gov/fuels/gasoline/pub/oxyrprt.pdf [Accessed 21 November 2012].

Callahan, T.J., Yost, D.M. & Ryan, T.W., 1985. *Acquisition and interpretation of diesel engine heat release data*. SAE Paper: 0148-7191/85/1021.

Ceviz, M.A. & Kaymaz, I., 2005. Temperature and air-fuel ratio dependent specific heat ratio functions for lean burned and unburned mixture. *Elsevier: Energy Conversion and Management*, 46: 2387-2404.

Chevron, 2009. *Motor gasolines technical review*. [Online] Available at: http://www.chevronwithtechron.com/products/documents/69083_MotorGas_Tech_Review.pdf [Accessed 03 November 2012].

Chun, K.M. & Heywood, J.B., 1987. Estimating heat-release and mass-of-mixture burned from spark-ignition engine pressure data. *Combustion Science and Technology*, 54: 133-143.

Danaher Industrial Controls, 2003. *Encoder application handbook*. [Online] Available at: http://www.dynapar.com/uploadedFiles/_Site_Root/Service_and_Support/Danaher_Encoder_Handbook.pdf [Accessed 04 December 2012].

Ebrahimi, R., 2011. Effect of specific heat ratio on heat release analysis in a spark ignition engine. *Scientia Iranica*, 18: 1231-1236.

Encoder Products Company, [S.a.]. *Optical encoders and accessories*. [Online] Available at: www.encoder.com/literature/optical-encoder-guide.pdf [Accessed 03 November 2012].

EUBIA, [S.a.]. *Bioethanol production and use*. [Online] Available at: http://www.erec.org/fileadmin/erec_docs/Projcet_Documents/RESTMAC/Brochure5_Bioethanol_low_res.pdf [Accessed 04 November 2012].

Ferguson, C.R. & Kirkpatrick, A.T., 2001. *Internal combustion engines applied thermosciences*. 2nd ed. New York: John Wiley & Sons.

Figliola, R.S. & Beasley, D.E., 2006. *Theory and design for mechanical measurements*. Danvers: John Wiley & Sons.

Fritz Kübler GmbH, 2012. *Accessories*. [Online] Kübler Available at: http://www.kuebler.com/PDFs/leaflet/drehgeber/english/zubehoer_kupplungen_en.pdf [Accessed 03 December 2012].

Fritz Kübler GmbH, 2012. *Incremental encoders*. [Online] Kübler Available at: http://www.kuebler.com/PDFs/leaflet/drehgeber/english/5000-5020_en.pdf [Accessed 03 December 2012].

Goering, C.E., 1998. *Engine heat release via spread sheet*. [Online] Available at: http://www3.abe.iastate.edu/ae342/AE342_2008/labs/lab3_IMEP/Lab%203_IMEP.pdf [Accessed 03 November 2012].

Heywood, J.B., 1988. *Internal combsution engine fundamentals*. New York: McGraw-Hill.

Honeywell sensing and control, 2012. [Online] Available at: http://sensing.honeywell.com/product%20page?pr_id=55990 [Accessed 03 November 2012].

Horiba, 2013. *Automotive test systems*. [Online] Available at: http://www.horiba.com/automotive-test-systems/products/mechatronic-systems/engine-test-systems/details/dynas3-ht-high-torque-915/ [Accessed 01 February 2013].

Kenny, W.J., 2010. *Instrumenting an internal combustion engine for in-cylinder pressure measurement*. Stellenbosch University.

Kistler, [S.a.]. *Measuring spark plug*. [Online] Available at: http://www.kistler.com/mediaaccess/000-022e-09.02.pdf [Accessed 21 November 2012].

Klein, M., 2007. *Single-zone cylinder pressure modeling and estimation for heat release analysis of SI engines*. Linköping University.

Koc, M., Sekmen, Y., Topgül, T. & Yücesu, H.S., 2009. The efects of ethanol-unleaded gasoline blends on engine performance and exhaust emissions in a spark-ignition engine. *Elsevier: Renewable Energy*, 34: 2101-2106.

Lancaster, D.R., Krieger, R.B. & Lienesch, J.H., 1975. Measurement and analysis of engine pressure data. SAE Paper: 750026.

Lapuerta, M., Armas, O. & Bermudez, V., 2000. Sensitivity of diesel engine thermodynamic cycle calculation to measurement errors and estimated parameters. *Elsevier: Applied Thermal Engineering*, 20: 843-861.

Lilly, L.R.C., 1984. *Diesel engine reference book*. Cornwall: Butterworth.

Lounici, M.S., Loubar, K., Balistrou, M. & Tazerout, M., 2010. Investigation on heat transfer evaluation for more efficient two-zone combustion model in the case of natural gas SI engines. *Elsevier: Applied Thermal Engineering*, 31: 319-328.

M5 Board, [S.a.]. *M5 Board*. [Online] Available at: http://www.m5board.com/vbulletin/e28-m5-discussion/140324-engine-rebuild-lhd-231-a-7.html [Accessed 03 November 2012].

Milnes, R., Deller, L. & Hill, N., 2010. *Ethanol Internal Combustion Engines*. [Online] Available at: http://www.iea-etsap.org/web/E-TechDS/PDF/T06_Ethanol%20ICEs_final_18Jun10_GS_OK_NH.pdf [Accessed 04 December 2012].

National Instruments, 2012. *NI USB-6351 X series data acquisition*. [Online] Available at: http://sine.ni.com/nips/cds/view/p/lang/en/nid/209071 [Accessed 05 November 2012].

NICNAS, 2004. *Sodium Alkylbenzene Sulfonate anti-vale seat recession additive*. [Online] Available at: www.nicnas.gov.au/publications/car/./pec_26_full_report_pdf.pdf [Accessed 21 November 2012].

Optrand Incoporated, [S.a.]. *M3x0.5 combsution pressure sensor*. [Online] Available at: http://www.optrand.com/fliers/m3x05.pdf [Accessed 21 November 2012].

Plint, M. & Martyr, A., 1995. *Engine testing theory and practice*. Tottenham: Hartnolls Limited.

Presto, [S.a.]. *Speed sensors*. [Online] Available at: http://www.presto.co.uk/pdf/data-0006.pdf [Accessed 03 November 2012].

Ricardo Inc., 2010. *Technical Assessment of the Feasibility of Introducing E15 Blended Fuel in U.S. Vehicle Fleet, 1994 to 2000 Model Years*. [Online] Available at: http://ethanolrfa.3cdn.net/934abeccc70545542f_96m6bugqf.pdf [Accessed 01 February 2013].

Rodrigo, C.C. & Sodré, J.R., 2010. Hydrous ethanol vs. gasoline-ethanol blend: Engine performance and emissions. *Elsevier: Fuel*, 89: 287-293.

SAPIA, 2008. *Petrol and diesel in South Africa*. [Online] Available at: www.sapia.co.za [Accessed 03 November 2012].

Schenck Pegasus GmbH, 1997. *Eddy-current dynamometer*. Darmstadt: Schenck.

Schifter, I. et al., 2011. Combustion and emissions behaviour for ethanol-gasoline blends in a single cylinder engine. *Elsevier: Fuel*, 90: 3586-3592.

Shehata, M., 2010. Cylinder pressure, performance parameters, heat release. specific heats ratio and duration of combustion for spark ignition engine. *Elsevier: Energy*, 35: 4710-4725.

Sierra Research, 2008. *Impact of MMT use in unleaded gasoline on engines, emissions control systems, and emissions*. [Online] Available at: http://cleanairinitiative.org/portal/system/files/73069_main.pdf [Accessed 21 November 2012].

Sodré, J.R. & Soares, S.M., 2003. *Comparison of engine power correction factors for varying atmospheric conditions*. [Online] Available at: www.scielo.br/pdf /jbsms/v25n3/a10v25n3.pdf [Accessed 03 November 2012].

Srinivasan, C.A. & Saravanan, C.G., 2010. Study of combustion characteristics of an SI engine fuelled with ethanol and oxygenated fuel additives. *Journal of Sustainable Energy and Environemnt*, 1: 85-91.

Tamers, M., [S.a.]. *Distinguishing between bioethanol and petroleum ethanol*. [Online] Available at: http://www.betalabservices.com/biofuels/petroleum-ethanol.html [Accessed 04 November 2012].

The fuel expert, 2010. [Online] Available at: http://www.fuelexpert.co.za/whatis octane.php [Accessed 27 January 2013].

Topgül, T., Yücesu, H.S., Cinar, C. & Koca, A., 2006. The effects of ethanol-unleaded gasoline blends and ignition timing on engine performance and exhaust emissions. *Elsevier: Renewable Energy*, 31: 2534-2542.

Ubysz, A., 2010. Problems of rotational mass in passenger vehicles. *Transport Problems*, 5: 33-40.

Van Basshuysen, R. & Schäfer, F., 2004. *Internal combustion engine handbook: basics, components, systems and perspectives*. Wiesbaden: Vieweg Verlag.

Verhelst, S. & Sheppard, C.G., 2009. Multi-zone thermodynamic modelling of spark ignition engine combustion - an overview. *Elsevier: Energy Conversion and Management*, 50: 1326-1335.

Williams, F.W., 1997. *Evaluation of hydrocarbon measurement techniques in class B fire environments*. [Online] Available at: www.dtic.mil/cgi-bin/GetTRDoc?AD=ADA321891 [Accessed 30 November 2012].

Wlodarczyk, M.T., Poorman, T., Arnold, J. & Coleman, T., [S.a.]. *Long-life fiber-optic pressure sensors for harsh environment applications*. [Online] Available at: http://www.optrand.com/ [Accessed 03 November 2012].

WWFC, 2009. *Ethanol guidelines*. Worldwide Fuel Charter.